technische universität dortmund

MAX PLANCK INSTITUTE OF MOLECULAR PHYSIOLOGY

Reconstitution of RhoGTPase membrane loading

Dissertation

Zur Erlangung des akademischen Grades eines Doktors der Naturwissenschaften

(Dr. rer. nat.)

der Fakultät für Chemie und Chemische Biologie der Technischen Universität Dortmund

Angefertigt am Max-Planck Institut für molekulare Physiologie in Dortmund

vorgelegt von

Michael Armstrong

April 2022

Tag der Abgabe der Dissertation: 01. April 2022
Von Michael Armstrong

Erstgutachter Prof. Dr. Philippe I. H. Bastiaens

Zweitgutachter Prof. Dr. Roger S. Goody

The work presented in this thesis was performed in the group of Dr. Peter Bieling in the Department of Systemic Cell Biology lead by Prof. Dr. Philippe I. H. Bastiaens at the Max Planck Institute of Molecular Physiology, Dortmund, Germany.

Eidesstattliche Versicherung (Affidavit)

Armstrong, Michael
Name, Vorname
(Surname, first name)

209514
Matrikel-Nr.
(Enrolment number)

Belehrung:

Wer vorsätzlich gegen eine die Täuschung über Prüfungsleistungen betreffende Regelung einer Hochschulprüfungsordnung verstößt, handelt ordnungswidrig. Die Ordnungswidrigkeit kann mit einer Geldbuße von bis zu 50.000,00 € geahndet werden. Zuständige Verwaltungsbehörde für die Verfolgung und Ahndung von Ordnungswidrigkeiten ist der Kanzler/die Kanzlerin der Technischen Universität Dortmund. Im Falle eines mehrfachen oder sonstigen schwerwiegenden Täuschungsversuches kann der Prüfling zudem exmatrikuliert werden, § 63 Abs. 5 Hochschulgesetz NRW.

Die Abgabe einer falschen Versicherung an Eides statt ist strafbar.

Wer vorsätzlich eine falsche Versicherung an Eides statt abgibt, kann mit einer Freiheitsstrafe bis zu drei Jahren oder mit Geldstrafe bestraft werden, § 156 StGB. Die fahrlässige Abgabe einer falschen Versicherung an Eides statt kann mit einer Freiheitsstrafe bis zu einem Jahr oder Geldstrafe bestraft werden, § 161 StGB.

Die oben stehende Belehrung habe ich zur Kenntnis genommen:

Official notification:

Any person who intentionally breaches any regulation of university examination regulations relating to deception in examination performance is acting improperly. This offence can be punished with a fine of up to EUR 50,000.00. The competent administrative authority for the pursuit and prosecution of offences of this type is the chancellor of the TU Dortmund University. In the case of multiple or other serious attempts at deception, the candidate can also be unenrolled, Section 63, paragraph 5 of the Universities Act of North Rhine-Westphalia.

The submission of a false affidavit is punishable.

Any person who intentionally submits a false affidavit can be punished with a prison sentence of up to three years or a fine, Section 156 of the Criminal Code. The negligent submission of a false affidavit can be punished with a prison sentence of up to one year or a fine, Section 161 of the Criminal Code.

I have taken note of the above official notification.

Dortmund,
Ort, Datum
(Place, date)

Unterschrift
(Signature)

Titel der Dissertation:
(Title of the thesis):

Reconstitution of RhoGTPase membrane loading

Ich versichere hiermit an Eides statt, dass ich die vorliegende Dissertation mit dem Titel selbstständig und ohne unzulässige fremde Hilfe angefertigt habe. Ich habe keine anderen als die angegebenen Quellen und Hilfsmittel benutzt sowie wörtliche und sinngemäße Zitate kenntlich gemacht.
Die Arbeit hat in gegenwärtiger oder in einer anderen Fassung weder der TU Dortmund noch einer anderen Hochschule im Zusammenhang mit einer staatlichen oder akademischen Prüfung vorgelegen.

I hereby swear that I have completed the present dissertation independently and without inadmissible external support. I have not used any sources or tools other than those indicated and have identified literal and analogous quotations.

The thesis in its current version or another version has not been presented to the TU Dortmund University or another university in connection with a state or academic examination.*

*Please be aware that solely the German version of the affidavit ("Eidesstattliche Versicherung") for the PhD thesis is the official and legally binding version.

Dortmund,
Ort, Datum
(Place, date)

Unterschrift
(Signature)

Acknowledgements

I would like to thank Dr. Peter Bieling for the opportunity to work on this fascinating project. There were moments of excitement, as well as bumps in the road along the way, but through this project, I think, we have developed a much deeper and meaningful understanding of the nature of the work outlined in this thesis. Additionally, I would like to thank him for all the guidance and support he has provided me with over my time in the group, not only for my project, but also my career and my development as a scientist. We have had many great and insightful discussions which I have always enjoyed.

To members of the Bieling Lab, I extend my thanks in all the support you have given me over the years, the ideas, the discussion, and the laughs. I would specifically like to thank Dr. Ilaria Visco for her continued support in this work, her guidance, intellectual input and ensuring I stayed sane during this process, it is deeply appreciated. In addition, I would like to thank Ankit Roy for all the hard work he has contributed to this project. Without these two people, the work presented in this thesis would not be as it is here.

The Bieling lab is embedded in the Department of System Cell biology headed by Prof. Dr. Philippe Bastiaens, and this environment has moulded my thinking as a scientist to a level I could not have anticipated. It has given me a view and mindset that I believe is unique to this department and will serve me for the rest of my career. This could not be achieved without the passion and drive of Philippe. I would like to thank him for all the discussions we have had and the input he has given me throughout my time in the department. Additionally, I would like to thank all the people who make this department what it is. You have all made it such an enjoyable place to be.

Thanks to Prof. Dr. Roger Goody, for his insights, contributions, and discussions during my thesis advisory committees. The IMPRS, Christa and Lucia, thank you for all the support and guidance during my time here. To the many people who have helped me throughout my time at the institute, weather that has been sharing a state-of-the-art microscope or your coffee machine, thank you.

Finally, I would like to thank my family and my partner Julia who have supported me unconditionally throughout this process and their ever-lasting support in my career.

Table of Contents

List of Figures

List of Tables

Commonly used abbreviations

aa	Amino acid
AF647	Alexa Fluor 647
Cy3	Sulpho-Cyanine 3
fL	Femtolitre
FRAP	Fluorescence recovery after photobleaching
GAP	GTPase-activating protein
GDF	GDI dissociation factor
GDP	Guanosine diphosphate
GEF	Guanosine exchange factor
GTP	Guanosine triphosphate
h	hour
ITSN	Intersectin
ivp	In vitro prenylation
k_D	Equilibrium dissociation rate constant
k_{off}	Dissociation rate constant
k_{on}	Association rate constant
M	Molar
min	Minutes
mL	Millilitre
MM	Minimal mix lipid composition
mM	Milimole
ms	Millisecond
NPF	Nucleation promoting factor
nM	Nanomole
PC	Phosphatidylcholine basic lipid composition
PM	Plasma membrane mimic lipid composition
pM	Picomole
RhoGDI/GDI	Guanosine dissociation inhibitor
s	Seconds
SLB	Supported lipid bilayer
SM	Single molecule
SUV	Small uni-laminar vesicles
$t_{1/2}$	Half-time
TIRF / SM-TIRF	Total internal fluorescence microscopy / Single molecule TIRF

μL	Microlitre
μM	Micromolar
μm	Micrometre
WASP	Wiskott-Aldrich syndrome protein
WAVE	A five-subunit protein complex (WAVE1, CYFIP1, ABI2, Nap1 and HSPC300) or orthologues

Abstract and Zusammenfassung

Abstract

The polarisation of membrane-bound signalling molecules that control the actin cytoskeleton, such as Rho-type GTPases and phosphoinositides is essential for the spatial organisation of cell shape. However, the ubiquitous solubilisation factor RhoGDI (Guanosine Dissociation Inhibitor) sequesters the majority of RhoGTPases in the cytosol, away from the membrane. Starting from defined complexes of RhoGTPases and RhoGDI, we investigate how RhoGTPases load onto membranes.
To this end, we reconstituted the recruitment of the RhoGTPase Cdc42 to supported lipid bilayers and followed this process by multi-colour single molecule imaging. This allowed us to investigate of the effects of several suggested regulators of Cdc42 recruitment. These included regulators catalytic cycle such as activating guanosine exchange factors (GEFs), the biochemical composition and characteristics of the membrane such as charge or lipid composition, and the use of cell lysate to probe for a still unidentified GDI dissociation factor (GDF).
By capturing these events as a high time resolution, it was possible to not only understand what modulates Cdc42 recruitment, but also to decipher at what point during the recruitment process GDI dissociated.
Using reconstitution along with powerful TIRF microscopy and the development of single molecule tracking approaches we showed that RhoGTPase separate from their solubilisation factor RhoGDI prior binding to the membrane. Furthermore, once separated from RhoGDI, it is the composition of the membrane itself which regulates the binding frequency of RhoGTPases at the membrane. We go on to show that, on a supported lipid bilayer, the GEF ITSN is incapable of promoting recruiting of Cdc42 alone, nor the Cdc42:GDI complex suggesting that the catalytic and spatial cycles of the RhoGTPases not coupled in the process of RhoGTPase membrane recruitment.
Finally, through the inclusion of cell lysate in our reconstitutions and in contrast to assumptions in the field, we observe no evidence for an essential active RhoGDI displacement factor (GDFs) that facilitates RhoGDI removal.

Zusammenfassung

Die Polarisierung von membrangebundenen Signalmolekülen wie Rho-Typ-GTPasen und Phosphatidylinositole, welche das Aktin-Zytoskelett steuern, ist massgeblich für die räumliche Organisation der Zellform verantwortlich. Der konsevierte Solubilisierungsfaktor RhoGDI (Guanosin-Dissoziationsinhibitor) sequestriert jedoch die Mehrheit der RhoGTPasen im Zytosol, weg von der Membran. Ausgehend von definierten Komplexen aus RhoGTPasen und RhoGDI untersuchen wir hier, wie RhoGTPasen in Membranen binden können.

Zu diesem Zweck rekonstituieren wir die Rekrutierung der RhoGTPase Cdc42 in oberflächen-gebundene Lipiddoppelschichten und verfolgen diesen Prozess durch Mehrfarben-Einzelmolekülbildgebung. Dies ermöglicht es uns, die Auswirkungen mehrerer vorgeschlagener Regulatoren der Cdc42-Rekrutierung zu untersuchen. Dazu gehörten Regulatoren des Katalysezyklus wie Guanosin-Austauschfaktoren (GEFs), die biochemische Zusammensetzung und Eigenschaften der Membran wie beispielsweise Ladung und die Verwendung von Zelllysat zur Untersuchung eines bisher unbekannten GDI-Dissoziationsfaktors (GDF).

Durch die Erfassung dieser Ereignisse mit hoher Zeitauflösung war es möglich, nicht nur zu verstehen, welche Faktoren die Cdc42-Rekrutierung modulieren, sondern auch zu beschreiben, an welchem Punkt während des Rekrutierungsprozesses GDI dissoziiert.

Unter Verwendung der Rekonstitution zusammen mit leistungsstarker TIRF-Mikroskopie und der Entwicklung von Ansätzen zur Verfolgung einzelner Moleküle zeigten wir, dass sich RhoGTPase von ihrem Solubilisierungsfaktor RhoGDI vor der Bindung an die Membran trennt. Darüber hinaus ist es nach der Trennung von RhoGDI die biochemische Zusammensetzung der Membran selbst, welche die Bindungshäufigkeit von RhoGTPasen an der Membran reguliert. Wir zeigen weiter, dass das der GEF Intersectin nicht in der Lage ist, die Rekrutierung von Cdc42 oder des Cdc42:GDI-Komplexes zu fördern. Dies deutet darauf hin, dass die katalytischen und räumlichen Zyklen der RhoGTPasen nicht im Prozess der RhoGTPase-Membranrekrutierung gekoppelt sind.

Schließlich beobachten wir durch die Einbeziehung von Zelllysat in unsere Rekonstitutionen, dass es im Gegensatz zu früheren Annahmen keine Hinweise auf einen aktiven RhoGDI-Verdrängungsfaktor (GDFs) gibt, welcher der die RhoGDI-Dissoziation erleichtert.

Introduction

The role of Rho-type GTPases in cell polarity and morphogenesis

Rho-type GTPases are master regulators of cell polarity and morphogenesis found in all eukaryotes. These 20 – 30 kDa proteins are integral to a wide spectrum of cellular functions in a large variety of organisms and transduce signals from cell surface receptors to intracellular signalling and cytoskeletal networks. Among the RhoGTPases, the three best studied and widely conserved family members are Cdc42, Rac1 and RhoA. Key to their cellular role is the development of spatiotemporal activity patterns, which locally control cell polarisation and morphology, a phenomenon which is critical to not only cytoskeletal polarisation but a large number of cellular processes and information integration[1,2].

The link between RhoGTPases and cell morphology was initially established through micro-injection of RhoA into fibroblasts, upon which a marked increase in actin stress fibres was observed[3]. Rac1 soon followed, showing its requirement in the development of membrane ruffles and lamellipodial protrusion[4]. Cdc42 was first identified as an essential cell cycle gene in yeast[5,6] and its mammalian homologs were subsequently shown to localise to the leading edge of protruding cells along with Rac1[7,8]. Resulting from their high degree of sequence similarity, the three classical RhoGTPases share biochemical and structural properties with other small GTPases of the Ras superfamily (Figure 1.) To carry out their function at the plasma membrane, RhoGTPases need to attach reversibly to membranes and bind to guanosine-di- or -tri-phosphate (GDP or GTP) in a regulated manner. As such, they contain a nucleotide-binding pocket, which is surrounded by the switch 1 and 2 regions. These switch regions undergo conformational changes in response to the identity of the bound guanine nucleotide, conferring the active state and facilitating effector binding when bound to GTP[9,10]. To localise to the inner leaflet of the plasma membrane, RhoGTPases contain a C-terminal prenylation motif, the so-called CAAX box, which consists of a cysteine followed by any two aliphatic amino acids and finally any amino acid[11,12]. RhoGTPases are subject to post-translational lipidation at the reactive cysteine within this motif, resulting in an enzymatically conjugated geranylgeranyl moiety. This hydrophobic lipid modification anchor inserts into the inner, cytosol-facing leaflet of the plasma membrane, thereby providing membrane affinity whilst allowing for diffusion within the membrane plane.

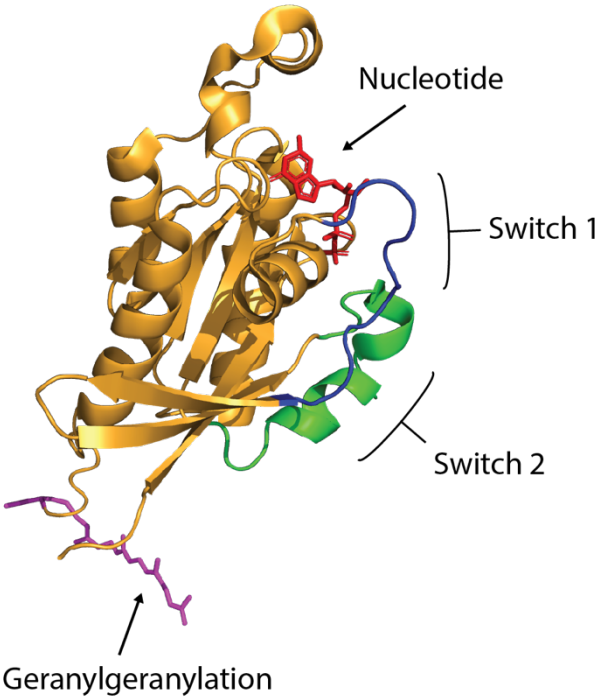

Figure 1. Crystal structure of Cdc42. Crystal structure of inactive Cdc42. The bound nucleotide (red) sits within the nucleotide pocket proximal to the switch 1 (blue) and switch 2 (green) regions. Geranylgeranyl-motif (magenta) at the C-terminus critical for membrane localisation. PDB:2H7O[13]

When bound to the plasma membrane and in an active state, Rho-type GTPases control cell morphology by several mechanisms including the regulation of the actin cytoskeleton. To do so, Rho-type GTPases interact with specific effector proteins, such as N-WASP and WAVE, so called nucleation promoting factors (NPFs) or formin-family proteins. When NPFs interact with their cognate active RhoGTPases, this results in the development of distinct actin networks[14,15], specifically branched actin at the leading edge and contractile networks at the rear.

Branched networks generate protrusive forces across the leading edge, allowing the membrane to be pushed forward. Conversely, at the rear of the cell retraction fibres classically patterned by active RhoA organisation[16], facilitate contractility. These distinct actin structures form at opposing cell edges but work in unison to produce directed movement.

A prerequisite for the spatial segregation of contractile and protrusive actin structures is the spatial patterning of RhoGTPases within the cell. Due to the closely coupled relationship between the RhoGTPases and the actin cytoskeleton, it has been of great interest to visualise active pools of RhoGTPases in live cells. As a result, a number of biosensors have been developed over the years[17] such as the one outlined in Figure

2A. These sensors revealed not only the localisation of the active Rho-type GTPases to the plasma membrane, but also their heterogenous activity distribution[7,18–20]. What is clear from the distribution of the Rho-type GTPases is that during protrusion/retraction events, these RhoGTPases must be tuned regarding localisation and activity for robust morphological output. As can be seen in Figure 2B, the activity patterns of Cdc42, which is located to the leading edge of cells during migration, largely overlaps with the Arp2/3-generated branched actin network at the front of the cell (Figure 2C). However, the picture is likely more complex than this, with several Rho-type GTPases located to the leading edge of the cell, with differing activity patterns believed to modulate different aspects of motility such as directional persistence and speed[7,19]. This spatiotemporal regulation and coordination of Rho-type GTPases is critical as cells must respond to numerous, time-varying cues and respond by stimulation of a distinct local cytoskeleton network.

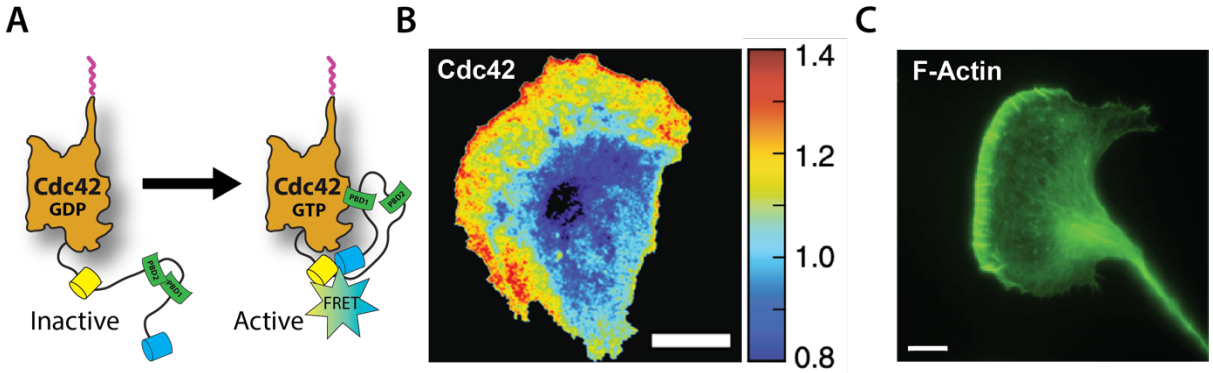

Figure 2. Active RhoGTPase distribution in the cell and corresponding actin network. (A) An example FRET sensor, utilising a single chain architecture, which reads activity by the release of autoinhibition between two p21 biding domains (PDB, green) when the GTPase is in an active state[21]. **(B)** Distribution of active Cdc42 within HeLa cells utilising a FRET sensor showing the highest population of active Cdc42 (red) is located at the leading edge, whilst the cell body shows lower levels of active Cdc42 (blue), scale bar 20 μm [7]. **(C)** Actin network of B16-F1 cells stained with phalloidin, the strong signal at the leading edge shows the protrusive actin network driving the cells leading edge, scale bar 10 μm [22].

The networks involved in polarisation of cells are very dynamic, able to respond rapidly and robustly. The RhoGTPases are no exception to this, requiring both activation and correct spatial distribution. Activity and localisation must be regulated in time and space, both at local and global length scales allowing the cell to not only polarise but modulate polarisation in an ever-changing environment. It is the coordination of RhoGTPase activity and localisation which allows for functional polarisation.

Two distinct biochemical cycles control RhoGTPase activity

The catalytic cycle of Rho-type GTPases

Rho GTPase can assume two alternating activity states as part of their catalytic cycle, depending on the nucleotide to which they are bound. To confer a cytoskeletal response, the Rho-type GTPases must be activated at the plasma membrane to interact with cytoskeletal regulators. RhoGTPases could theoretically, in isolation, spontaneously activate by dissociation of their bound GDP and mass action could drive the loading of the GTP nucleotide, which is significantly more abundant in the cytoplasm of living cells[23,24]. Similarly, Rho-type GTPases could also rely on their innate ability to hydrolyse GTP to revert to an inactive state. This innate ability is not specific to the RhoGTPases but indeed all Ras superfamily members given the level of sequence similarity[25–28]. These spontaneous processes are, however, insufficient to explain RhoGTPase behaviour in vivo because of a number of kinetic considerations. First, the spontaneous dissociation of bound nucleotide is incredibly slow with a half-life of around 5 h[29]. The same holds true for the intrinsic hydrolysis rates for Rho-type GTPase, with a half-life of around 5 – 20 min[30]. These rates are incompatible with rapid cellular responses to stimuli such as cell migration. Additionally, such a GTPase autonomous mechanism would not easily allow for the formation of spatial patterns, as the Rho-type GTPase could be spontaneously activated anywhere and not solely at a polarisation site at the plasma membrane. Instead, nature has evolved an array of regulatory proteins that kinetically promote both activity transitions. Exchange of GDP for GTP is kinetically promoted by guanosine exchange factors (GEF) which facilitate conversion the GTPase to an active, GTP-bound form at a vastly increased rate[29]. To inactive the Rho-type GTPases, GTPase activating protein (GAP) proteins promote nucleotide hydrolysis at rates orders of magnitude faster than the intrinsic hydrolysis rate[30]. Details of the mechanisms involved in GEF-mediated activation and GAP-mediated inactivation of Rho-type GTPases are discussed in the subsequent chapters.

The spatial cycle of Rho-type GTPases

The active fraction of the Rho-type GTPases must be located at the membrane to actuate cytoskeletal dynamics. However, the binding of RhoGTPases to the plasma membrane is a reversible process, a characteristic shared with other Ras superfamily members with considerable flux between membrane-bound and cytosolic pools[31]. All

Ras superfamily members undergo prenylation at their C-termini, facilitating membrane localisation. Therefore, solubilisation factors play a critical role to maintain sizable cytosolic pools of these proteins. In the absence of solubilisation factors, most prenylated GTPases mislocalise and, in the case of RhoGTPases, also undergo degradation[32,33]. The alternating events of reversible membrane binding and cytosolic solubilisation constitute a "spatial cycle" that is, as with the catalytic cycle of GTPases, tightly controlled. The control of the spatial cycle of RasGTPase has most extensively been studied for Ras itself in pioneering work by the Bastiaens lab. The solubilisation factor PDEδ unloads its farnesylated client Ras at perinuclear membranes by displacement through active Arl-family GTPases. Ras is then transported towards the plasma membrane by vesicular transport. This active system maintains a stable steady-state localisation of Ras at the PM[34]. RhoGTPases however, differ in once crucial aspect from Ras in their interaction with solubilisation factors. PDEδ-mediated solubilisation of Ras occurs in a nucleotide independent manner[35], whereas Guanosine dissociation inhibitor (GDI/RhoGDI) preferentially solubilises the inactive form of RhoGTPases[36,37] although with only around a two-fold difference in affinity[38]. This ability to discriminate active from inactive RhoGTPases is thought to be fundamental in RhoGTPases polarisation.

Despite active RhoGTPases being localised to the membrane via prenylation at the c-terminus, it was initially surprising to find them dominantly localised in the cytosol[39], maintained RhoGDI. Similar to PDEδ, RhoGDI solubilises RhoGTPases by shielding the GTPase geranylgeranyl moiety from the cytoplasm by inserting it into a hydrophobic pocket. This means that cellular membranes and RhoGDI compete for RhoGTPase binding resulting in majority of RhoGTPases being retained in an inactive state bound to RhoGDI in the cytosol[32,36,40], and an active fraction dominantly localised to the plasma membrane. The selective accumulation of the active RhoGTPases at the plasma membrane mirrors the localisation of their activating GEFs[41], suggesting a link between the spatial and activity cycles. However, the exact biochemical nature of the coupling between these two cycles has remained enigmatic. What makes this question even more fascinating is that both cycles are coordinated with a relatively small set of regulators. Below, the RhoGTPases as well as each of these limited set of regulator classes is discussed in detail, highlighting how they function individually and collectively to produce cell polarity in Rho-type GTPase activity, which ultimately leads to distinct cytoskeletal morphologies.

The Rho-type GTPase family

Found in all eukaryotes, Rho-type GTPase (as well as other Ras subfamily members) belong to the most highly conserved proteins amongst those involved in cell signalling[42]. With over 22 members in mammals, and orthologues in many other organisms such as yeast and the related Rho of plant (ROP) proteins in plants[42], the Rho-type GTPases are essential in a wide range of processes including, but not limited to, formation of cell protrusions such as filopodia[43–45], lamellipodia[4], neurite extensions and axons in neuronal development[46,47], cell-cell adhesion[48] and protrusion/retraction events[16,19] to list but a few.

A rather beautiful set of images from Hall and co-workers in the late 1990s illustrates how these active Rho GTPase can result in these diverse cell morphologies[49] (Figure 3).

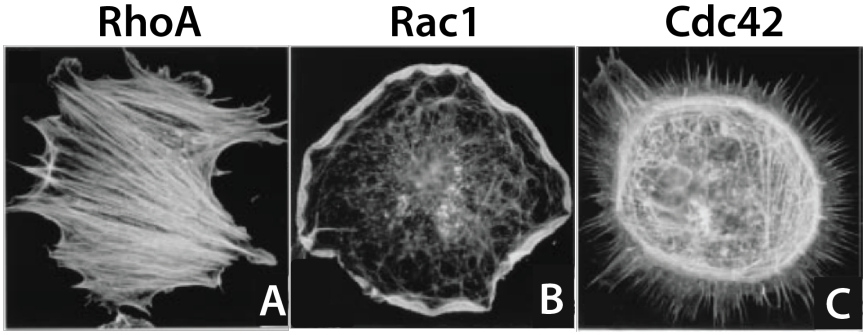

Figure 3. Activation of the classical RhoGTPases produces a distinct cytoskeletal response[49]. (A) Addition of growth factor lysophosphatidic acid activates Rho producing stress fibres. **(B)** Microinjection of constitutively active Rac induces lamellipodia. **(C)** Microinjection of FGD1 (an exchange factor (GEF) of Cdc42) leads to filopodia formation. Swiss 3T3 fibroblasts. No scale bar is provided in original literature; however, it is noted cell sizes are ≈ 75 μm.

Classically, the three Rho-type GTPases were believed to act as switch-like factors to promote specific actin-based structures involved in cell polarity and motility; RhoA in stress fibre and focal adhesion formation, Cdc42 in filopodia formation and Rac1 in lamellipodia formation[49]. While this general picture still holds true today, it is now understood that the role of Rho-type GTPases in such processes is much more adaptive and dynamic than presented in the classical view. Through the development of activity sensors and advance microscopy techniques it has been revealed that the networks of the individual RhoGTPases and their regulators are strongly entwined.

Use of such modern-day visualisation approaches illustrates how RhoGTPases, despite being controlled by a relatively limited set of regulator classes, show distinct spatial patterns (Figure 4) which lead to the long observed morphological changes.

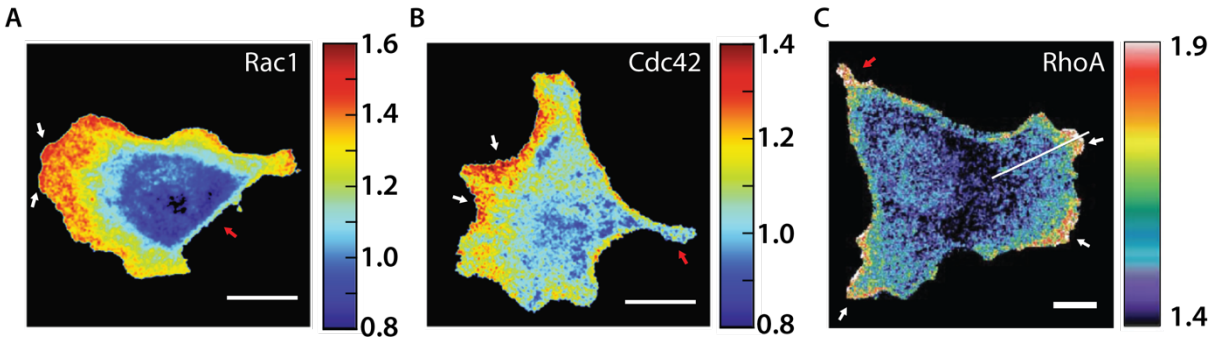

Figure 4. Activity patterns of the three classical RhoGTPases. (A) Rac1 shows strongest activity (red) at areas of protrusion within the cell (white arrows) and lowest activity (blue) at areas of retraction (red arrows)[7] HeLa cells, scale bar 20 µm. **(B)** Cdc42 shows similar distribution to Rac1, with strongest activity (red) at protrusion sites (white arrows) and lowest activity (blue) at areas of retraction (red arrows)[7] HeLa cells, scale bar 20 µm. **(C)** RhoA activity distribution showing strongest activity (red) at sites of retraction (red arrow) and reduced activity (blue/purple) at protrusive regions (white arrows)[50], MEF cells, scale bar 10 µm.

Despite being involved in distinct processes, Rho-type GTPases share many fundamental commonalities with other members of the Ras superfamily. This is not surprising, given the large degree of amino acid identity, particularly within subgroups such as the Rac subgroup (up to 93% identity between members[42,51]). However, a critical region of divergence is the hypervariable region (HVR) at the very C-terminus of Rho and Ras GTPases. The HVR contains several sequence elements (Figure 5A) essential for membrane targeting within the cell. Critical to proper targeting is the post-translational prenylation at the so-called CAAX box (Red highlight box sequence Figure 5A), which consists of a cystine followed by any two aliphatic amino acids and finally any amino acid[11,12].

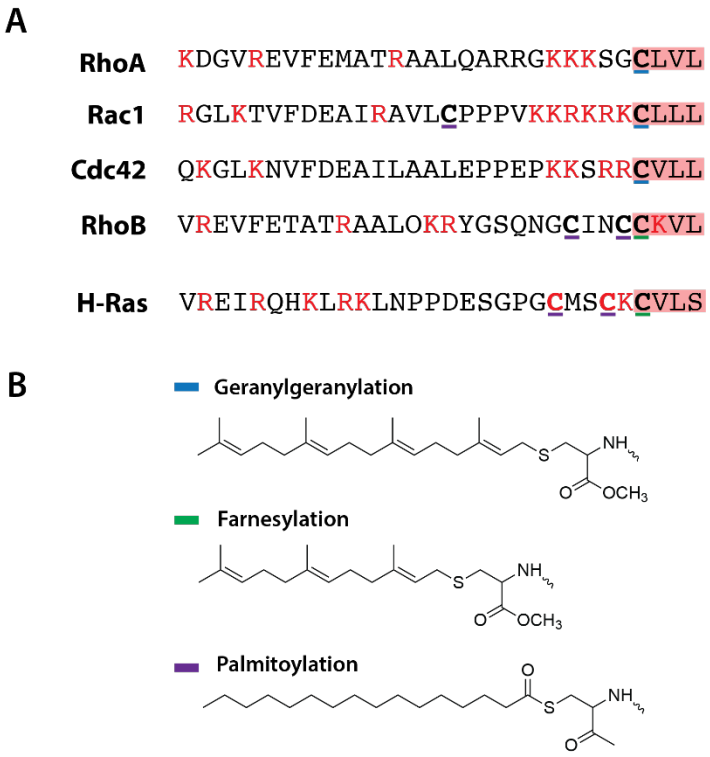

Figure 5. Sequence comparison of C-termini of Ras superfamily GTPases. C-terminal alignment of membrane targeting sequences of human GTPases[12]. **(A)** CAAX motif residues are indicated by red box, basic residues are indicated by red typeface. Bold typeface indicates a reactive cystine with the corresponding modification in colour as an underline. **(B)** Modifications at C-terminus of GTPases, Geranylgeranylation (blue), Farnesylation (green) and Palmitoylation (purple).

Most RhoGTPases are conjugated to a geranylgeranyl moiety via type I Geranylgeranyltransferases (GGTaseI), however farnesylation by Farnesyltransferase (Ftase) can also occur in a fraction of cases (Figure 5B)[52,53]. Whether farnesylation occurs simply a consequence of limited enzyme specificity or, alternatively, serves a specific biological function is currently unknown. Prenylation within this motif is followed by cleavage of the three remaining amino acids and carboxymethylation of the terminal cysteine[54]. The geranylgeranylation process is likely irreversible since no enzymes have been characterised until now that can remove it. The prenyl anchor, together with a positively charged stretch of amino acids (Figure 5A) of variable sequence and length immediately upstream of the CAAX motif, constitute the main interface for membrane association[55]. In addition to these sequence elements, several Rho-type GTPases such as also contain additional cysteine residues within or upstream of the HVR, which can undergo reversible palmitoylation[56–59] (Figure 5A). All of these modifications have been shown to both regulate localisation[57,60], and additionally modify interaction with other regulators, such as in the case of a brain-specific Cdc42 isoform which is impaired in interaction with

RhoGDI when the GTPase was prenylated and palmitoylated[61]. The ability to modulate GTPase behaviour is not constrained to palmitoylation. Phosphorylation of Rho-type GTPases has been proposed as an additional regulatory layer[55]. Specifically, phosphorylation of Cdc42 has been proposed to weaken RhoGDI binding[62,63]. In the case of Rac1, phosphorylation by ERK and AKT have shown to promote GTPase translocation to the nucleus[64] and inhibition of GTP binding[65] respectively. For RhoA, phosphorylation by PKA has been shown to negatively regulate interaction with the effector ROCK[66]. Other, more indirect mechanisms of phospho-regulation, based on competition of different RhoGTPases for RhoGDI binding have also been proposed. For instance, PKG-mediated phosphorylation of RhoA was reported to increase its affinity for RhoGDI, leading to an increased Rac1 membrane recruitment and activity in turn[67]. Such a mechanism captures an important facet of RhoGTPase biology. As RhoGDI is promiscuous in binding to its RhoGTPase clients with comparable affinities, considerable crosstalk can be expected to arise from RhoGDI competition. The relative abundance of both RhoGDI and distinct RhoGTPases as well as the kinetic constraints on the interaction between them would be critical determinants of such crosstalk. However, crosstalk and feedback between distinct RhoGTPases and their associated regulators certainly goes beyond simple competition for RhoGDI and is an intense area of current research. The sheer number of regulators of RhoGTPases, especially at the level of GEFs and GAPs, combined with their known degree of promiscuity renders the understanding of entire RhoGTPase networks, a daunting challenge. However, here an attempt will be made to summarise the main modes of regulation as well as crosstalk and feedback, mediated by the different regulator classes in the subsequent chapters. The understanding of such crosstalk and interaction dynamics sheds light onto the potential mechanisms involved in regulation of RhoGTPase spatial and catalytic dynamics.

A limited set of Rho-type GTPases regulator types

RhoGDI

The master regulator of the spatial cycle of RhoGTPases is RhoGDI. Unlike the stunning degree of diversity of RhoGEFs and GAPs, there only 3 GDIs encoded in the genome of mammals[68], GDI1, GDI2 and GDI3. RhoGDI1 is the most abundant and well-characterised isoform. Interestingly, RhoGDI1 shows very little client specificity,

interacting with numerous Rho-type GTPases including all three of the classically studied examples, Cdc42, Rac1 and RhoA with similar affinity[69–71]. A lack of client specificity holds also true for RhoGDI2. This less ubiquitously expressed RhoGDI isoform[13,72,73] is typically found in haematopoietic cells however binds to its RhoGTPase clients with significantly lower affinity due differences in sequence of the N-terminal regulatory arm[74,75]. RhoGDI3, the most divergent of the family, on the other hand has been shown to be rather selective in its Rho-type GTPases interactions, predominantly binding to RhoB and RhoG[76,77]. Furthermore, RhoGDI3 possesses a unique N-terminal extension which targets it to the Golgi complex as well as other cellular endomembranes[78], differing from the other two RhoGDIs that are not membrane-localised but distribute throughout the cytoplasm[79]. In this work, I will focus on RhoGDI1 as it is the most ubiquitously expressed form.

RhoGDI has three distinct biochemical activities. As the name suggests, it was first observed to strongly slow down both the slow spontaneous exchange as well as the loading of the nucleotide to Rho-type GTPases in complex with RhoGDI[80]. RhoGDI binding also inhibits the intrinsic hydrolysis activity of the GTPase[81]. These effects result from the specific binding mode between RhoGTPases and RhoGDI. The N-terminal regulatory arm of GDI wraps around the GTPase protecting the switch regions (switch 1 and switch 2) as well as the nucleotide-binding pocket (Figure 6.)[13]. When bound to RhoGDI, the structural dynamics of these regions required for the transition between distinct states are restricted, effectively locking the GTPase into the specific nucleotide state in which it was encountered by RhoGDI.

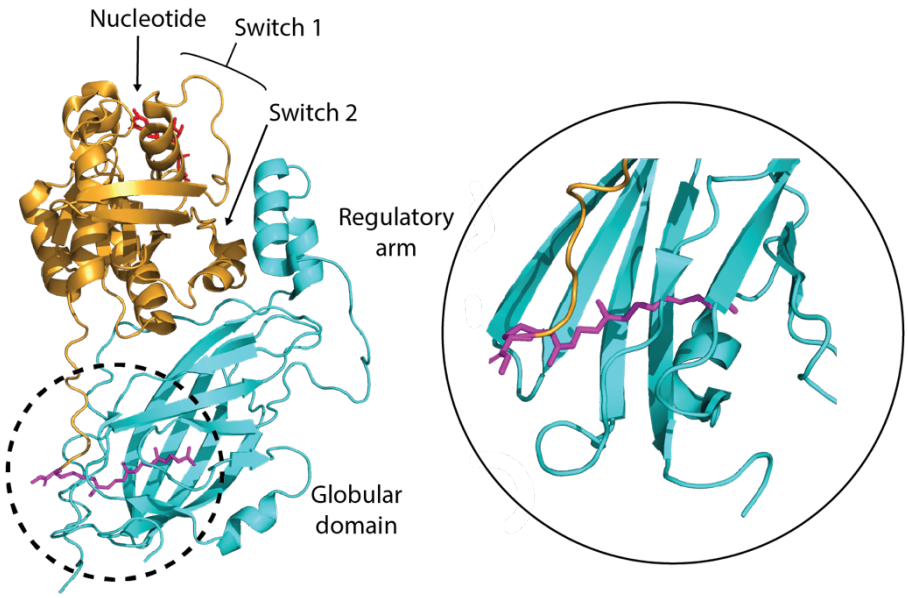

Figure 6. Crystal structure of RhoGDI in complex with Cdc42[13]. RhoGDI (Cyan) complexed with inactive Cdc42 (Orange) is retained in complex by interaction between the regulatory arm of RhoGDI and the switch regions of Cdc42. Additionally, the geranylgeranyl motif at the C-terminus of Cdc42 (magenta) interacts with the globular domain of RhoGDI (inset), shieling this hydrophobic region preventing membrane interaction. PDB:2H7O[13].

Secondly, in addition to the negative regulation via the N-terminal arm of RhoGDI, the globular domain also serves a critical function in Rho-type GTPase regulation. Despite being geranylgeranylated, 90-95% of Rho-type GTPase are localised throughout the cytosol, not to membranes[32,36,40]. This is due to the interaction between the isoprenoid moiety and RhoGDI. RhoGDI binds to the isoprenoid moiety of the Rho-type GTPase via a hydrophobic pocket within its globular domain shielding the moiety and preventing association to the membrane[82] (Figure 7). In the absence of binding to a membrane or a RhoGDI client, RhoGTPases with an exposed isoprenoid moiety are unstable and do not remain soluble[32] which can allow them to be subject to degradation[33].

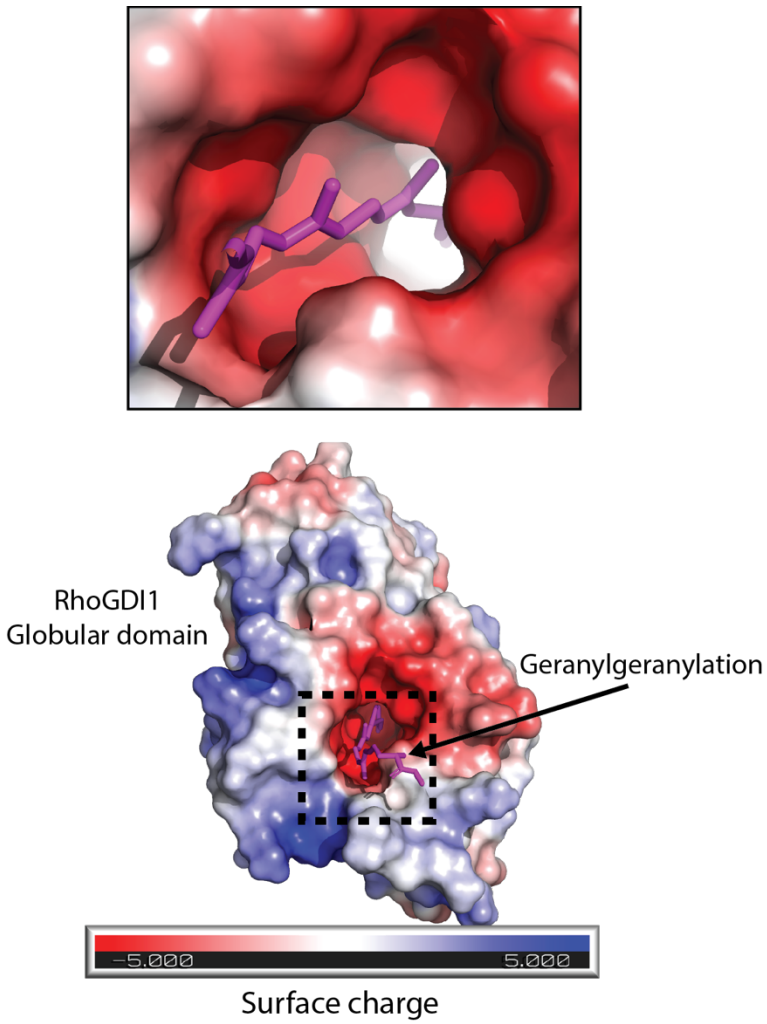

Figure 7. Structure of globular domain of RhoGDI shielding the prenyl-motif of RhoGTPases. The insertion of the geranylgeranyl motif of Cdc42 (upper inset) is orchestrated by the hydrophobic, positively charged lipidation-motif and the negatively charged cleft (indicated by red surface, lower) found within the globular domain of RhoGDI. Surface charge predicted using PyMol[83]. PDB:2H7O[13].

The interaction between RhoGTPases and RhoGDI show high affinity (picomolar regime) and corresponding slow dissociation ($t_{1/2} \approx 60$ min)[84] suggesting that once bound to a RhoGDI molecule, the release of the RhoGTPase to allow for membrane association is incredibly slow. This appears incompatible with the rapid time scales of RhoGTPase polarisation observed in cells[85]. How these two seemingly opposed observations coexist is unclear. It has been suggested that the large pool of RhoGTPases maintained in the cytosol by RhoGDI could be the source of the RhoGTPases recruited to the membrane. Knockout of RhoGDI should lead to a pronounced phenotype on both Rho-type GTPase localisation and function as this should lead to a drastic reduction of the soluble pool of RhoGTPases as well as excess mis-localisation to endomembranes. Such results might be anticipated to greatly alter

the functional signalling properties. While such effects on localisation have indeed been robustly observed in several systems, the functional consequences of genetic RhoGDI removal, while partially controversial, have been generally surprisingly mild. Knockdown of RhoGDI in COS7 cells for instance did not abolish Rac1 activity dependent membrane ruffling[86]. Similarly, RhoGDI-binding deficient Cdc42 was still able to induce the formation of filopodia when overexpressed[87]. However, in the same experiments a marked increase in localisation of RhoGDI to the Golgi apparatus was noted and Cdc42 was found exclusively at membranes and no longer in the cytosol. The maintenance of a functional cytoskeletal organisation and response after RhoGDI loss was similarly observed in other model systems. Deletion of the single RhoGDI orthologue RDI1 in yeast, for instance, generated viable cells that were similar to wildtype in terms of growth, mating and cell morphology[88]. The absence of a cytosolic pool in the case of RhoGDI1 and RDI1 knockouts, yet unimpaired growth (in the case of organisms or cells) and budding (in the case of yeast) would suggest that there is still sufficient localisation and activation of the GTPases at the membrane.

These data combined suggest that any role of RhoGDI in RhoGTPase delivery to, or extraction from, membranes might be functionally dispensable. However, not all results in literature support this notion. Other work using RhoGDI binding-deficient Cdc42 has shown a mis-localisation of Cdc42 to the perinuclear region and very little at the plasma membrane[89] contrasting other results, suggesting that RhoGDI does play a role in Cdc42 targeting to the plasma membrane. Similar experiments using a RhoGDI binding deficient Rac1 mutant could demonstrate a lack of Rac1 translocation to the plasma membrane in response to Hepatocyte growth factor (HGF)[90], further supporting this theory.

How can these seemingly conflicting findings of a dispensable RhoGTPase:GDI interaction and RhoGTPase delivery by RhoGDI be reconciled? Firstly, some cell types could compensate the lack of RhoGDI1 with RhoGDI2, due to biding promiscuity. Additionally, other RhoGTPase interactors such as caveolin1 may be able to act as alternative solubilising factors[91]. However, the observation of the loss of the cytosolic pool of Rho-type GTPases after RhoGDI1 removal suggests that such potential compensatory effects are minor. Alternatively, other mechanisms of plasma targeting of Rho-type GTPases have been suggested. Work in budding yeast has implicated vesicle trafficking as the major driver of Rho-type GTPase plasma membrane localisation after GDI removal[92]. Such actin-dependent, polarised Cdc42

delivery via “hitchhiking” on vesicles might be sufficient for Cdc42 polarity and associated morphological changes. As mentioned earlier, Rdi1 knockout in yeast showed no strong phenotype in terms of Rho-type GTPase polarity, however, when vesicle cycling was also blocked, Cdc42 polarity was rapidly lost.

A further hypothesis to explain the above behaviours could be the existence of a membrane bound fraction of the Rho-type GTPase which is dynamically maintained allowing for rapid GTPase activation at the membrane when necessary. The loss of RhoGDI may cause mis-localisation of the soluble pool, but any membrane bound fraction would simply remain at the PM, and once activated by membrane associated GEFs, could facilitate cytoskeletal dynamics.

However, as mentioned previously, with a half-life of around 1 hour for dissociation from GDI resulting in an incredibly stable cytosolic fraction, how would such a dynamic RhoGTPase fraction exist? RhoGDI preferentially binds to the GDP bound form of Rho-type GTPases, however RhoGDI can also bind to the GTP active form of RhoGTPases[38], although with reduced affinity and increased dissociation rates resulting in a half-life of ≈ 2.5 min[84]. The interaction between RhoGDI and its RhoGTPase client shields RhoGAP interaction[93] preventing GAP-mediated hydrolysis as well as intrinsic hydrolysis. Therefore, active RhoGTPases in association with GDI, could provide a primed pool of already active RhoGTPases which dissociates from its RhoGDI client much faster. Due to the nature of the interaction between RhoGDI and RhoGTPases, specifically the switch regions and the prenyl moiety, perhaps a mechanism whereby the reduction in affinity of active RhoGTPases to GDI coinciding with the GTPase prenyl tail exchanging between GDI and membranes results in an accelerated dissociation rate compared to inactive RhoGTPase-GDI dissociation in solution. Furthermore, this fraction would not require GEF activation as it would arrive at the membrane in its active state, able to directly interact with effectors. As active RhoGTPase have been shown to be extracted by GDI[38], this could produce a dynamically maintained pool between the membrane and in the cytosol of active RhoGTPases and a large, more stable cytosolic reservoir of RhoGTPases in the inactive GDP-bound state.

These open questions in terms of the pools of Rho-type GTPases warrant further investigation.

Guanosine Exchange Factors (GEFs)

RhoGTPases bind GDP and GTP with comparable and high affinity. Due to the highly conserved nature of the nucleotide binding pocket, Ras-superfamily members show affinities in the picomolar regime[94,95], much higher than the concentration of these nucleotides in the cytoplasm[96]. At equilibrium, nearly all RhoGTPases should therefore contain an associated nucleotide. However, because of their low intrinsic nucleotide dissociation rate, they cannot rapidly exchange from their GDP-bound inactive state to the GTP-bound active state. Guanosine exchange factors (GEFs) have evolved to promote this exchange and break through this kinetic bottleneck in activation. There have been more than 80 RhoGEFs identified in the human genome that can be separated into two evolutionarily distinct families. First the Dbl-like GEFs with 70[97–99] and second the DOCK family with 11 members[99,100]. This means that the are many more GEFs than RhoGTPases, suggesting that there is significant overlap in substrate specificity and potentially also redundancy in function. This indeed appears to be the case, as there are over 25 GEFs that can activate all three classical Rho-type GTPases Rac1, Cdc42 and RhoA[97,98]. Despite this abundance and potential overlap, defects in a single GEF can lead to disease (Table 1).

Table 1. RhoGEF protein information[97,101–103]**.** Information regarding example RhoGEFS, their family, and known defects associated to mutation.

GEF Protein	Family	Defect	Reference
Dbl	Dbl-like	Defective dendrite elongation	104
ITSN	Dbl-like	Impaired brain function, suggested role in Down syndrome and Alzheimer disease	105–107
Tiam1	Dbl-like	Impaired oncogenesis	108
DOCK2	DOCK	Long term survival of cardiac allografts, problematic post-transplant operations	102
DOCK8	DOCK	Combined immunodeficiency syndrome	101,103,109

All of these GEFs appear to be controlled through inducible recruitment to cellular membranes and/or the release of intra- or inter-molecular autoinhibition[97]. Notably, these mechanisms are not mutually exclusive and most GEFs seem to utilise a combination of them to acquire spatial and temporal specificity as detailed below. The general mode of action from an energetic perspective of all GEFs is the stabilisation of the nucleotide-free GTPase transition state. However, the specific means by which

GEFs achieve this differs substantially for distinct GEF types. To understand how RhoGEFs carry out their cellular roles, a deeper look at how these two families function is required.

Dbl-family GEFs were first identified from diffuse B-cell-lymphoma cells, hence the founding GEF was named Dbl[110,111]. Dbl contains a region of around 240 amino acids homologous to a region of the *S. cerevisiae* protein Cdc24, which activates Cdc42 during yeast budding and polarity. Dbl and Cdc24 thus represent the initial members of this large and diverse gene family. In their role of promoting nucleotide exchange at cellular membranes, Dbl-like GEFs contain several important, conserved domains, most importantly the catalytic ~ 200 aa Dbl homology (DH) domain, and the subsequent regulatory ~ 100 aa Pleckstrin homology (PH) domain. Both are found as a conserved module in all Dbl-like GEFs (Figure 8), with flanking domains strongly varying between individual family members.

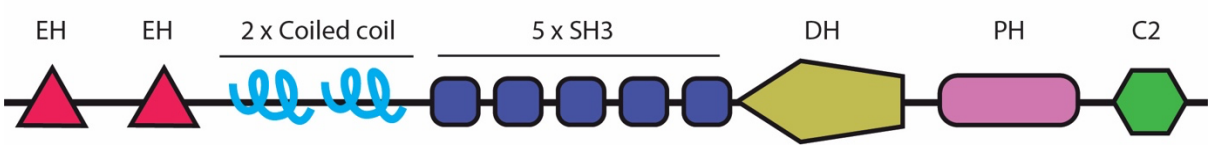

Figure 8. Domains of the Cdc42 specific Dbl-family GEF ITSN. The Dbl-like GEF contains the catalytic DH domain responsible for promoting nucleotide exchange, it is also residues in this domain which confer specificity to Cdc42. The PH domain is important for phosphoinositide binding as well as other proteins in the actin cytoskeletal network. The SH3 domains are responsible for binding to a range of downstream effectors such as WASP. The EH domains are involved in Ca^{+} binding[112], the C2 domain is involved in membrane targeting[113].

The exchange of nucleotide is mediated by the interaction between the catalytic domain of the RhoGEF and its client RhoGTPase. In the case of the Dbl-like RhoGEF ITSN, this interaction occurs between the DH domain of ITSN and the switch 1 region of Cdc42[114] (Figure 9). In addition to interactions with the switch 1 region, conserved hydrophobic regions within the switch 2 region anchor the GTPase to a hydrophobic cleft on the surface of the DH domain of the GEF. Finally, conserved residues of Lys and Asn within the DH domain of the GEF make significant interactions with the switch two region of the GTPase to contribute to exchange potential[97].

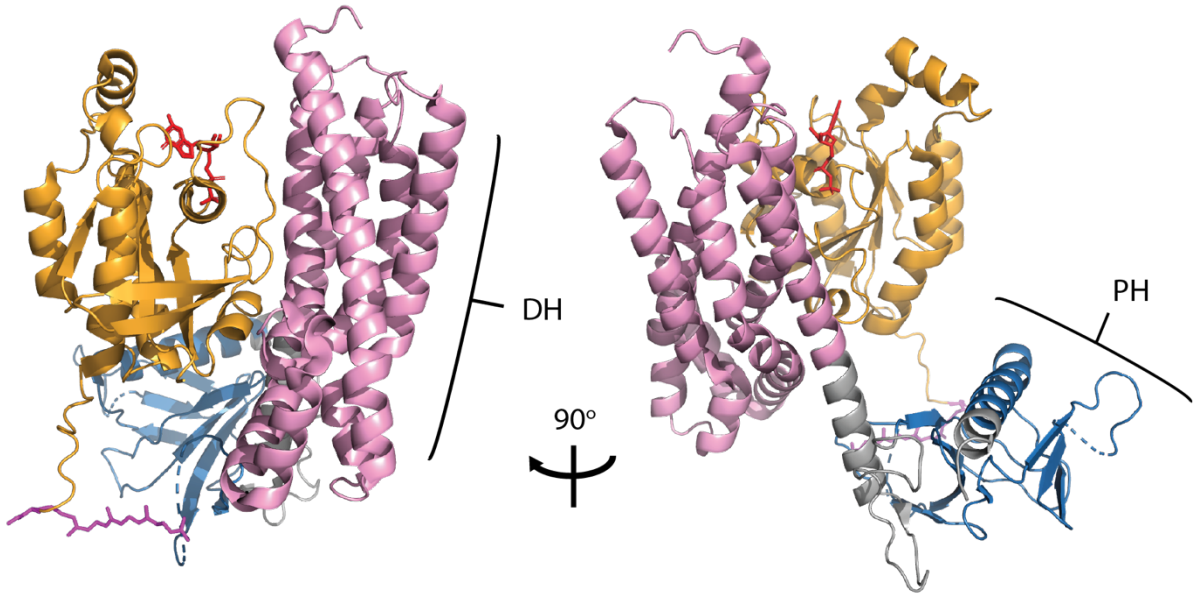

Figure 9. Crystal structure of Intersectin in complex with Cdc42[114]**.** The DH domain of Intersectin (ITSN, pink, left) interacts with the switch regions of Cdc42 (orange) to destabilise the nucleotide (red). The PH domain of ITSN (blue, right) allows for interaction with phosphoinositide lipids and perhaps other proteins such as ezrin. PDB 1KI1.

High affinity binding to the guanosine nucleotide requires a coordinated Mg^{2+} ion[96]. In contrast to other Ras-related GTPases[115–117], the DH domain of RhoGTPase GEFs does not directly insert into the nucleotide binding cleft, but rather disorganises the binding pocket allosterically to reduce the affinity of the Mg^{2+} cofactor[97]. This promotes the formation of an GEF:RhoGTPase intermediate, devoid of nucleotide and Mg^{2+}. Due to the higher concentration of GTP over GDP within the cell, GTP is preferentially loaded into the pocket of the GTPase and once again stabilised with Mg^{2+} resulting in an active GTPase molecule[118]. In principle, GEFs can exchange GTP and GDP nucleotides indiscriminately. Directionality is merely the result of the higher cellular concentration of GTP compared with GDP.

The regulatory PH domain directly C-terminal to the catalytic DH region (Figure 9) also plays an important role for GEF functionality. In many cases, this PH domain directly contributes to membrane association of GEFs by interacting with distinct phosphoinositide lipids[119], which are often enriched at sites of RhoGTPase activity. Differential recruitment of distinct GEFs to specific regions within the cell would offer a level of spatial control of GTPase activation. Indeed, many GEFs have been shown to localise to sites of RhoGTPase activity within the cell[120], many are found at the plasma membrane, even within specific membrane localisation such as the leading or trailing edges in the cases of Tiam1[121,122] or ITSN[123,124]. This phenomenon of selective

GEF recruitment[29] has been suggested to establishment of front-back polarity[121,122]. In some cases, this localisation has been linked to the presence of specific phosphoinositides at membranes, for example, with DH-PH constructs of Tiam1 and ITSN GEFs showing specificity for phosphoinositides, PI(3)P, PI(4,5)P_2 respectively[119] via PH domain interaction. This suggests that GEF activity can dynamically respond to a changing membrane composition[125]. In other cases, this PH domain does not seem to interact with phosphoinositides, but rather plasma membrane-associated proteins such as ezrin[126]. Ezrin and related ERM (ezrin, radixin and moesin) proteins act as bi-functional crosslinkers between the plasma membrane and the proximal actin cortex. As such, their accumulation at the membrane depends on the presence of cortical actin, which is itself nucleated by RhoGTPase activity. Such a GEF recruitment mechanism, indirectly promoted by actin, has been speculated to provide positive feedback between actin nucleation and RhoGTPase activity.

The DOCK (dedicator of cytokinesis) protein family contains eleven members (DOCK 1-11), which are evolutionarily and structurally unrelated to the Dbl-like GEFs. All DOCK GEFs identified until now appear to act on Rac1 and Cdc42, but not RhoA[99]. DOCK GEFs possess a conserved catalytic domain known as the DOCK Homology Region 2 (DHR2)[127] and a phosphoinositide binding domain (DHR1) responsible for targeting DOCK GEFs to the membrane via phosphoinositide interactions[127–129] (Figure 10).

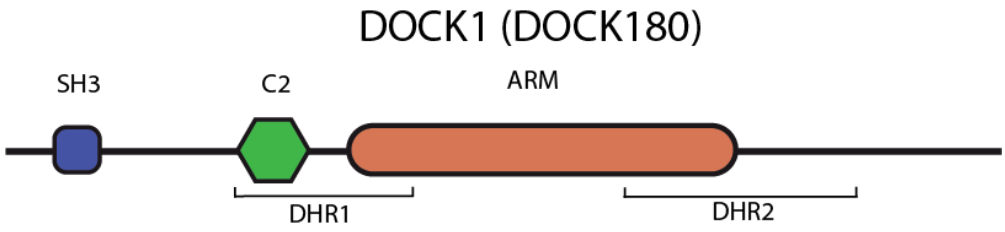

Figure 10. Domain architecture of DOCK1(DOCK180)[97,128,129]**.** DOCK1 (DOCK180) is a Rac1 specific DOCK family GEF of the DOCK-A subgroup. The Src-homology-3 (SH3) domain typically binds to polyproline regions in other proteins, often downstream effectors of the RhoGTPases. The C2 domain is another modular signalling domain that can induce membrane–protein, or protein–protein interactions after binding several Ca2+ ions. The ARM domain is an ~40 amino-acid-long tandemly repeated sequence motif involved in the formation of suprahelical structures used to engage other proteins, typically those containing ARM-arrays themselves. The DHR1 domain is responsible for phosphoinositide interactions, whilst the catalytic DHR2 facilitates nucleotide exchange.

The DOCK family is further divided into 4 subfamilies based on sequence similarity. DOCK-A and B subfamilies contain the DOCKs 1 – 5 and share an SH3 domain at

their N-terminus (DOCK1 example in Figure 10). The DOCK-D subfamily (DOCKs 9-11) possess a PH domain at their N-terminus. Finally the DOCK-C subfamily possesses solely the DHR domains[99]. A critical differentiator between the DOCK-A/B and DOCK-C/D subfamilies is substrate specificity with DOCK-A/B exclusive to Rac1 and DOCK-C/D harbouring mixed specificity (see Table 2)[99].

Table 2. Summary table of DOCK family RhoGEFs

DOCK Family	DOCK protein	Addition domains	Specificity
DOCK-A	DOCK1	SH3	Rac1
	DOCK2	SH3	
	DOCK5	SH3	
DOCK-B	DOCK3	SH3	Rac1
	DOCK4	SH3	
DOCK-C	DOCK6	-	Cdc42 + Rac1
	DOCK7	-	
	DOCK8	-	Cdc42
DOCK-D	DOCK9	PH	Cdc42
	DOCK11	PH	
	DOCK10	PH	Cdc42 + Rac1

The mechanism of nucleotide exchange and interaction with client RhoGTPases is rather similar to Dbl-like GEFs, with the DHR2 domain interacting with the switch regions to facilitate nucleotide release[99]. Regulation on the other hand differs somewhat. As discussed in the Dbl-like GEFs, the PH domain allows for localisation of GEFs to the plasma membrane either via phosphoinositide interaction or through interaction with membrane-associated proteins. While some DOCK GEFs do possess a PH domain at their N-terminus (Table 2), the majority do not. Some DOCK proteins seem to assemble into hetero-oligomeric complexes. DOCKs 1 – 5, for instance bind to the engulfment and cell motility (ELMO) proteins via their conserved SH3 domain[130–132]. There are three ELMO proteins in mammals, but all of them appear to act as scaffolds, because none of them contains apparent catalytic domains[133]. GEF activity seems nonetheless depend on interaction since it has been shown that in human kidney cells, Rac1 activation was inhibited when the interaction between DOCK180 (DOCK1) and ELMO was disrupted[127]. Furthermore, when the interaction with DOCK180 (DOCK1) is maintained but localisation of ELMO is inhibited by sequence deletion, cells failed to localise DOCK180 at the lamellipodia. This resulted in migration defects and suggests that localisation of DOCK180 to the lamellipodia by ELMO localisation plays a role in cell migration[130].

The release of autoinhibition appears to be an important mode of regulation for both Dbl- and DOCK-type GEFs. Most, but not all Rho GEFs display only marginal activity when overexpressed and are constitutively activated by truncations of sequences upstream of the catalytic DHPH domain module[41,134]. The GEF Vav has been show to undergo release of autoinhibition by phosphorylation within its N-terminal extension, which usually occludes the DH catalytic site[135]. Additionally, for ITSN1L, the DH domain is autoinhibited by a short stretch of amino acids between its SH3 domains and its catalytic DH domain[136,137]. This inhibition is released by effector interaction with the SH3 domains such as N-WASP[137]. This provides an interesting avenue of feedback, as active GTPases recruit NPFs such N-WASP, the in turn increases GEF activity.

Besides release of autoinhibition, membrane localisation of the GEF in itself has been proposed to greatly activate nucleotide exchange as a result of dimensionality reduction[138]. Mobile attachment of both GEFs via lipid or protein interactions, as well as GTPases via prenylation, promotes their diffusional encounter in the plane of the membrane. Other positional effects, such as a favourable orientation of the catalytic domain of GEFs or even GTPases at the membrane might also contribute[139]. Specifically, the interaction of the PH domain with membrane lipids has been proposed to orient the adjacent DH domain relative to membrane-bound Rho GTPases, suggesting why these domains are invariably found in tandem in all Dbl-type GEFs. Regardless of the precise origin, the kinetic effect of membrane recruitment on nucleotide exchange kinetics can be extremely potent, as shown in the well-studied example of SOS in Ras activation. Binding both Ras and SOS to lipid bilayers increases the rate of activation up to 500 fold compared to similar concentrations of both reactants in solution[140]. Similar effects can be anticipated for RhoGEFs. Indeed, the induced recruitment of catalytically active GEFs to the plasma membrane by optogenetic or chemical inducible dimerisation is sufficient to activate RhoGTPase in vivo[141,142]. Notably, induction of activity appears to depend on membrane identity, because GEF recruitment to other endomembranes does not elicit a similar GTPase response compared to the plasma membrane[143]. All these points combined suggest that RhoGEFs act on inactive GTPases already present in the membrane and do not directly stimulate their recruitment from solution. However, more work is required to determine the exact relationship between membrane binding and GEF-mediated activation of Rho-type GTPases.

GTPase-activating proteins (GAPs)

RhoGTPases possess the ability to catalyse the hydrolysis of GTP to GDP+P_i intrinsically. However, this process is rather slow with half-lives of several minutes[144]. In the early 1990's, a class of regulators was identified that kinetically promote GTP hydrolysis[111,145] via a conserved 150 residue domain (the GAP domain)[146] (Figure 11). These RhoGAP proteins selectively bind to active GTP-bound RhoGTPases to catalyse the hydrolysis of the β-γ phosphodiester bond within the associated nucleotide, at rates that exceed intrinsic hydrolysis by several orders of magnitude[30].

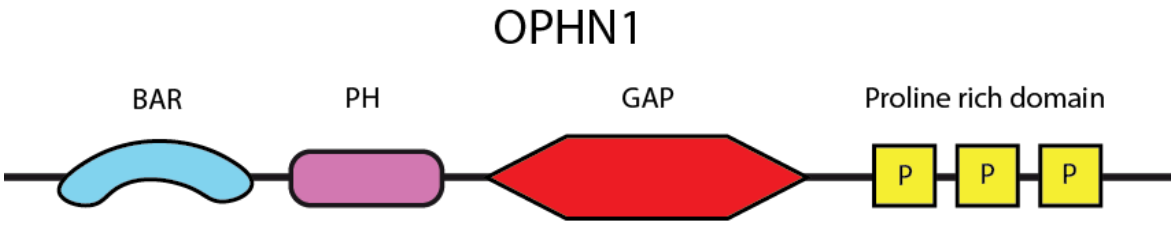

Figure 11. Domain architecture of the RhoGAP OPHN1[30]**.** OPHN1 is a RhoGAP, with promiscuous activity towards a number of RhoGTPases including Cdc42, Rac1 and RhoA. The GAP domain, a conserved domain in RhoGAPs catalyses the hydrolysis of GTP to GDP by the GTPase. The PH domain has roles in phosphoinositide binding. BAR domains act as curvature sensing modules. The proline rich domain allows for interaction with other regulators which contain SH3 domains such as ITSN, proposed as a mechanism of feedback.

By now, over 80 RhoGAPs (far more than RhoGTPases themselves) have been identified in humans[146,147]. As with the RhoGEFs, a key remaining unanswered question is why there are so many distinct GAP family members to downregulate far fewer Rho-type GTPases found many eukaryotic organisms? Even more so than for RhoGEFs, GTPase promiscuity of GAPs poses a conceptual challenge, since are no RhoGAP proteins that appear to be truly specific for a single RhoGTPase[30]. With so many family members and low specificity, regulation of RhoGAPs is an exciting area of current research.

Importantly, RhoGAP specificity might arise through differential targeting of the RhoGTPases and the RhoGAPs within the cell. For instance, RhoGAPs such as OPHN1 or SRGAP3 show little specificity between the Rho-type GTPase but each possess a curvature sensing BAR domain[30] (Figure 11). BAR domains allow for recruitment to areas with high curvature such as the leading or trailing edges of cells. This would provide a mechanism of specificity, allowing BAR-domain-containing RhoGAPs to act more selectively on Rho-type GTPases which are also located at areas of high curvature[148] or segregated spatially as seen in Figure 4. In addition, most

RhoGAPs are large, multi-domain proteins that often contain numerous putative interaction partners such as kinases, which might tune their activity or localisation[149,150].

It has been postulated that RhoGAPs could provide an avenue of RhoGTPase crosstalk. As previously mentioned, many RhoGAPs, such as OPHN1 possess a N-terminal putative lipid-binding PH domain thought to be required for phosphoinositide binding[30]. This could provide recruitment of RhoGAPs to areas of increased phosphoinositide concentrations[150]. This membrane composition would likely also recruit RhoGEFs via their PH domain. However, as discussed RhoGEFs, typically exhibit greater client specificity than RhoGAPs. Phosphoinositide patches could lead to RhoGEF recruitment and activation of specific client RhoGTPases, but simultaneous inactivation, via RhoGAP, of many RhoGTPases in a non-specific manner, allowing for the development of active patterns of specific RhoGTPases. Localisation of RhoGAPs to sites of high RhoGTPase activity could also provide opportunity for catalytic-cycle-regulator interaction. The RhoGEF ITSN has been shown to interact with RhoGAP CdGAP[123]. ITSN is specific for Cdc42 activation and CdGAP has activity towards Cdc42 and Rac1[151]. This interaction, mediated by the central domain of CdGAP, was suggested to result in a conformational change involving the proline rich domain of CdGAP leading to the inhibition of the GAP activity of CdGAP. This means that the Cdc42-activating GEF ITSN could also lead to increased level of active Rac1 at the membrane due to down-regulation of CdGAP activity, illustrating another example of putative feedback.

In addition to spatial regulation, RhoGAPs undergo modifications which alter their activity towards Rho-type GTPases, specifically phosphorylation and/or ubiquitination[55]. In the case of DLC1 shows enhanced activity when phosphorylated by PKA, dimerisation is facilitated which leads to an increase in GAP activity[152]. Conversely, when phosphorylated by ERK, p190ARhoGAP is inhibited in GAP activity resulting in Rho-dependent focal adhesion formations[153] showing that RhoGAPs themselves can be both positively and negatively regulated by phosphorylation. Due to the large number of diverse RhoGAP family members, a lot remains unknown regarding their regulation and potential avenues of crosstalk.

Effector protein interactions and coordination of actin networks

The actin cytoskeleton is a dynamic filament network that shapes, supports and exerts forces on membranes[154], which is essential for processes such as cell morphogenesis, motility[14,155] and cell division[156,157]. Cells possess large amounts of polymerisable actin, which is maintained by its own set of regulators and provides the thermodynamic energy for polymerisation-based protrusion of the plasma membrane[158],[159]. However, to exert pushing forces in a directional manner, actin growth needs to be spatially controlled. Pulling forces on membranes are also exerted through actin filaments that are contracting through the action of myosin II motor proteins whose activity is subject to spatial regulation[160,161]. The spatial control and the coordination of pushing and pulling forces at the plasma membrane is mainly exerted by Rho-type GTPases[19]. To modulate cytoskeletal activity Rho-type GTPases interact with a plethora of effector proteins.

In the case of protrusive actin network architectures such as filopodia and lamellipodia at the leading edge (Figure 12), several downstream interaction partners for active Rho-type GTPases have been identified. The most relevant activities in this context are so-called nucleation promoting factors (NPFs) such as the (N-)WASP and WAVE complexes that activate the branching nucleation activity of the Arp2/3 complex.

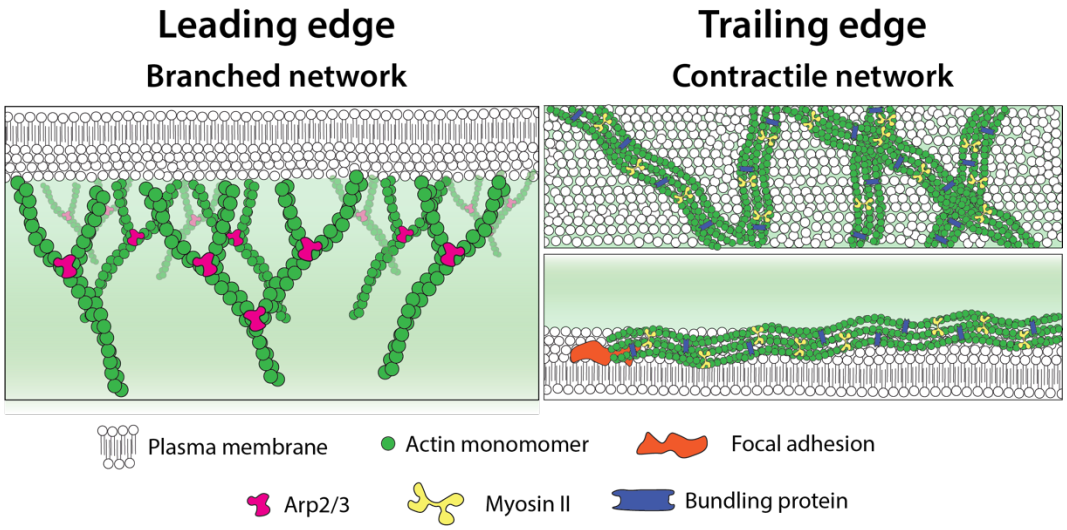

Figure 12. Distinct actin networks of branched networks and contractile networks. The production of a branched actin network (left) allows for transmission of force to the cell membrane pushing the leading edge forward. Arp2/3 binds to existing mother filaments and facilitates nucleation of a daughter filament at a distinctive 70° angle. Contractile networks (right) rely on the parallel bundling of actin filaments and the activation of motor proteins which produce pulling forces. This force is transferred to the membrane via anchoring through focal adhesions.

Both (N-)WASP and WAVE are controlled by regulated autoinhibition. In the case of (N-)WASP, recruitment to active Cdc42 and $PI(4,5)P_2$ lipids within the plasma membrane releases intramolecular autoinhibition allowing its VCA domain to bind to and activated the Arp2/3 complex[162,163]. WAVE on the other hand is part of a five subunit complex known as the wave regulatory complex (WRC) made up of WAVE, Pir121, Nap1, Abi1 and HSPC300[164,165]. Similar to N-WASP, WAVE can receive inputs from Rho-type GTPases and phosphoinositides, however Rac1 and $PI(3,4,5)P_3$ in this case[166,167]. Recruitment through these membrane-associated molecules again leads to the liberation of the Arp2/3 activating VCA domain within the WAVE complex. Once activated at the plasma membrane, these NPFs recruit the Arp2/3 complex to form a ternary complex with an existing actin filament to create a filament branch[168–170]. The incorporation of new monomers elongates daughter filament branches from the pre-existing mother filament at a 70° angle[171]. Activation of Arp2/3 branching at selective regions of the plasma membrane, together with other factors that control the length of the nucleated filaments such as capping protein (CP) forms the biochemical basis of branched actin network assembly. However, NPFs such as N-WASP and WAVE are regulated by factors in addition to the ones outlined above. Specifically, membrane curvature has been suggested to influence localisation and activity of these NPFs. For WASP, this was shown to localise to positive (inward) curvature created by cells crawling over bead recruiting the arp2/3 to these sites[172]. The WAVE complex can be seen as a propagating linear “wave” structure in the lamellipodia via feedback loops[173] including IRSp53 (an I-BAR domain protein, capable of sensing curvature) recruitment[174], stimulating actin polymerisation which then strips the WAVE complex from the membrane[175].

At the rear of the cell, contractility is classically patterned by active RhoA. Rho Kinase (ROCK) is an effector of RhoA[176–178], and plays a major role in mediating the rearrangement of the actomyosin cytoskeleton[179]. Activation of ROCK via interaction between the Rho binding domain (RBD) of ROCK and RhoA[180] results in the phosphorylation of the myosin light chain (MLC)[181] of myosin II inducing actin contraction[179,182–185]. This pulling force is generated as the myosin II motors are linking actin filaments which are arranged parallel to one another. The maturation of these contractile bundles can result in large fibres known as stress fibres[180,186,187]. Stress fibres form between adhesive patches of integrin receptors known as focal adhesions[188] and are bundled together by a range of cross-linking and/or bundling

proteins such as α-actin or filamin[184]. Despite what is known regarding the role of RhoA in this process, much remains elusive regarding how the filaments, which make up these bundles are initiated.

As is clear from all the previously discussed regulators, spatial coordination of these interactions is paramount, with all these interactions taking place at specific regions of the plasma membrane. The integration of biochemical and morphological inputs at the level of the effector proteins can generate distinct actin structures that would be difficult to achieve by single input such as RhoGTPases alone. Notably, deformation of the membrane, classically seen as simple output of signalling and cytoskeletal activity, feeds back onto, and influences all these regulators and the cytoskeleton itself.

The plasma membrane and its influence on RhoGTPases

The plasma membrane is not simply static barrier that retains the cellular contents, but is in fact a dynamic supramolecular structure that receives, processes and distributes biochemical signals[189]. Populated by integral and peripherally associated proteins, it is formed of a lipid bilayer which is dynamically maintained through a combination of lipid synthesis, chemical conversion and vesicle fusion and fission events[190]. Phospholipids in the context of the plasma membrane serve several general functions. The structure of phospholipids with their hydrophobic acyl chains produces a bilayer into which hydrophobic moieties, such as the prenyl tail of RhoGTPases can partition. Specific phospholipids can also act as first and second messengers in signal transduction[190], and influence protein-membrane interactions[191,192].

Phospholipid composition therefore constitutes an important factor in determining the identity of a membrane within the cell. The inner leaflet of the plasma membrane is formed of phosphatidylcholine (PC), phosphatidylethanolamine (PE), phosphatidylinositol (PI) (the phosphorylation state of which can be interconverted, but $PI(4,5)P_2$ being the most abundant one), phosphatidylserine (PS) and sphingomyelin (SM)[190]. This negatively charged surface, depending on its exact relative fraction of these lipids, can recruit different Rho GTPase, as well as their activators as previously discussed. The PM therefore functions as specialised compartment on which RhoGTPases and these regulators concentrate to self-organise in to micro-scale activity patterns. These activity domains polarise many distinct cell types and organise distinct cellular protrusions. For example, neutrophils form a protrusive leading edge as they move towards their target, neurons establish distinct projections such as axons

and dendrites and epithelial cells polarise into basolateral and apical domains. All these cell protrusions rely on the spatial regulation of plasma membrane composition and Rho-type GTPase activity.

One class of membrane phospholipids particularly critical to membrane identity are the phosphoinositide (PI) lipids. These lipids make up a minor fraction of membrane lipids, but are found in all cellular membranes of eukaryotic cells[193]. The interconversion of PI lipids to various states of phosphorylation via lipid kinases and phosphatases (Figure 13) allows for enrichment of specific phosphoinositide species in distinct membrane compartments or even in distinct zones of a continuous bilayer such as the plasma membrane. The plasma membrane typically contains PI, PI(3)P, PI(4)P, PI(5)P, $PI(4,5)P_2$, $PI(3,5)P_2$ and $PI(3,4,5)P_3$[193,194].

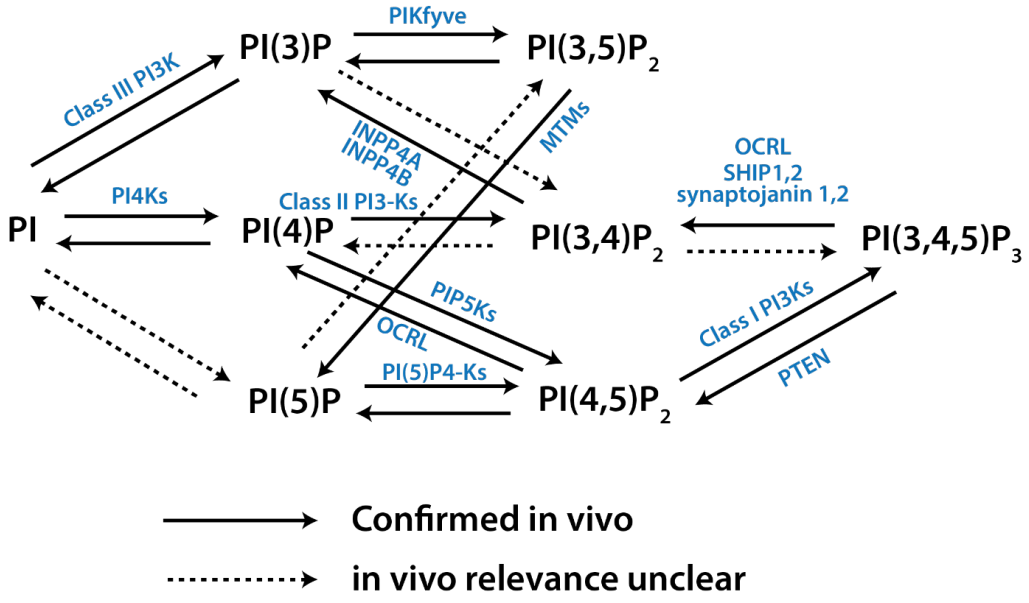

Figure 13. Interconversion of phosphoinositide lipids in the plasma membrane[193,195,196]**.** Phosphatidylinositol (PI) is an abundant component of the plasma membrane. Critically, through the action of lipid phosphatase and kinases, PI can be modified to a myriad of phosphorylation states conferring membrane identity and crucially for RhoGTPase signalling, interaction with specific regulators of the catalytic cycle. Many of these lipid regulators themselves are influenced by the activity state of the RhoGTPases, providing a powerful mechanism of feedback.

Similar to RhoGTPases themselves, several PIP species show polarised distribution[197] and are closely linked to a large number of cytoskeletal and signalling regulators[198]. Local conversion of PIP lipids has been shown to be critical in the formation of cytoskeletal structures such as lamellipodia or filopodia and processes such as endocytosis and re-polarisation to change cell direction[85,194,195].

The number of peripheral membrane proteins that interact with distinct PIP species is rather large. For example, close to 400 proteins can be pulled down from mammalian cell extracts using $PI(3,4,5)P_2$ and $PI(4,5)P_2$ coated beads[199]. Interestingly, many of these PIP interactors are regulators of the GTPase catalytic cycle, such as specific Dbl- and DOCK-family GEFs. In addition, there is coupling between the phosphatases and kinases responsible for this PIP interconversion and the RhoGTPases. This link appears to be bi-directional, as some RhoGTPases such as Rac have been shown to directly stimulate some PI3K isoforms[200–202] which are responsible for the production of $PI(3,4,5)P_3$ from $PI(4,5)P_2$ (Figure 13), thereby providing potential positive feedback via subsequent GEF recruitment to the generated phosphoinositides. This positive feedback loop between Rac1 and $PI(3,4,5)P_3$ is best established in the process of neutrophil migration and relies on the $PI(3,4,5)P_3$ responsive Rac1 GEFs such as P-Rex1[203]. These examples point toward a strong interplay between the GTPase activity cycle and the lipid composition of the membrane.

Besides molecular composition, mechanical properties of the plasma membrane such as tension and curvature have also been shown to influence RhoGTPase signalling and cell polarity in general. Specifically, the role of membrane tension in RhoGTPase signal has been an area of intense research recently. In neutrophil migration, membrane tension has been identified as the long range inhibitor for leading edge formation[204]. Experiments showed that increasing tension is sufficient for long-range inhibition of both branched actin assembly and Rac1 activation. While the underlying mechanism is still a matter of debate, this shows that membrane tension is both a consequence of, as well as an inhibitory input to, leading edge signalling and membrane protrusion. However, whether membrane tension is indeed a global property that rapidly equilibrates across the entire plasma membrane as required for such a long-range mechanism is presently unclear. The classical fluid mosaic model posits that phospholipids would be sufficiently mobile to respond to and rapidly dissipate any gradients in membrane tension[205,206]. Recent experiments, however, have shown that such rapid propagation of tension does not occur in the plasma membrane of eukaryotic cells and that tension can indeed be maintained locally[207]. Reasoning given for this is that by the inclusion of transmembrane proteins linking the PM to the actin cortex prevents this tension by resisting membrane flow.

It can be seen that the membrane is a dynamic environment. The interconversion of phosphoinositide species, changes in shape, distribution of tension all of which

feedback onto the proteins which are interacting on the surface. Understanding, on a fundamental level, what the plasma membrane contributes to RhoGTPase polarity establishment is an area of great interest. Developing a deep knowledge about how this critical regulator in polarity is coupled to the Rho-type GTPase network, particularly the role the plasma membrane plays in RhoGTPase recruitment is a subject in this thesis.

Plasma membrane targeting of Rho GTPases

Despite extensive research over several decades, the mechanism by which Rho-type GTPases target the plasma membrane is presently unclear. One of most long-standing questions is how RhoGTPases can shed their solubilisation factor RhoGDI given the tight interaction between them. Notably, the previously measured affinities for this interaction vary substantially, from low picomolar[84] to micromolar[36,70,84,208]. Part of this variance may be due to technical differences such as the use of chemical labels or the identity of the prenyl moiety on the Rho-type GTPase, all of which can influence interaction strength. The most technically sound in vitro experiments, however, show a sub-nanomolar dissociation constant. How such a tight complex allows for the formation of sufficiently large pools of active GTPases within the PM is not entirely clear. If the dissociation constant for RhoGDI is indeed sub-nanomolar, it would be much lower than for lipid bilayers[209]. This affinity can vary depending on lipid composition, however is in the order of 0.5 μM for the most favourable cases reported in literature[210]. Despite this presumed disparity in affinity, the equilibrium partitioning between membrane and GDI binding by RhoGTPases at steady state might shift according to their relative abundance. RhoGDI levels appear to be near stoichiometric to the total concentration of Rho-type GTPases[54] in the cytosol of animal cells. Based on the localisation of the majority of RhoGTPases to the cytosol, it might be expected that the balance favours GDI binding. The concentration of Rho-type GTPases likely varies but has been estimated between 50 and 120 ng/10^6 cells (of cell lines investigated, MDCK, COS1 and ECV) with RhoGDI being estimated between 150 – 280 ng/10^6 cells[54]. Assuming a total cell volume of around 1750 fL[211], of which 50% may be occupied by the endomembrane system[159] this would give a cytoplasmic concentration of ≈ 10μM RhoGDI and ≈ 9μM total RhoGTPases. However, one major uncertain quantity is the effective concertation of membrane lipids, not only as part of the plasma membrane, but also the extensive endomembrane system inside

eukaryotic cells. The plasma membrane surface area of MDCK cells has been estimated by imaging to be around 4000 μm^2, obtained from approximations relying on the spreading area of adherent cells[212]. With an average area per lipid of 0.553 nm^2 of the inner plasma membrane leaflet[213] and using an average molecular weight for the predominant PM lipids (PC, PS, PE and cholesterol)[213] one can estimate concentration of around 100 μM of total plasma membrane lipids. For a simple competition model, these concentrations and affinities, result in an equilibrium partitioning that approximates observations in cells (95% cytosolic GTPase:GDI complexes and 5% membrane associated GTPases). Notably, the local effective concentration of the inner leaflet of the plasma membrane might rise in areas with low surface to volume ratios such as lamellipodia or filopodia. One of the key confounding issues of this simple model is the high abundance of endomembranes that might exceed the plasma membrane surface area by two orders of magnitude[214].

Whichever assumptions are made about the equilibrium partitioning between the GDI- and the membrane-associated pool, the central issue appears to be a kinetic one. The spontaneous dissociation of RhoGTPase:RhoGDI complexes is presumably much slower than the rapid changes in RhoGTPase activity that can be observed in live cells[36]. Given this high kinetic stability of RhoGTPase:RhoGDI complexes, perhaps there is an as-yet uncharacterised factor which facilitates increased Rho-type GTPase dissociation and membrane recruitment. Indeed, active displacement of solubilisation factors, so called GDI dissociation factors (GDFs), has been demonstrated for other small GTPases of the Ras superfamily. Ras itself, for instance, sheds its solubilisation factor PDEδ through active Arl2GTPases that locally act as GDFs at perinuclear endomembranes[34]. Notably, PDEδ strongly differs from RhoGDI in contacting exclusively the prenyl group[215] and no other regions of its client GTPase. The specific allosteric release mechanism established for PDEδ would likely not function in the case of RhoGDI for this and other structural reasons. On the other hand, an unrelated GDF-based mechanism has been suggested also for the Rab-type GTPases.[216]. Pra1 and the yeast homolog Yip3 appear to promote the release of RabGDI from some, but not all RabGTPase clients[217,218], but the biochemical mechanism is not well defined. DrrA (SidM) was also suggested to act as a GDF[219], however later biochemical work has shown that RabGDI is displaced via the GEF activity of DrrA/SidM[220].

In the case of the Rho-type GTPases, no bona-fide GDF has been identified thus far, there are however potential candidates. The aforementioned ezrin and additional

proteins such as radixin as well as p75 neutrophin have been reported to promote the displacement of RhoGDI from its client RhoGTPase[221–223]. This mechanism was suggested to function by interaction between the N terminus of ezrin (and other ERM proteins) and RhoGDI, resulting in competition of binding to RhoGTPases and promoting activation levels of RhoGTPases by acting as a GDI sink[222,224]. The data is similar for p75 neutrophin, despite suggesting an interaction between p75 neutrophin and RhoGDI whilst in complex with RhoA, this interaction may require additional inputs from RhoGEFs to promote activation and separation of RhoA. None of the above candidates have been shown to kinetically promote the separation of the RhoGDI from its RhoGTPase client, hence the identity of a RhoGDF remains elusive.

In the absence of strong candidates for widely conserved GDFs, other, more indirect means of RhoGDI release were proposed. As mentioned above, phosphorylation of either GDI or RhoGTPases might lower affinity and kinetically promote GDI release[67,225–227]. An alternative hypothesis is that the membrane itself might act as a GDF. It has been suggested that the stability of the RhoGDI:RhoGTPase complexes could be modulated by the interaction with lipids including phosphoinositides[228], with some data showing activation of Rho-type GTPases only in presence of lipids[229]. However, most of these experiments do not discriminate between simple competition between GDI and membranes at equilibrium and other potentially more direct effects on the kinetics of GDI release. Given the bipartite interaction of RhoGDI with the switch regions on one hand and the prenyl moiety on the other (as discussed earlier), a “handover” mechanism could be envisioned with the prenyl tail exchanging between GDI and membranes at an accelerated rate compared to the complete dissociation of GDI in a single step.

Finally, GEFs have long been debated to act as GDFs, predominantly because of two reasons: first, they can discriminate between distinct RhoGTPases and are themselves controlled by signalling activity[97,230], hence they could provide spatio-temporal control to GDI release. Second, inducible recruitment of catalytically active GEFs to the plasma membrane of living cells via optogenetic or chemically-induced dimerisation is sufficient to elicit signalling activity for many RhoGTPases[7,231]. However, whether GEFs indeed facilitate RhoGTPase membrane recruitment by promoting RhoGDI release or whether they simply activate a pool of inactive RhoGTPases already present at the membrane is not clear. Importantly, structural considerations argue against a direct involvement of GEFs in RhoGDI displacement.

The N-terminal regulatory arm of RhoGDI and the catalytic domains of both Dbl- and DOCK-type RhoGEFs extensively overlap at the RhoGTPase switch regions. This strongly suggests that these interactions are mutually exclusive and that GEF-mediated activation can only take place after membrane binding of RhoGTPases[13,232,233]. However, given that the two main GDI interaction sites of RhoGTPases are somewhat distant and partially separable, one could conceive a hand-over mechanism, related to the one described above: Dynamic undocking of the N-terminal arm of GDI might occasionally liberate the GEF binding site and opportunistic nucleotide exchange could destabilise the GDI:RhoGTPase complex. Such a displacement mechanism however is highly speculative, as the structural dynamics of the GDI:GTPase complex are not known and a trimeric RhoGTPase:GDI:GEF complex has not been observed.

In conclusion, how Rho-type GTPases target the plasma membrane remains poorly understood. Fewer than a handful of putative factors have been implicated in the displacement of RhoGDI in vivo, however direct biochemical evidence supporting this is lacking. Understanding the biochemical mechanisms of RhoGTPase targeting to lipid membranes and the timing of the release of RhoGDI are the major objectives of this thesis.

Objectives

This thesis aims, through a bottom-up reconstructive approach, to understand the sequence of events leading to the recruitment of RhoGTPases from their GDI complex to the membrane. As outlined above, there are numerous potential mechanisms by which this process can be regulated. Using biochemical assays, advanced dual-colour single molecule microscopy techniques and reconstitutions of increasing complexity to uncouple the factors involved in RhoGTPase recruitment, this thesis aims to capture discrete events of RhoGTPase membrane association and answer several interesting questions.

First, how are RhoGTPases recruited to membranes? GEFs, specific membrane lipids and displacement factors have all been suggested to be involved but the exact mechanism remains elusive[234]. Specifically, it is unclear whether the dissociation of the RhoGTPases from GDI is occurring independently from membrane recruitment or is discrete step within the membrane loading process. Furthermore, what is the influence of activity state? Are membrane recruitment and nucleotide exchange coupled[235] or uncoupled[68] events, is GEF-mediated activation required to localise RhoGTPase to the membrane or is GTPase activation an uncoupled, subsequent process?

There is much complexity to be understood in the recruitment of RhoGTPases to the plasma membrane and the development of functional polarisation. Through reconstitution of RhoGTPase loading, this thesis aims to understand the nature of the coupling between the spatial cycle, mediated by RhoGDI, and the catalytic cycle, regulated by RhoGEF. Additionally, how does a cell-like environment mimicked by the addition of cell lysate alter recruitment dynamics? Can we provide evidence for the exitance of a GDF-like activity for RhoGTPase?

Results

Isolation of stoichiometric, dual-labelled RhoGTPase:RhoGDI complexes

The first objective was to obtain a pure, homodimeric complex of geranylgeranylated RhoGTPases and RhoGDI with orthogonal fluorescent labels on either protein. We initially focussed on bacterially expressed Cdc42, which we enzymatically geranylgeranylated in vitro by recombinant GGTaseI (see methods). We opted for this strategy, as we previously discovered that overexpression and purification of RhoGTPases from insect cells results in a heterogenous prenylation state[236] with an appreciable fraction of unprenylated and mis-farnesylated protein (I. Visco unpublished results). This in vitro approach, despite lacking cleavage of the three terminal amino acids and methyl esterification[237] as in vivo, produces a protein with functional geranylgeranyl-motif, confirmed by membrane recruitment, and GDI dissociation assays (Dr. Ilaria Visco[38]). To isolate geranylgeranylated from residual unprenylated Cdc42 after in vitro prenylation, we employed size-exclusion chromatography in the presence of CHAPS micelles, which allows for the removal of non-prenylated as well as GGTase1 (Figure 14A). The prenylated species showed a shorter retention time due to the increase in molecular weight by the interaction with detergent micelles via the prenyl tail (Figure 14A). We confirmed by mass spectrometry that Cdc42 prepared in this manner is homogenously geranylgeranylated (I. Visco unpublished results).

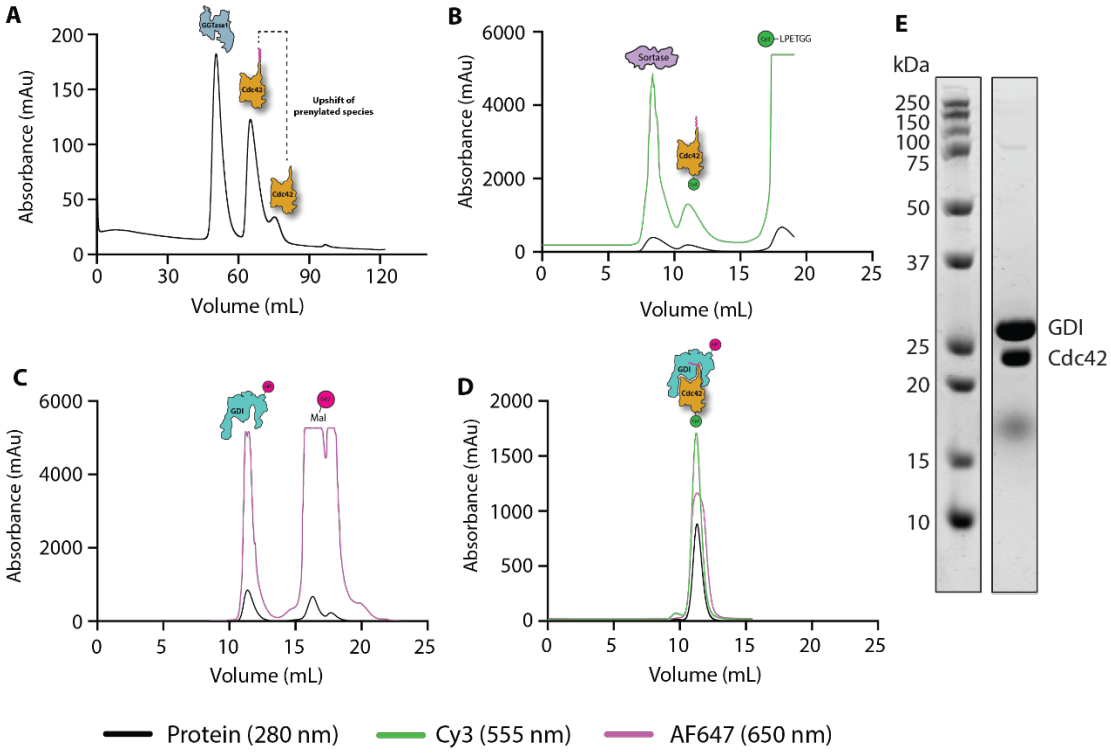

Figure 14. Biochemistry of in vitro produced Cdc42:RhoGDI complex. (A) 280 nm absorbance profile during gel filtration of Cdc42. In vitro prenylated Cdc42 was separated from the unprenylated fraction via size exclusion chromatography. By using detergent (prenylation buffer, see methods) prenylated Cdc42 showed an upshift relative to the unprenylated species and was a distinct peak from the GGTase1 allowing for selection of the desired fraction. **(B)** Gel filtration profiles of labelled Cdc42 via 280 nm (protein) and 555 nm (cy3). Following sortase mediated peptide ligation of a Cy-3 peptide to Cdc42, the labelled, prenylated Cdc42 was separated from the free peptide and sortase via size exclusion chromatography. The Cdc42 peak was identified by the coincidence of 280 and 555 nm absorbance signal. **(C)** Gel filtration profile of RhoGDI. To separate RhoGDI from free dye, size exclusion chromatography was used. Coincidence of 280 (protein) and 650 (AF647) nm allowed for selection of the labelled GDI peak. **(D)** Gel filtration profile of Cdc42:RhoGDI complex. Stochiometric amounts of Cdc42 and RhoGDI were mixed and passed over a size exclusion chromatography column. The absorbance at 280 (protein) 555 (Cy3) and 650 (AF647) nm overlapping in a single peak confirmed the formation of the complex. **(E)** SDS-PAGE gel of Cdc42:GDI complex. Complex stoichiometry was confirmed by SDS-PAGE gel. Cdc42 and GDI labelled on the right of gel. Labelling ratio was determined for this complex of 74% Cdc42 labelling and 92% RhoGDI labelling.

Once isolation of geranylgeranylated Cdc42 was achieved, to allow for visualisation in microscopy experiments, Cdc42 as well as its interaction partner RhoGDI, must be labelled. Previous studies mostly relied on N-terminal tagging of GTPases with fluorescent proteins such as GFP. N-terminal Fluorescent protein-tagging however, impairs the localisation and function of many RhoGTPases[38], indicating that RhoGDI binding might be altered. To circumvent this issue, a Cy3-labelled short peptide was conjugated to GTPase the N-terminus via sortase mediated peptide ligation (sortagging)[238] (see methods) (Figure 15), followed by gel filtration in the presence of CHAPS. By following absorbance at multiple wavelengths, it was possible to identify proteins and peptides (at 280 nm) and fluorescent dyes at their appropriate

wavelengths (555 nm in the case of Cy3). Through the difference in molecular weight of the components, it was possible to isolate the Cy3-labelled, geranylgeranylated Cdc42 (Figure 14B).

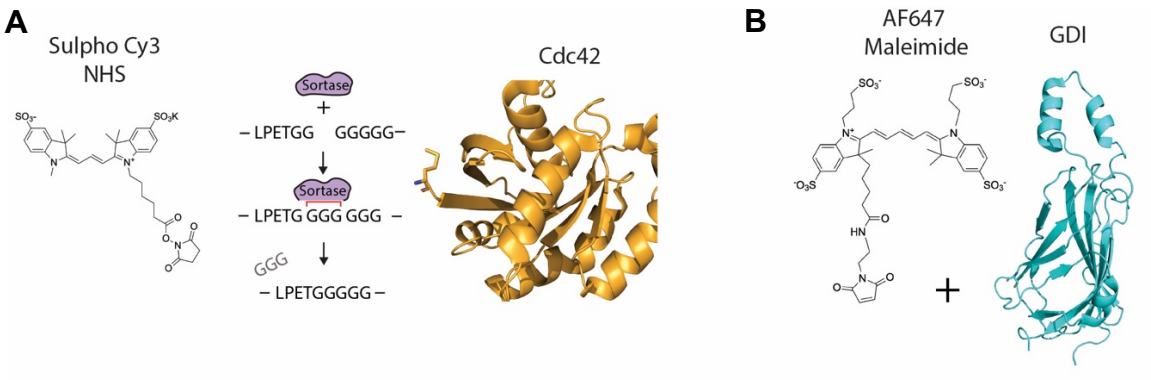

Figure 15. Protein labelling biochemistry. **(A)** Sortase mediated peptide ligation to the N-terminus of Cdc42. The NHS ester of SulphoCy3 was conjugated to the primary amine of the LPETGG peptide. This peptide sequence along with the pentaglycine motif found at the N-terminus of the Cdc42 construct used here form the recognition sequence of sortase. Sortase conjugates this peptide to the N-terminus of Cdc42, with a GGG-cleavage product, resulting in the labelled Cdc42. **(B)** Maleimide chemistry for RhoGDI labelling. The RhoGDI construct contains a single reactive cysteine (Cys78) in the globular domain amenable to labelling. AF647-maleimide was used to label this reactive cysteine producing the labelled GDI component for complex formation.

RhoGDI was fluorescently labelled with AF647-maleimide on its single exposed cysteine (Cys78), followed by gel filtration to remove excess free dye (Figure 14C) (see methods). This residue lies on the surface of the globular IG domain of RhoGDI and faces away from the GTPase client. We have previously shown that labelling at this position does not alter RhoGDI function (I. Visco unpublished results). This provided the labelled components for recruitment reconstitutions.

To form the Cdc42:RhoGDI complex, both proteins were combined at a 1:1 stoichiometry and gel filtered in the absence of detergents. In the absence of detergent any Cdc42 which was not bound to GDI was lost through non-specific interaction with the column resin. Tracking of three wavelengths 280 (protein), 555 (Cy3) and 650 (AF647) nm allowed for the identification of the heterodimeric complex (Figure 14D). SDS PAGE of the combined peak fractions confirmed stoichiometric amounts of Cdc42 and GDI (Figure 14E). Labelling ratio was determined for this complex of 74% Cdc42 labelling and 92% RhoGDI labelling (see methods).

Cdc42 and GDI form an extremely high affinity and long lived complex

RhoGDI is known to bind very tightly to the inactive, GDP-bound form of Rho-type GTPases[81,84,239,240]. The vast majority of soluble RhoGTPases in the cytoplasm are

therefore bound to RhoGDI[32,36,40]. To probe the kinetic stability of our dual-labelled, heterodimeric complex in vitro, we followed its dissociation by measuring the loss in sensitised emission, (exploiting the FRET pair of the labels), over time after the addition of a large excess of unlabelled RhoGDI (Figure 16). The resulting time curve could be well fit by a double exponential decay function. Dissociation kinetics yielded a fast rate of 0.003 s^{-1} yielding a $t_{1/2}$ of 4.1 min, this rate made up 32% of the data. The slow rate was 0.0003 s^{-1} a $t_{1/2}$ of 42 min (Figure 16).

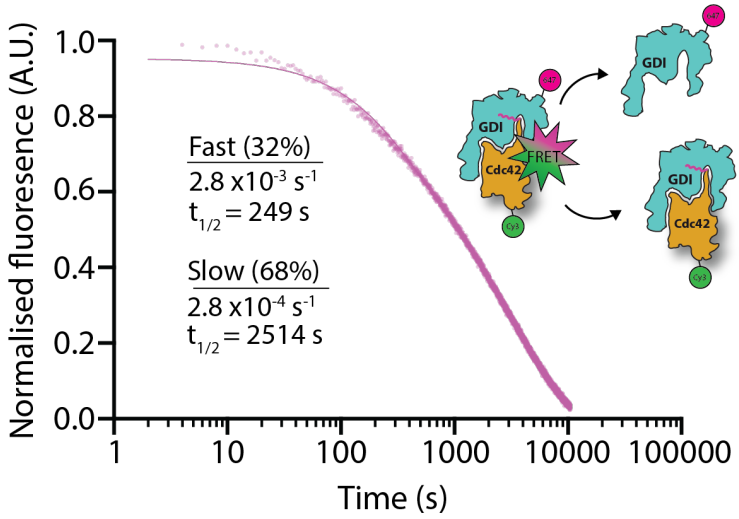

Figure 16. Rho GDI dissociation kinetics. 80 nM of Cy3-Cdc42 complexed in situ with 120 nM of AF647-RhoGDI with a dark-chase of 5000 nM unlabelled RhoGDI. Ratiometric FRET between Cy3-Cdc42 and AF647-GDI measured at intervals of 2 s for 20000 s. A two phase decay fit generates a fast rate of dissociation of 2.8 $x10^{-3}$ s^{-1}, making 32% of the population and a slow dissociation rate of 2.8 $x10^{-4}$ s^{-1} making up the remainder (68%).

This confirmed that our isolated heterodimeric complex was extraordinarily stable kinetically, with dissociation rates comparable to those measured in literature[84].

We next asked how RhoGDI complex formation affects Cdc42 activation. Because the interaction sites between the RhoGEFs and Cdc42 are occluded by the N-terminal arm of Rho GDI[13,114], we hypothesised that our isolated heterodimeric complex should be impervious to activation by RhoGEFs. To test this, we carried out nucleotide exchange assays in the presence of a minimal catalytically active fragment of the Cdc42 GEF Intersectin1 (ITSN, see methods) and free mant-GTP supplied in solution. As expected, free Cdc42 (in the absence of RhoGDI) rapidly exchanged its nucleotide in the presence of the GEF, as indicated by the increase in fluorescence (Figure 17 orange line). Addition of a 1.5X molar excess of unlabelled RhoGDI potentially inhibited nucleotide exchange, showing only a marginal increase in fluorescence

(Figure 17 cyan line). Similarly, our isolated, dual-labelled RhoGDI:Cdc42 complex also showed minimal nucleotide exchange over time (Figure 17 Purple).

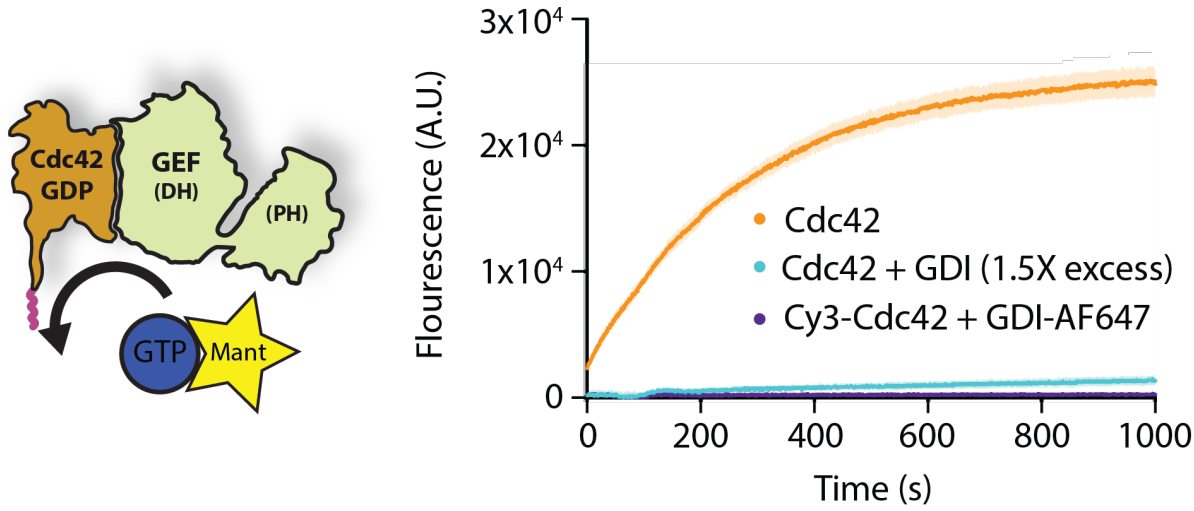

Figure 17. Nucleotide exchange assays utilising ITSN. 120 nM of Cdc42 alone, or in complex with RhoGDI (either stoichiometric complex or 1.5X molar excess GDI) was added along with a final concentration of 1.167 μM Mant GTP. The nucleotide exchange was stimulated by the addition of 1.6 nM of ITSN-DH-PH and mant fluorescence measured (365 nm Ex, 440 nm Em) every 5 s for 5000 s. Error (shaded) SD.

These data support the conclusion that this complex is extraordinarily stable and shielded from activation by GEF (ITSN) in solution. We next studied the mechanistic consequences of RhoGDI binding on RhoGTPase membrane recruitment and GEF-mediated activation in more complex reconstitution assays.

Reconstitution of membrane associated RhoGTPase activity in the presence of cell lysates

Several groups have previously reconstituted Cdc42- and Rac1-induced actin assembly from lipid bilayers of defined composition (including phosphatidylinositols) using cell extracts[164,241]. This suggests that all molecular requirements for RhoGTPase activation other than membranes, including any potentially essential GDF activity, should be contained in cell lysates. Based on established protocols, we prepared concentrated pig-brain lysate[164,242] (see methods) and used silica beads coated with lipid bilayers of varying composition to test for Cdc42 recruitment and activation.

Specifically, as published in litrature[164] we prepared silica beads coated with membranes consisting of phosphatidylcholine (PC), phosphatidylinositol (PI) and phosphatidylinositol-4,5-bisphosphate ($PI(4,5)P_2$) (48:48:4 molar ratio) (Figure 18A). This strongly negatively charged membrane composition, which here we name

minimal mix (MM) has been previously been shown to promote the recruitment and activation of Rac1 and Cdc42 via PI(4,5)P_2-responsive GEFs. In addition to lipid-coated beads, we added profilin-actin and a fluorescently labelled actin filament binding probe (AlexaFluor647-UTRN$_{261}$, see methods) and our in vitro prepared Cdc42 (in the absence of GDI) to the pig brain lysate. The presence of concentrated lysate did not disrupt the continuity of the membrane as indicated by a fluorescent membrane marker (RhodE-PE) (Figure. 18B). More importantly, assembly of halos and polarised tails of polymerised actin surrounding the lipid-coated beads was readily observed (Figure. 18B), indicating membrane recruitment and activation of RhoGTPases and interaction with regulators such as NPFs from cell extract stimulating actin polymerisation.

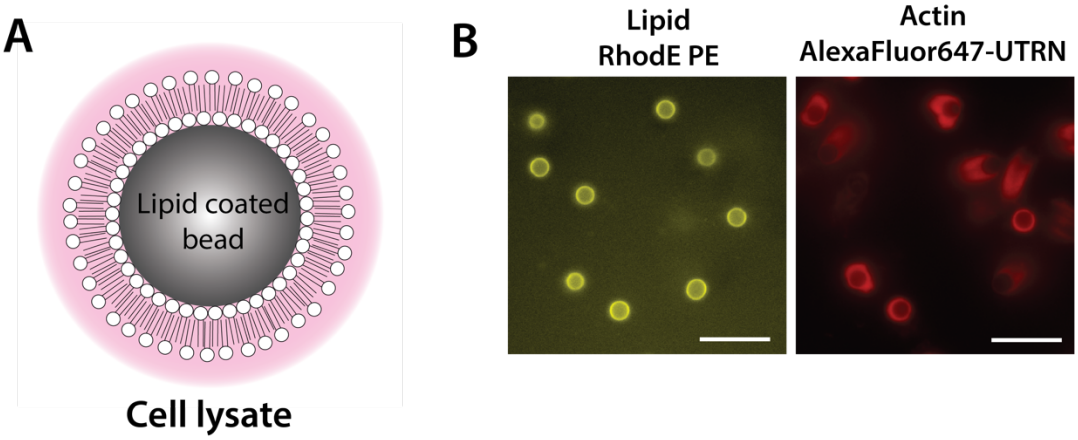

Figure 18. Functional lysate produces actin network. (A) Cartoon of lipid coated bead in cell lysate. MM lipid bilayer 3 μm beads were prepared to act as a surface for actin network formation. **(B)** Widefield image of beads showing lipid membrane (left) and an actin network (right). Cell lysate of ≈ 40 mg/mL total protein content (estimated by Bradford) was activated with 1X energy mix (30 mM phosphocreatine, 4 mM ATP, 4 mM $MgCl_2$, pH 7.4) and 1X salt mix (120 mM KCl, 10 mM EGTA, 40 mM 3-phosphoglycerate) prior to use in experiments. To this 0.1 μM Alexa647-UTRN$_{261}$, 7 μM profilin actin and 0.5 μM Cy3-Cdc42 was added. Beads were incubated 2 min and imaged. Scale bar 10 μm.

Next, we probed the recruitment of Cdc42 from exogenously supplied, labelled Cdc42:RhoGDI complexes (Figure 19). Membrane binding of Cdc42 could indeed be robustly observed under these conditions (Figure 19A). However, the level of membrane-associated Cdc42 at steady state was surprisingly similar in the presence and absence of cell lysates (Figure 19B), suggesting that membrane recruitment was not strongly affected by any components found in the cell lysate.

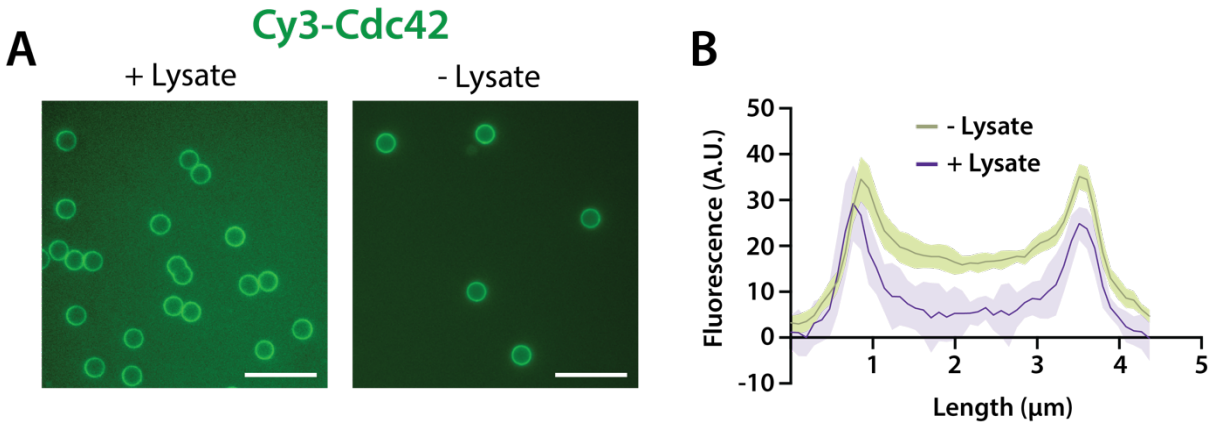

Figure 19. Cdc42 recruitment to lipid coated beads. (A) Widefield microscopy image of lipid coated beads (MM mix) and recruited Cdc42 (Cy3). Cell lysate (left) of ≈ 40 mg/mL total protein content (estimated by Bradford) mixed with 1X energy mix, (30 mM phosphocreatine, 4 mM ATP, 4 mM $MgCl_2$, pH 7.4), 1X salt mix (120 mM KCl, 10 mM EGTA, 40 mM 3-phosphoglycerate), 0.1 μM Alexa647-$UTRN_{261}$, and 0.5 μM Cy3-Cdc42:GDI complex were added to beads supporting a MM composition lipid bilayer. In the absence of lysate, extraction buffer (20 mM HEPES pH 7.4, 100 mM KCl, 1 mM EGTA, 0.1 mM EDTA, 2 mM MgCl2 2.5 mM DTT, 0.5 mM ATP) was used instead. Beads were incubated 2 min and imaged. Scale bar 10 μm. **(B)** An intensity line scan across the bead illustrating Cy3 (Cdc42) fluorescence intensity in the presence and absence of cell lysate. Error (shaded) SD.

This left several open questions, due to the use of dark (unlabelled) RhoGDI from these results, it was unclear if Cdc42 is arriving alone, or in complex with the RhoGDI, only that there is a Cdc42 signal at the surface of the bead. Additionally, in this end point assay, we could not determine whether the loading rate of the Cdc42 is altered under differing experimental conditions.

We concluded that the presence of a functional lysate was not required for the recruitment of Cdc42 to the surface of the lipid coated bead. Using more advanced microscopy techniques, specifically, single molecule TIRF in dual colour, we aimed to capture the moment of Cdc42 arriving at the membrane. This would allow an understanding of the nature of the Cdc42 recruitment, including the kinetics of binding and whether the GTPase arrives in complex with RhoGDI.

Reconstitution of fluid supported membranes

Localisation of Intersectin to supported lipid bilayers

Induced recruitment of RhoGEFs to the plasma membrane has been shown to activate RhoGTPases in vivo[231]. We therefore reconstituted this reaction geometry in a simplified in vitro system to probe whether RhoGEF localisation to the plasma membrane is necessary and sufficient to recruit Rho-type GTPases. To minimise potential confounding effects of soluble GEFs, we immobilised a His-tagged, minimal

catalytically active Cdc42 GEF (Alexa488-ITSN(DHPH)-His_{10}) via Ni-NTA lipids to supported lipid bilayers (SLBs)[243] (Figure 20). Similar constructs have been employed for Cdc42 activation in live cells. In addition, we previously confirmed that this particular construct potently activates geranylgeranylated Cdc42 when recruited to membranes in vitro (Dr. Ilaria Visco, unpublished data).

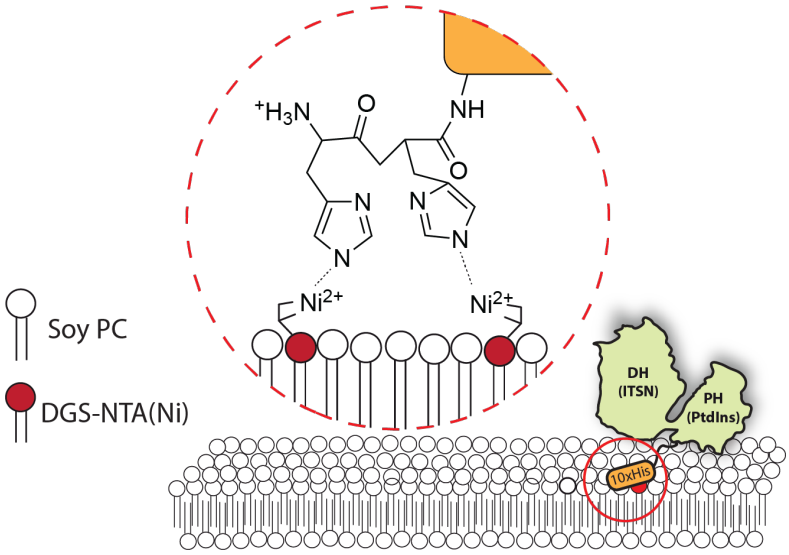

Figure 20. Ni-NTA lipid chemistry. ITSN-DH-PH-His_{10} localisation was achieved using DGS-NTA(Ni) lipids within the bilayer. His-tagged proteins initially bind to a single NTA(Ni) lipid however, due to lateral diffusion of the chelator lipids, additional nickel-histidine interactions may accumulate, forming long-lived multidentate protein-lipid complexes. To this end, ITSN was incubated for > 45 min[243].

ITSN was immobilised on DGS-NTA(Ni)-containing SLB for > 45 min allowing for multi-valent nickel binding, therefore maximising stability of the His-Ni interaction[243]. To confirm increased concentrations of NTA(Ni) lipids, 1% in these experiments. NTA(Ni) lipids allow us to modulate the density of GEF on the membrane therefore by confirming membrane formation was achieved with 1% NTA(Ni) we are therefore confident < 1% will be stable in all SLB preparations. Membrane attachment was specific, because control bilayers lacking the metal-chelating lipid showed little GEF signal by TIRF microscopy. We then monitored the kinetics of GEF dissociation from the membrane under continuous buffer flow (Figure 21). A $t_{1/2}$ of > 100 h was measured, which showed that once associated to the SLB, the ITSN was stably attached over the time course required for the recruitment and activation experiments (typically < 2 minutes).

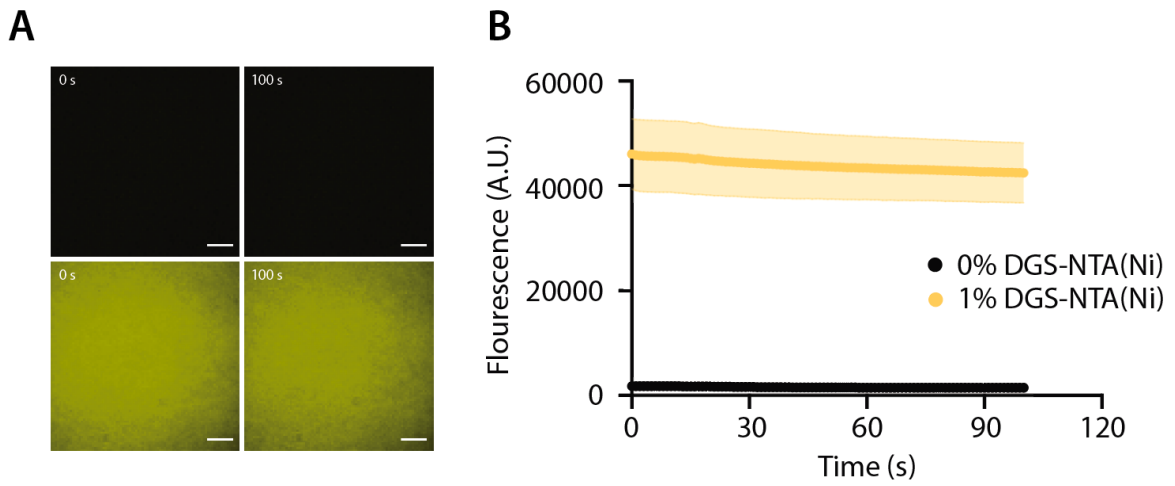

Figure 21. HIS-tagged ITSN stability on supported lipid bilayers. Following incubation of 1 μM 488-ITSN-DHPH-His10 for > 45 min, a flow of GEF buffer (50 mM HEPES pH 7.5, 50 mM NaCl, 2 mM MgCl2, 0.5 mM β-mercaptoethanol) was pumped across the SLB at a rate of 10 μL/min. **(A)** Fluorescence of 488-ITSN-DHPH-His10 at 0s and after 100 s of washing on SLBs containing 0% (upper) and 1% (lower) NTA(Ni) lipids. **(B)** Fluorescence intensity was measured for 20 min. Data was fitted with a mono-exponential decay for the full data set. Data here clipped to the first 100 s to represent stability of ITSN at the SLB during the time course of SM SLB experiments. Scale bar 20 μm. Error (shaded) SD.

Such a stable interaction between ITSN and the membrane also ensured a negligible solution fraction of GEF after protein was flowed into the imaging chamber. We therefore were now in the position to study the recruitment of RhoGTPases to membranes containing with high densities of catalytically active GEF.

Production of bilayers of varying lipid compositions

The use of supported lipid bilayers allowed for the investigation of the effect of a number biochemical parameters on Cdc42 membrane loading. This included the lipid composition of the SLB itself, as varying lipid species could be included at differing ratios, as well as the incorporation of membrane-associated regulators such as RhoGEFs. Specifically, we opted for three distinct lipid compositions (Figure 22, Table 11(methods)). First, a simple bilayer of net neutral charge (99.75% phosphatidylcholine (PC), 0.25% DGS-NTA-Ni) referred to as “PC”. Second, a strongly negatively charged membrane previously used for reconstitution of RhoGTPase signalling from cell extracts as explained above (PC:PI:PI(4,5)P_2:PE-PEG5000:DGS-NTA-Ni in a 47.25:48:4:0.5:0.25 percent molar ratio) which we refer to as minimal mix or “MM”. Finally, a membrane composition resembling the inner leaflet of the plasma membrane (derived from literature[190] and personal communication with Dr. I. Levental) of (PC :PE:PS:PI(4,5)P_2:Chol:PE-PEG5000:DGS-NTA-Ni in a

26.25:26.5:22.5:4:20:0.5:0.25 molar ratio) which was termed PM-mimic or “PM”. The low (0.25%), invariant fraction of DGS-NTA in all three membrane types allowed for the controlled recruitment of regulatory proteins such as GEFs via oligo-histidine tags.

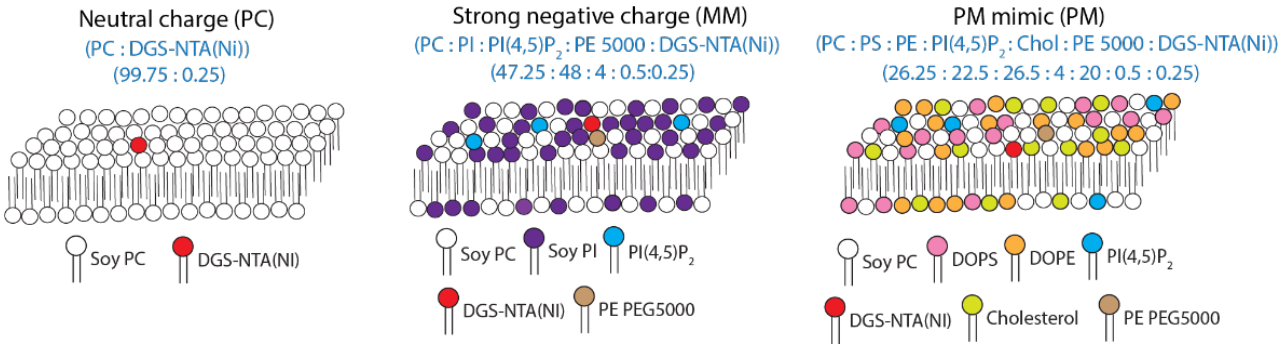

Figure 22. Supported lipid bilayer compositions. Three bilayer compositions were used here, a neutral membrane, termed PC, comprised of 99.75% phosphatidylcholine (PC), 0.25% DGS-NTA-Ni), A strongly negatively charged membrane (MM) comprised of PC:PI:PI(4,5)P_2:PE-PEG5000:DGS-NTA-Ni (47.25:48:4:0.5:0.25 percent molar ratio). A membrane composition resembling the inner leaflet of the plasma membrane termed PM, consisting of PC:PE:PS:PI(4,5)P_2:Chol:PE-PEG5000:DGS-NTA-Ni (26.25:26.5:22.5:4:20:0.5:0.25 molar ratio).

Before reconstitution the recruitment of Cdc42 to artificial membranes, we first checked membrane fluidity and stability for each of the lipid compositions used by fluorescence recovery after photobleaching (FRAP). Absence of membrane fluidity is indicative of a discontinuous bilayer with unfused vesicles, which can arise in the case of complex lipid mixtures such as the ones used in this work. To visualise the lipid component of the membrane, we formed bilayers in the presence of trace amounts of a fluorescent lipid (RhodE-PE, 0.01%). We observed that both simple PC and plasma membrane mimicking membrane compositions displayed a uniform distribution of the fluorescent label, whereas the MM exhibited a non-uniform partitioning between dim and bright areas, indicative of phase separation (Figure 23 MM).

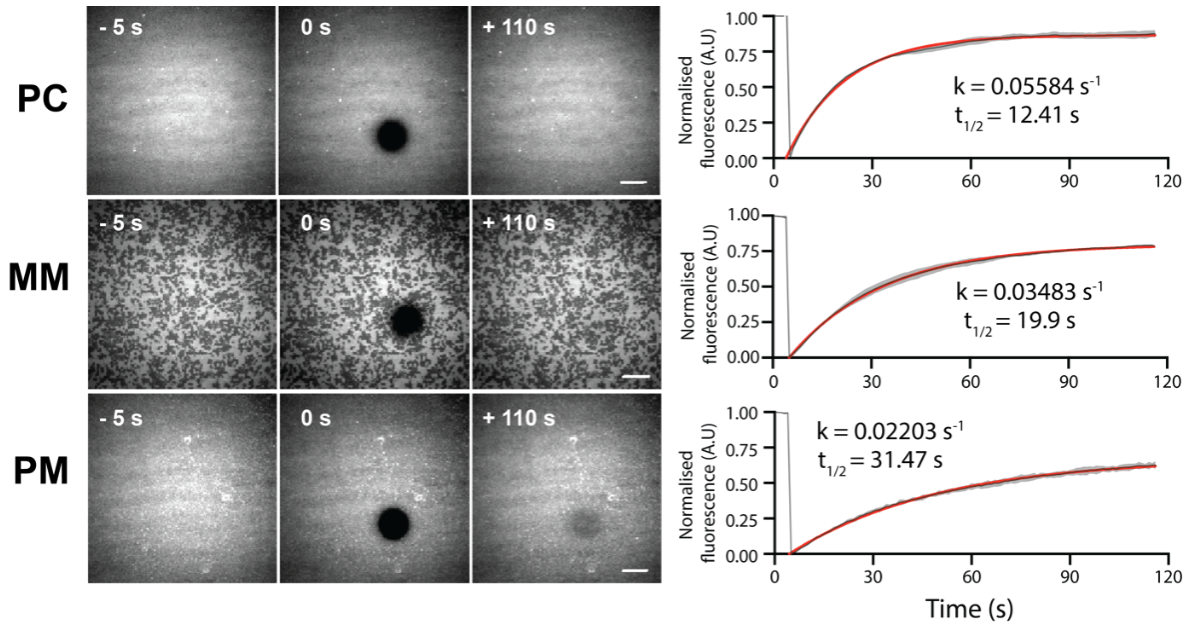

Figure 23. Confirmation of bilayer fluidity via FRAP microscopy. SLBs of all three lipid compositions were imaged for 5 s (1 s intervals) prior to a 3 s bleach phase at 100% laser power. Following bleaching imaging continued at a time interval of 1 s for 2 minutes (scale bar 20 μm). Time traces of the normalised fluorescence intensity FRAP region were taken and a single-phase association was fitted to establish recovery rates. Error SD.

We then bleached a small circular region in the field of view and followed fluorescence recovery over time by TIRF imaging (Figure 23). All three lipid compositions showed recovery after bleaching, albeit with slightly varying half-times, with PC showing the fastest recovery with a $t_{1/2}$ of 12.41 s, MM with a $t_{1/2}$ of 19.9 s and finally PM with a $t_{1/2}$ of 31.47 s. The slow-down in lateral lipid mobility in the two latter cases were likely due to the loss of flexibility in the hydrophobic phase of the bilayer due to poly-unsaturated acyl chains and the presence of cholesterol, respectively. Regardless, these measurements confirm that all bilayers produced are fluid and sufficient for SLB recruitment assays.

Visualisation of Cdc42 membrane recruitment at single molecule resolution

After confirmation of a fluid bilayer across the three lipid compositions, we could focus on the visualisation of Cdc42 recruitment. Because both Cdc42 and RhoGDI were incompletely labelled, we first obtained a reference for the maximal degree of co-localisation that can be expected our under specific imaging conditions. To this aim, we first visualised individual dual-labelled Cdc42:RhoGDI complexes, which were stably bound to PEG-passivated glass surfaces. Briefly, we introduced a biotin handle in the N-terminal peptide tag of Cdc42 (see methods) and recruited the isolated

heterodimeric complex to neutravidin-coated surfaces passivated with biotin-PEG-poly-lysine[159]. We confirmed that surfaces prepared in this manner allowed for the specific and stable immobilisation with little background binding. Surface recruitment was performed from low solution concentrations (100pM) of freshly diluted heterodimeric complexes to minimise premature dissociation prior to surface binding. Individual molecules of surface-bound Cdc42 (green) and RhoGDI (magenta) as diffraction-limited spots could readily observed by simultaneously imaging both 561 and 640nm channels (Figure 24). These spots were stationary due to the lack of a fluid membrane support, allowing for optimisation of spot detection, tracking and colocalisation analysis. Co-localisation of Cdc42 and RhoGDI (magenta) signals was evident for a significant fraction of cases, shown by white spots in the merge panel (Figure 24). To analyse the total colocalisation events the spot coordinates of the Cdc42 and RhoGDI signals at each time point were used to project a map of co-localised spots (colocalised recruitment panel). We determined that 34.9 ±8.49% of Cy3-Cdc42 molecules colocalised with Alexa647-RhoGDI molecules under these conditions. The presence of an appreciable non-colocalised fraction can likely be attributed to incomplete dual labelling, complex dissociation in solution and bleaching. This measurement sets a benchmark for the maximal colocalisation percentage to which recruitment on bilayers can be compared.

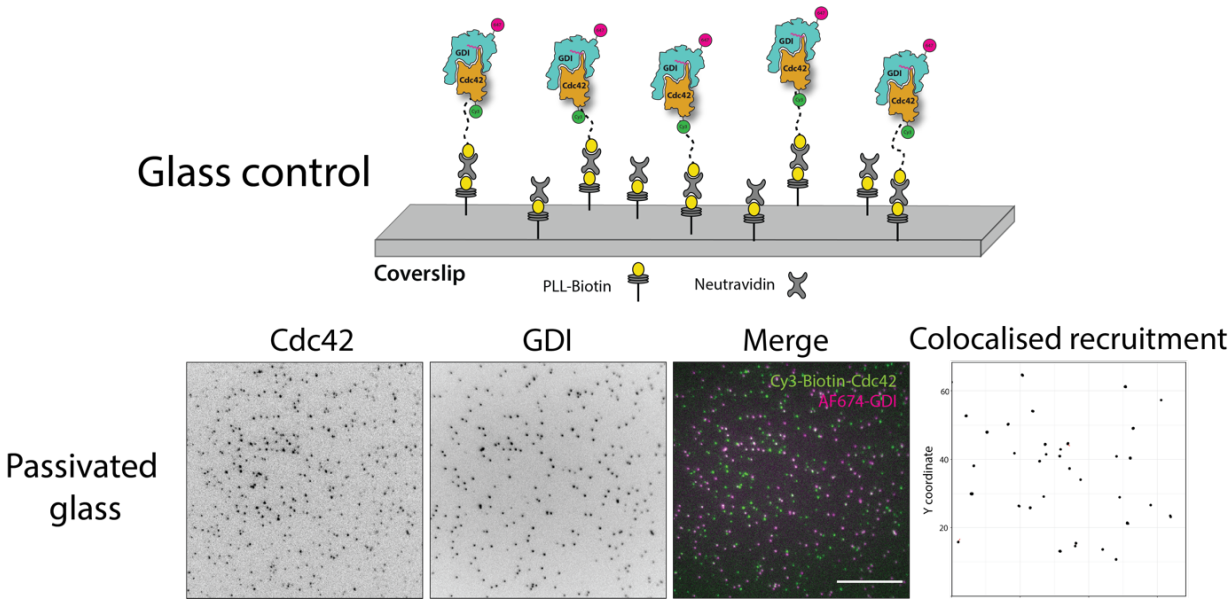

Figure 24. Dual colour single molecule TIRF controls for colocalised recruitment. Cartoon of biotin-neutravidin mediated recruitment of Cdc42:GDI complexes onto a passivated glass surface (upper). Single molecules of Cdc42, RhoGDI and a merge (time projection over 10 frames) (lower). Colocalised recruitment shows the arrival of new Cdc42 spots which were colocalised with a RhoGDI spot within the first 3 frames of landing. Scale bar 20 μm.

The ability to capture association of a Cdc42 or GDI molecule to the membrane and subsequently track these molecules allowed for investigation into several parameters (discussed in subsequent chapters). Not only did it allow for establishing a recruitment rate of Cdc42, but also to differentiate when a Cdc42 molecule arrives alone or in complex with a RhoGDI (Figure 25).

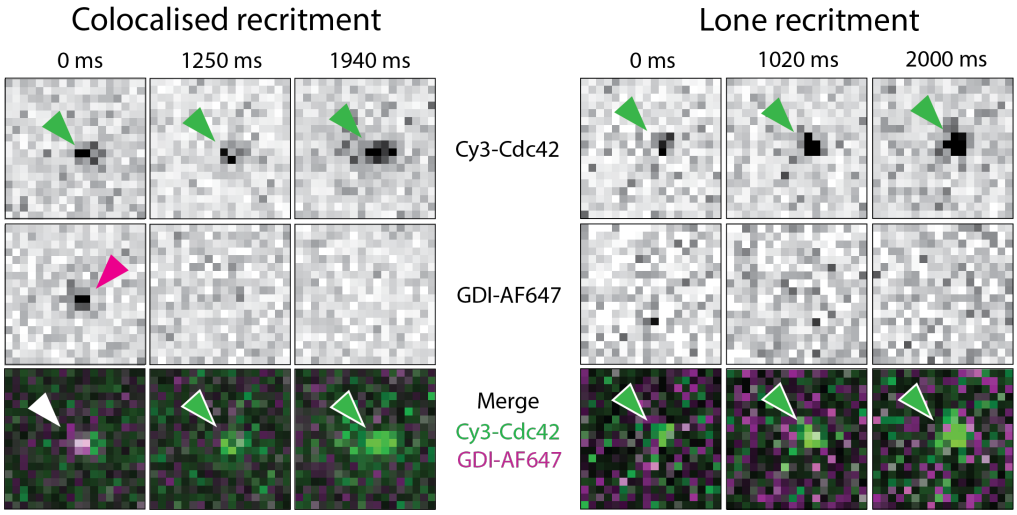

Figure 25. Classification of single molecule recruitment events. Examples of recruitment of Cdc42 spots both colocalised (left) and lone recruitment (right). In the colocalised example, as a Cdc42 spot is recruited (green arrow, 0 ms, upper row) a RhoGDI molecule is also visible at the point of recruitment (purple arrow middle row), which appears as a white spot in the merge channel (white arrow, bottom row). Cdc42 continues to remain colocalised until GDI is lost at 1250 ms (middle row, and bottom row (green arrow)). Cdc42 signal remains until 1940 ms. In the case of lone recruitment, the Cdc42 appears alone (upper and lower rows, green arrow) and remains visible for 2000 ms.

A Cdc42 molecule was considered to have arrived at the membrane with GDI if, within the first 3 frames, there was the appearance of a colocalised signal. The example on the left of Figure 25 shows the moment of recruitment of the colocalised signal (0 ms) the frame at which the GDI signal was lost (1250 ms) and the final frame prior to loss of the Cdc42 signal (1940 ms). Figure 25 (right) shows the appearance of a lone Cdc42 molecule (0s) and its final frame prior to signal loss (2000 ms).

Together, these results show that the Cdc24:RhoGDI complex can be robustly observed at the single molecule level, and specific event dynamics visualised.

We next utilised these recruitment assays on supported lipid bilayers to determine what fraction of the Cdc42 molecules arrive at the membrane in complex with RhoGDI (Figure 26A). As observed with the control, the moment of Cdc42 recruitment could be observed in a single molecule regime. Furthermore, due to the nature of the interaction, via prenyl-tail insertion into the membrane, Cdc42 molecules could now

be observed diffusing on the SLB (indicted by tracks in colocalised recruitment panels) (Figure 26B).

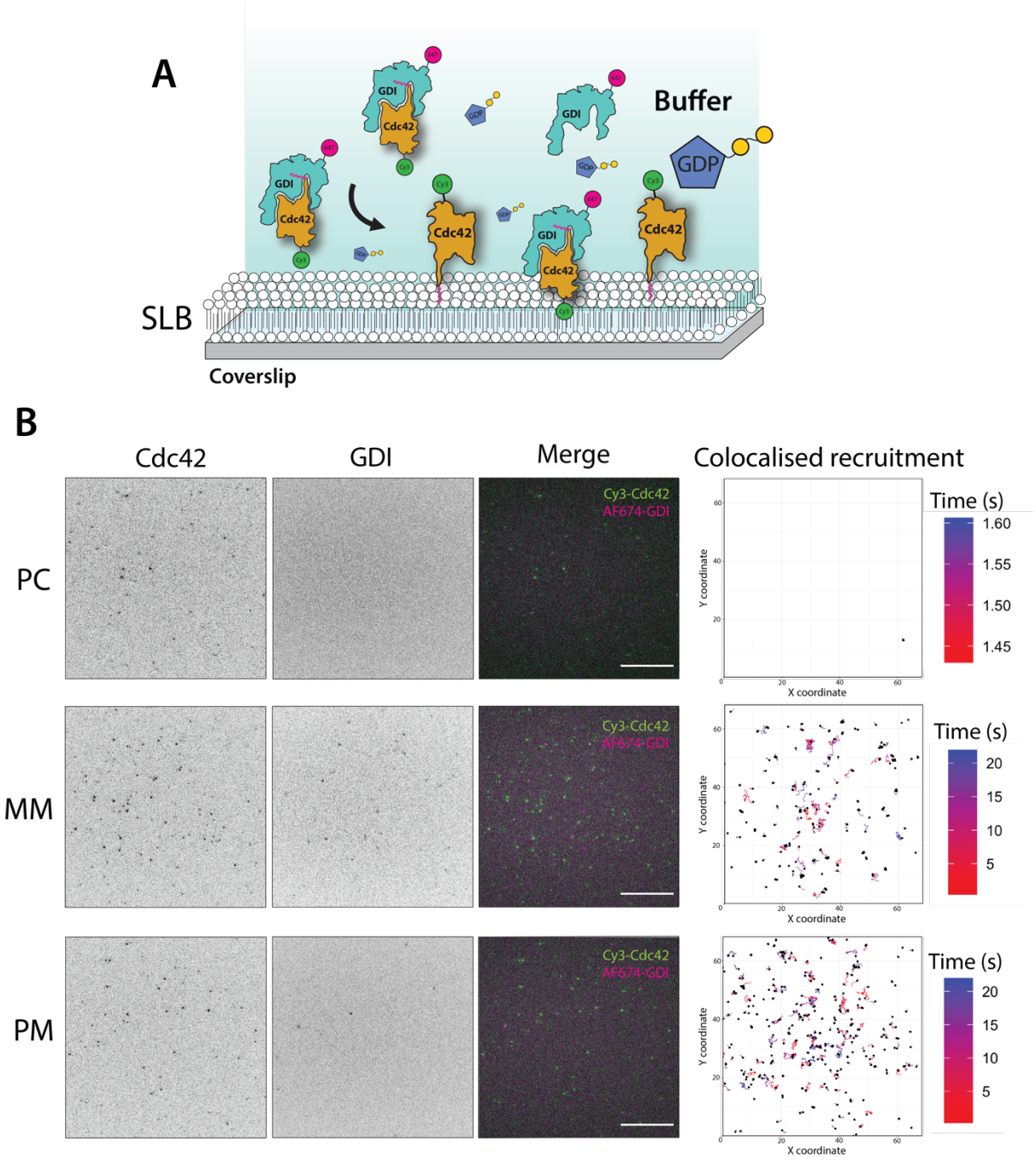

Figure 26. Single molecule recruitment to supported lipid bilayers. **(A)** Cartoon of physiological mediated recruitment of Cdc42:GDI complexes onto a supported lipid bilayers. **(B)** Single molecules of Cdc42 (first column), RhoGDI (second column) and a merge (third column) across three lipid compositions (PC, upper row, MM middle row, PM bottom row). Colocalised recruitment shows the arrival of new Cdc42 spots which were colocalised with a RhoGDI spot within the first 3 frames of landing. Scale bar 20 μm. Time heat projection indicated the time elapsed in the movie for each point within the trajectory of Cdc42 molecule which showed colocalisation on membrane recruitment.

From these images it can be observed that the amount of colocalised recruitment of Cdc42 and GDI seemed to increase with the increasing negative charge of the MM and PM compositions. Furthermore, absolute spot number of Cdc42 increased.
These data show that, as in the control data, we could reliably visualise Cdc42 and GDI molecules arriving at the membrane as a high time resolution. Furthermore, we could track these molecules to visualise colocalisation events while molecules were at the membrane surface. To truly understand recruitment rates however, we utilised data analysis techniques developed in house to quantify parameters such as landing rate and colocalisation, essential to understand RhoGTPase recruitment dynamics.

Reconstitution of Cdc42 recruitment to membranes

Membrane composition but not GEF modulates recruitment of Cdc42

To visualise the process of membrane recruitment of Cdc42 at the level of single molecules, we supplied low (100 pM) concentrations of freshly diluted, dual-labelled RhoGDI:Cdc42 complexes to SLBs. To study the impact of membrane-associated GEF activity, we carried out these experiments in the presence or the absence of SLB-immobilised ITSN(DHPH)-His_{10}, with excess of either GTP or GDP nucleotide in buffer (Figure 27 A and D). Besides GEF presence, we also varied the biochemical properties of the membrane itself by using either PC, MM or PM lipid compositions. We imaged recruitment synchronously in both 561 (Cdc42) and 640 (RhoGDI) nm channels at maximal time resolution (continuous acquisition, 22 ms time interval) to capture the moment of membrane association of individual Cdc42 molecules. This high time resolutions should allow us capture even a very rapid loss of the RhoGDI signal (unbinding up to rates of ≤ 50 s^{-1}) upon membrane association, should the Cdc42 arrive in complex with RhoGDI.
To quantify these observations from the single molecule movies captured, we utilised our advanced single molecule tracking scripts (developed in-house[244], see methods). This powerful tool allowed us to focus solely on authentic recruitment events leading to persistent membrane binding, excluding any spurious, highly transient interactions between Cdc42 and the membrane. This was achieved via an automatic tracking routine (see methods) and excluding of Cdc42 tracks that lasted less than 100 ms (five frames).
To understand the contribution of ITSN presence on the membrane on recruitment kinetics of RhoGTPases, we first quantified the rate of Cdc42 membrane binding at

the single molecule level. Strikingly, ITSN presence only marginally affected the rate of membrane recruitment, irrespective of the specific lipid composition or the presence of either GTP (Figure 27B) or GDP (Figure. 27E) in solution. In a minority of cases, presence of ITSN(DHPH)-His_{10} even slightly (less than two-fold) reduced Cdc42 landing rate (Figure 27B), potentially due to steric effects linked to the high density of GEFs on the membrane. This suggest that Cdc42 encounters the membrane independently of binding to GEFs and that nucleotide exchange occurs after and not upon membrane recruitment. The latter statement is in line with the near identical landing rates observed in experiments carried out in either GDP or GTP.

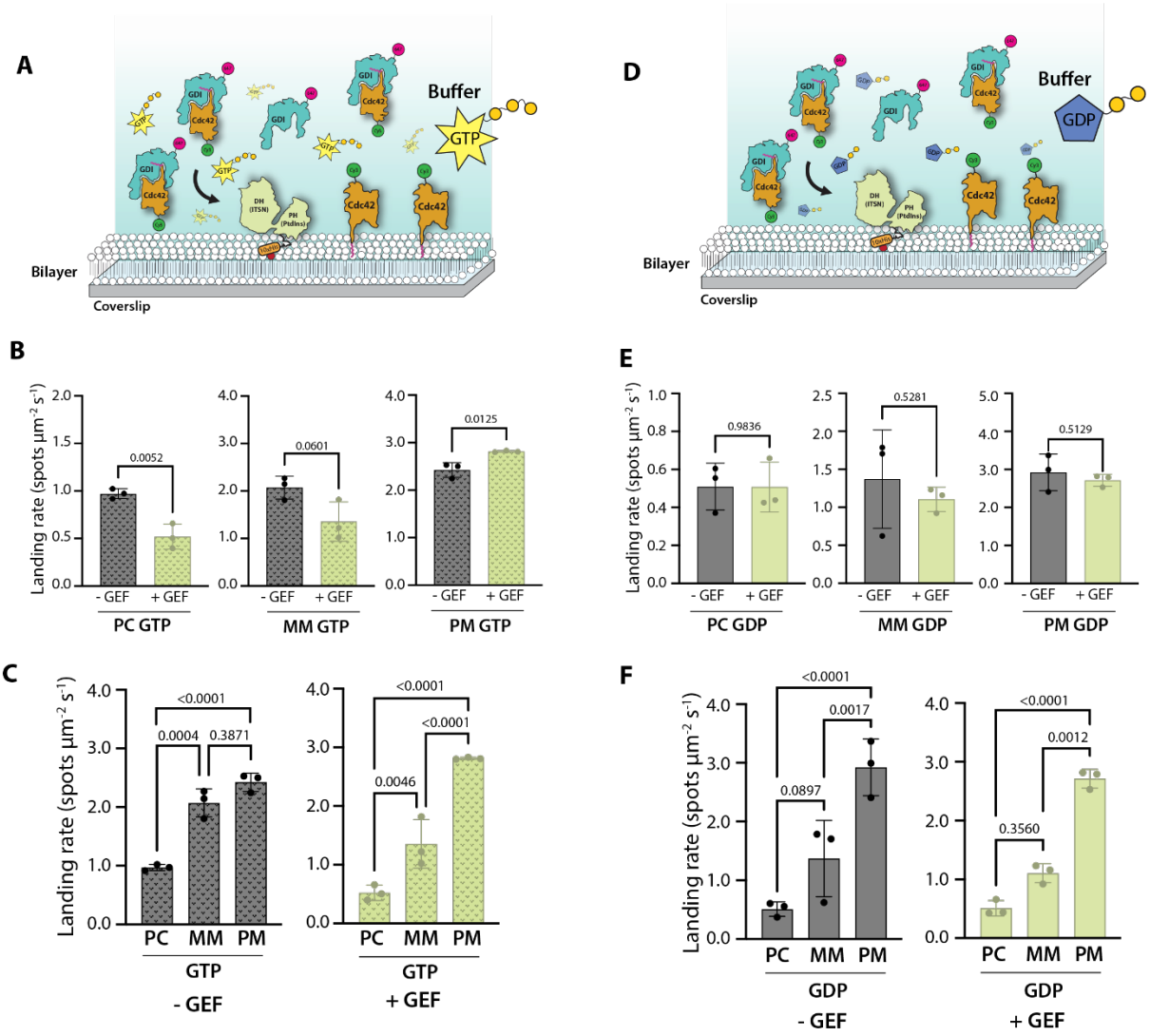

Figure 27. Measuring Cdc42 recruitment rates in the absence of cell lysate. (A) Cartoon of experimental geometry for GTP-buffer experiments. **(B + C)** Landing rate (mean) of Cdc42 spots per $\mu m^2\ s^{-1}$ in GTP-containing buffer. Three lipid conditions PC, MM and PM (left to right) in the presence and absence of ITSN-DH-PH-His_{10} (B) and comparison of rates across lipid conditions (C). **(D)** Cartoon of reaction geometry utilising GDP-containing buffer. **(E + F)** As with B+C however utilising GDP-containing buffer. All experiments used 100 pM Cy3-Cdc42:RhoGDI-AF647 complex. Data presented from 1000 frames (22 s) N = 3, error = SD. Statistical comparisons: B and E, unpaired t-test, C and F 2-way ANOVA. Cdc42 spots were considered to be membrane associated once track lengths were ≥ 5 frames (110 ms) Error bars SD.

However, the rate at which the Cdc42 was recruited differed across the lipid compositions used. When compared to the recruitment rate observed on PC SLBs, the MM and PM compositions both showed an increased rate of landing (by 2.1-fold and 2.5-fold respectively in GTP experiments, along with 2.6-fold and 5.7-fold in GDP experiments) (Figure 27 C and F). This suggests that the composition and the charge of the membrane may positively contribute not only to the stability of RhoGTPase on membranes as shown previously[193,210,245], but also to Cdc42 recruitment.

Cdc42 arrives at the membrane in the absence of RhoGDI

The lack of an influence of GEF presence on the rate of GTPase membrane binding does not exclude GTPases loading into membranes while still bound to RhoGDI. To investigate relationship between RhoGDI dissociation and membrane loading of Cdc42, we probed the fraction of colocalisation between Cdc42 and RhoGDI at the time of the initial membrane recruitment. The percentage of Cdc42 molecules which landed on the various membrane compositions (termed recruitment events) which were colocalised with a RhoGDI signal were compared to the biotin recruitment control (the theoretical maximum colocalisation potential) (Figure 28B and E). Once again, the influence of ITSN on colocalisation was investigated

All lipid compositions, in both GTP and GDP conditions, showed that Cdc42 co-localisation was dramatically lower than that of the control, in some cases showing no colocalisation recruitment events at all (Figure 28B and E). When compared to control colocalisation PC, MM and PM lipids showed a reduction in colocalisation of 116-fold, 27-fold and 6.6-fold respectively GTP buffer and 450-fold, 10-fold and 6.3-fold respectively for GDP buffer.

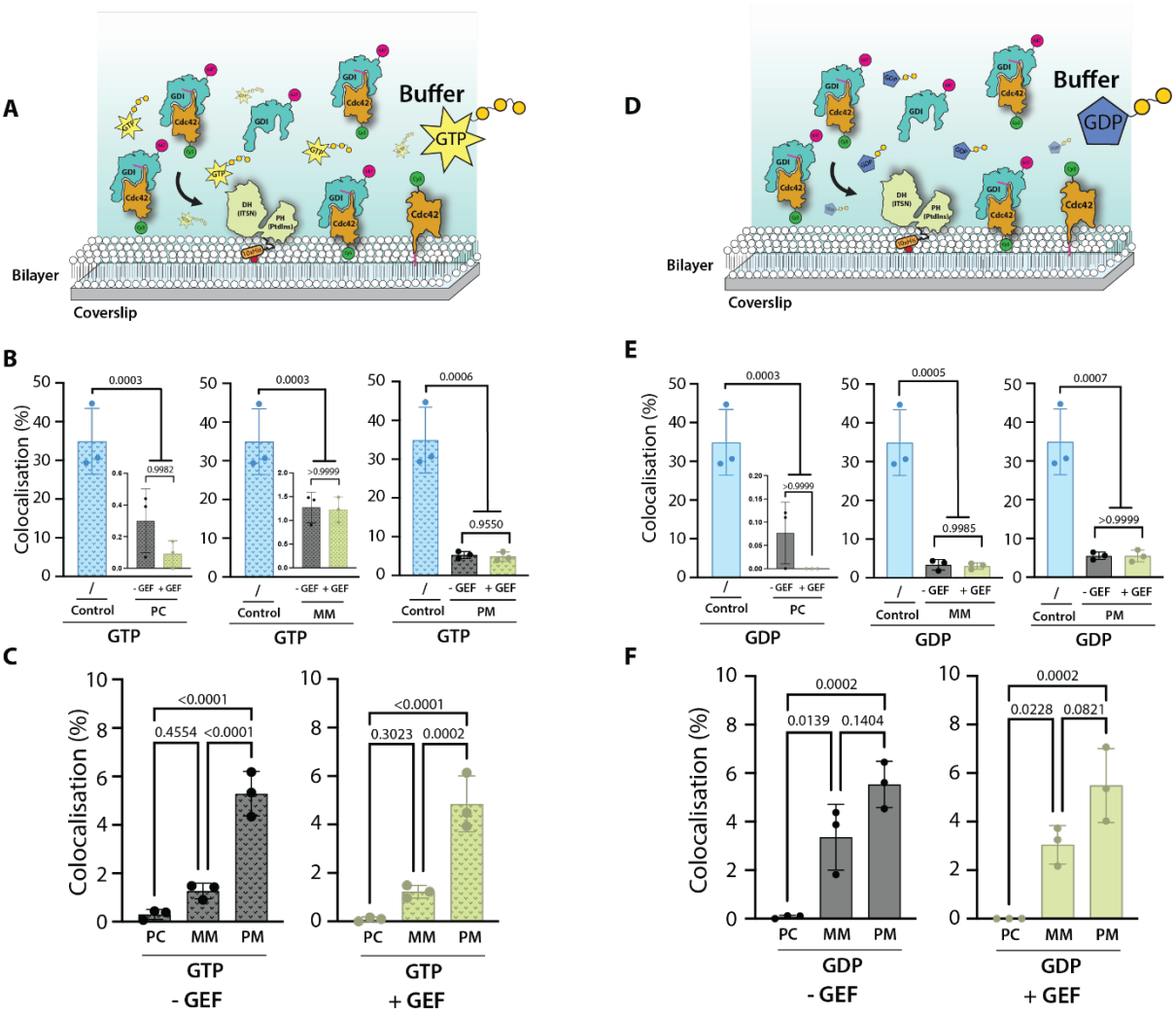

Figure 28. Colocalisation of Cdc42 and RhoGDI upon membrane recruitment in the absence of cell lysate. **(A)** Cartoon of experimental geometry for GTP-buffer experiments. **(B)** Colocalisation percentage of Cdc42 landing events (mean) in GTP-containing buffer. Three lipid conditions PC, MM and PM (left to right) in the presence and absence of ITSN-DH-PH-His_{10}, colocalisation fraction compared to biotin-based recruitment control (blue). **(C)** Comparison of colocalisation percentage across lipid conditions. **(D)** Cartoon of reaction geometry utilising GDP-containing buffer. **(E + F)** As with B+C however utilising GDP-containing buffer. All experiments used 100 pM Cy3-Cdc42:RhoGDI-AF647 complex. Colocalisation as a percentage of Cdc42 spots. Cdc42 spots were considered to be membrane associated once track lengths were ≥ 5 frames (110 ms). Data presented from 1000 frames (22 s) N = 3, error = SD. Statistical comparisons: B and E, unpaired t-tests and 1-way ANOVA, C and F 2-way ANOVA. Error bars SD.

Regarding the influence of GEF localisation to the membrane, no influence the levels of Cdc42:RhoGDI colocalisation was observed, with colocalisation percentages comparable to the SLBs lacking ITSN, an observation true for all three lipid compositions (Figure 28 B + E). However, when comparing colocalisation percentages between lipid compositions (Figure 28 C and F), a trend becomes apparent. In GTP buffer, when compared to PC, colocalisation increases 4.2-fold and 17.6-fold respectively for MM and PM compositions, with 43.6-fold and 71.9-fold increases for

MM and PM in GDP conditions. Critically however, despite the trend of increasing colocalisation across the PC, MM and PM compositions, the fraction of colocalisation remains very low (< 6%) to that observed in the positive control. This suggests that the vast majority of the Cdc42 as lost its RhoGDI client before arriving at the membrane and that the presence of GEF does not alter this. Furthermore, it appears that the inclusion of GDP or GTP does not influence this, further supporting that the activation of Cdc42 is independent of recruitment and not occurring whilst in complex with RhoGDI.

However, as there was an increase in colocalisation in conditions of negatively charged lipids, despite the fraction of colocalised Cdc42 remaining low, we were interested as to what could be a likely explanation. It was observed that there are large numbers of GDI spots appearing in the negatively charged lipid experiments. When the number of GDI spots was counted, there was a 25-fold increase in the amount of GDI spots detected on PM membranes as compared to PC (Figure 29). With all of these interaction events being incredibly short lived, (the majority 1 frame, 22 ms).

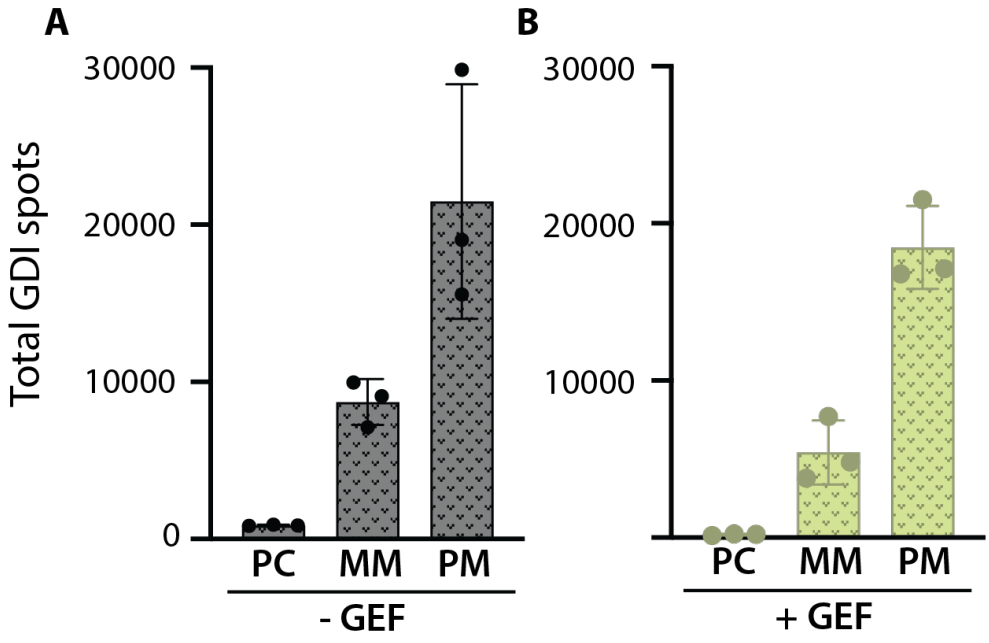

Figure 29. GDI spots landing on SLBs of varying composition in the presence and absence of GEF. The number of spurious interactions between RhoGDI and the plasma membrane across lipid conditions in the presence and absence **(A)** and presence **(B)** of GEF in GTP conditions. 100 pm Cdc42:GDI complex was introduced. Data presented from 1000 frames (22 s) N = 3. Error bars SD.

The observation of increased colocalisation rates in the MM and PM mixes is likely due to the negative charge on these SLBs. Negative charge appeared to result in spurious interaction between the RhoGDI, likely via positively charged patches located on the globular domain (Figure 7) and the membrane, slightly increasing the fraction of Cdc42 molecules showing colocalisation, (Figure 28).

This suggested that electrostatic charge could influence the interaction dynamics between RhoGDI and the membrane, however this influence was likely not a primary recruitment mechanism of the Cdc42:GDI complex as the colocalised fraction on Cdc42 remained low as compared to the positive control.

Cell lysate does not provide a mechanism whereby Cdc42 landing rate is increased

The above experiments were all carried out in GEF buffer to probe the minimum components required for membrane loading. However, there are many factors which have been implicated in the regulation of the Cdc42:RhoGDI complex which may influence landing rate such as those discussed in previous chapters. Cell lysates contain all the ingredients necessary to promote actin network development as shown in Figure 18 and literature[164,241]. Should there be any effects of post-translational modifications to RhoGDI or Cdc42, or the action of a GDF which facilitated an improved RhoGTPase recruitment rate, then this could be expected to result in an increased landing rate of Cdc42 in the reconstitution. We therefore repeated the recruitment assays in the presence of concentrated pig brain lysate. Briefly, the hard-spun lysate, activated using energy and salt mixes (see methods), was used in place of buffer. Freshly diluted Cdc42:RhoGDI was added to this mix along with the desired nucleotide, and flowed onto the SLB which, where necessary had been incubated prior with ITSN.

Looking first at the effect of ITSN on Cdc42 landing rate, as with buffer-based experiments, there was no influence of the recruitment rate of Cdc42 in the presence or absence of ITSN, both for GTP and GDP samples (Figure 30 B and E). This suggested that ITSN supplied exogenously does not increase the landing rate of Cdc42 even in the presence of functional cell lysate.

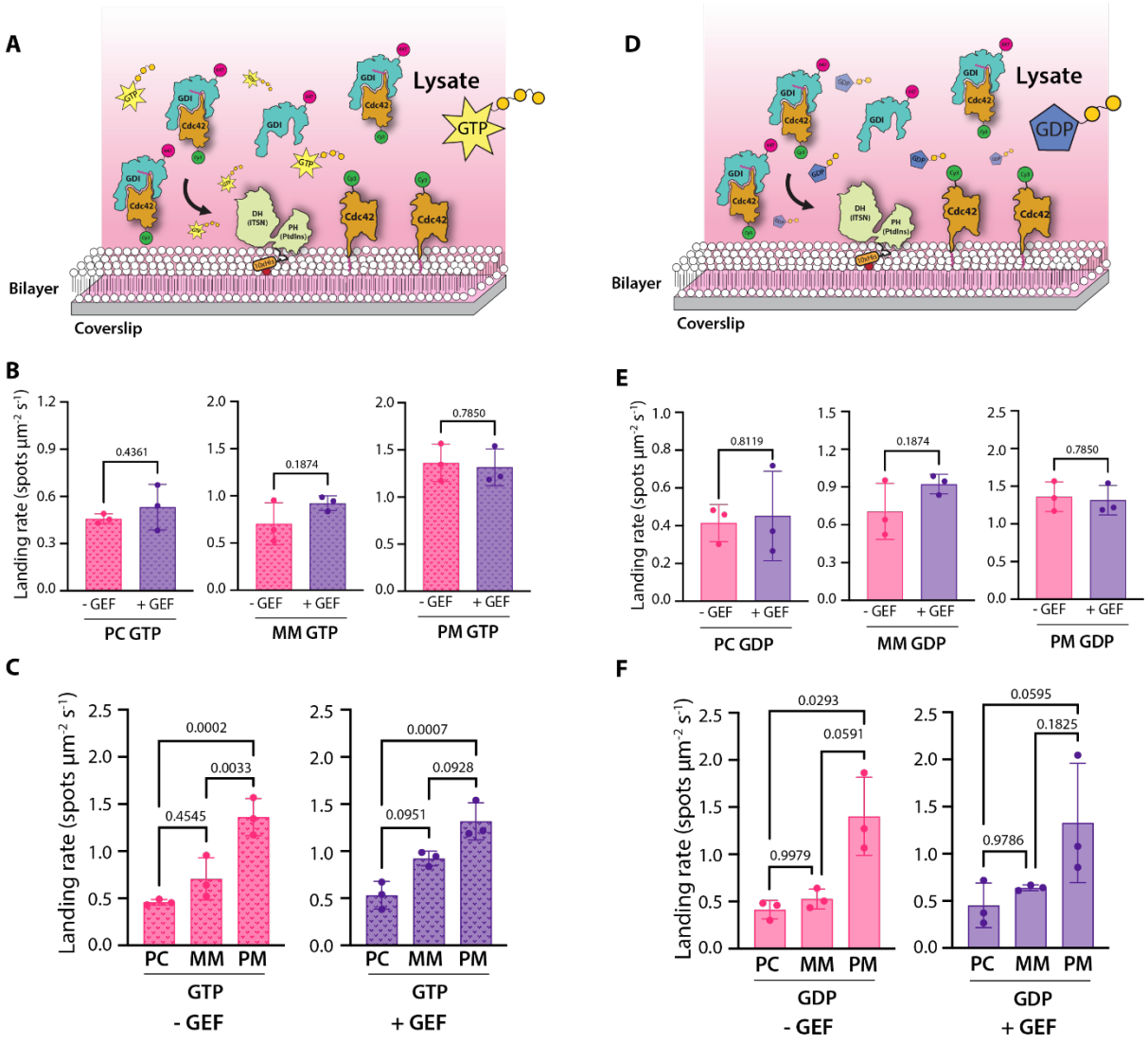

Figure 30. Measuring Cdc42 recruitment rates in the presence of cell lysate. (A) Cartoon of experimental geometry for GTP-buffer experiments. **(B + C)** Landing rate (mean) of Cdc42 spots per $\mu m^2\ s^{-1}$ in GTP-containing lysate. Three lipid conditions PC, MM and PM (left to right) in the presence and absence of ITSN-DH-PH-His_{10} (B) and comparison of rates across lipid conditions (C). **(D)** Cartoon of reaction geometry utilising GDP-containing lysate. **(E + F)** As with B+C however utilising GDP-containing buffer. Lysate was activated with energy mix (30 mM phosphocreatine, 4 mM ATP, 4 mM $MgCl_2$, pH 7.4) and salt mix (120 mM KCl, 10 mM EGTA, 40 mM 3-phosphoglycerate) prior to use in experiments. All experiments used 100 pM Cy3-Cdc42:RhoGDI-AF647 complex. Data presented from 1000 frames (22 s) N = 3. Statistical comparisons: B and E, unpaired t-test, C and F 2-way ANOVA. Error bars SD.

As in buffer-based experiments, the lipid membrane compositions appeared to influence landing rate with and increase compared to PC of 1.5-fold and 3-fold for MM and PM compositions respectively in GTP experiments and 1.3-fold and 3.4-fold in GDP experiments.

The landing rates observed are slightly lower, but comparable to that of buffer-based experiments suggested that the lysate was not providing an GDF-like component that

is facilitating the increased recruitment of Cdc42 to the SLB. Furthermore, the inclusion GEFs, both exogenous and endogenous (present in the cell lysate) was also not resulting in an increased Cdc42 landing rate. The influence of lipid composition holds up somewhat, with an increase of Cdc42 landing on MM composition and even more so on PM mix (Figure 30 C and F).

Colocalised recruitment is likely a rare occurrence in cells

Because of the slight reduction in landing rates in the presence of cell lysate compared to buffer-only experiments, we wondered whether lysate presence was stabilising the Cdc42:GDI complex which might result in an increase in colocalisation percentage. We therefore measured the fraction of colocalised Cdc42 that colocalised with GDI upon recruitment in the presence of cell lysate. As above, the hard-spun lysate, activated using energy and salt mixes, was used in place of buffer. Freshly diluted Cdc42:RhoGDI was added to this mix along with the desired nucleotide, and flowed onto the SLB which, where necessary had been incubated prior with ITSN.

Colocalisation in GTP and GDP samples was a minor fraction when compared to the positive control, with 41-fold, 47-fold and 44-fold lower colocalisation for PC, MM and PM respectively for GTP conditions. GDP conditions were comparably low, with 28-fold, 55-fold and 29-fold lower colocalisation for PC, MM and PM compositions respectively Figure 31 B and E).

Consistent with all previous results presented here, ITSN localisation to the SLB did not provide an altered colocalisation fraction, remaining comparable to the absence of ITSN across all lipid composition conditions (Figure 31B and E). This again supports the conclusion that the presence of RhoGEFs at the SLB do not modulate the amount of Cdc42 observed in complex at the surface.

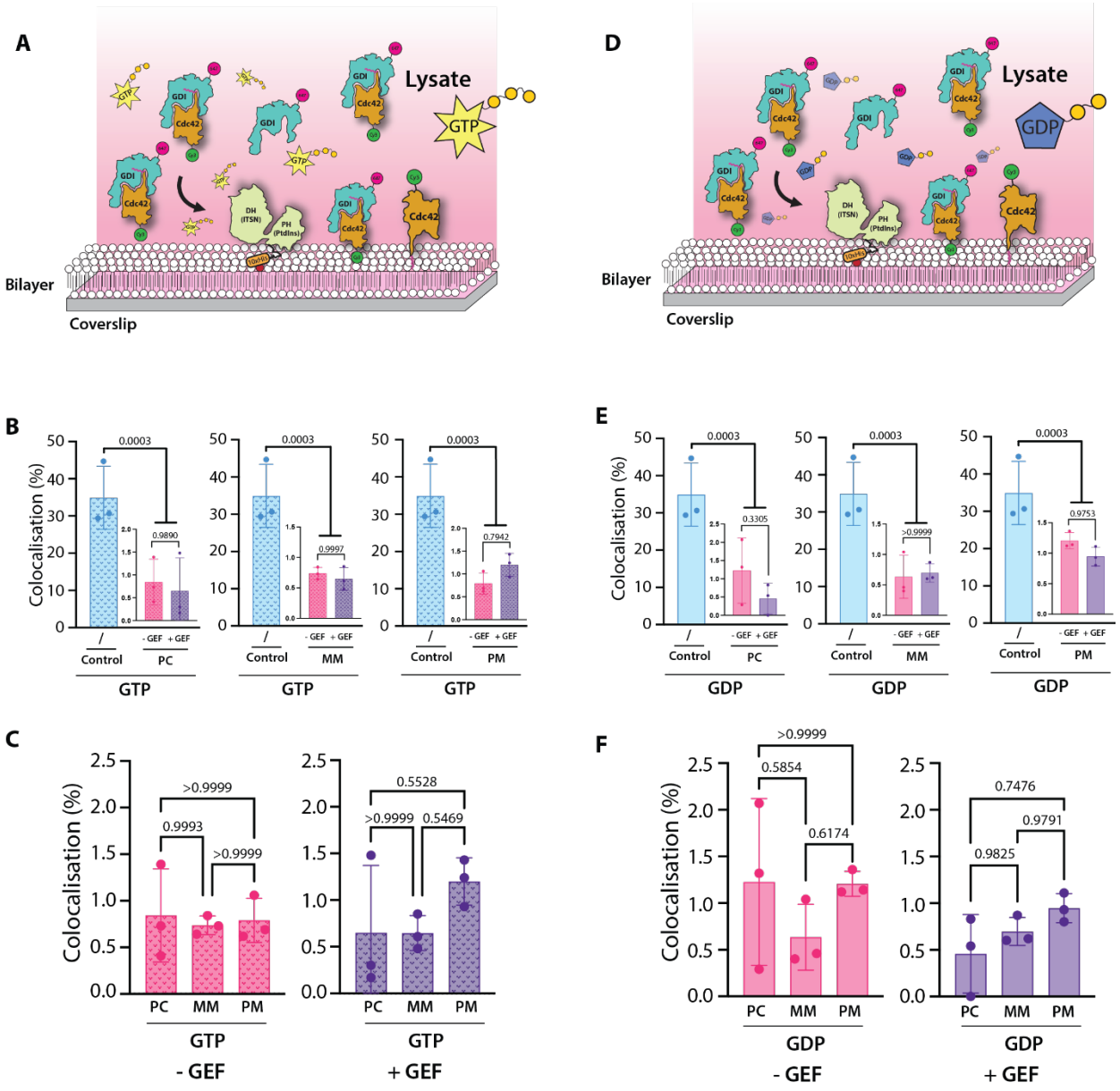

Figure 31. Colocalisation of Cdc42 and RhoGDI upon membrane recruitment in the presence of cell lysate. (A) Cartoon of experimental geometry for GTP-buffer experiments. **(B)** Colocalisation percentage of Cdc42 landing events (mean) in GTP-containing lysate. Three lipid conditions PC, MM and PM (left to right) in the presence and absence of ITSN-DH-PH-His_{10}, colocalisation fraction compared to biotin-based recruitment control (blue). **(C)** Comparison of colocalisation percentage across lipid conditions. **(D)** Cartoon of reaction geometry utilising GDP-containing lysate. **(E + F)** As with B+C however utilising GDP-containing lysate. All experiments used 100 pM Cy3-Cdc42:RhoGDI-AF647 complex. Colocalisation as a percentage of Cdc42 spots. Cdc42 spots were considered to be membrane associated once track lengths were ≥ 5 frames (110 ms). Data presented from 1000 frames (22 s) N = 3, error = SD. Statistical comparisons (see methods). Lysate was activated with energy mix (30 mM phosphocreatine, 4 mM ATP, 4 mM $MgCl_2$, pH 7.4) and salt mix (120 mM KCl, 10 mM EGTA, 40 mM 3-phosphoglycerate) prior to use in experiments. Data presented from 1000 frames (22 s) N = 3. Statistical comparisons: B and E, unpaired t-tests and 1-way ANOVA, C and F 2-way ANOVA Error bars SD.

Interestingly the trend observed in the absence of cell lysate of an increased colocalisation fraction for MM and PM lipids was nearly eliminated by the inclusion of

cell lysate. By including cell lysate, the fraction of co-localised Cdc42 and GDI falls below 1.5% across all conditions (Figure 31 C + F). The absolute number of GDI molecules observed as compared to buffer-based experiments is dramatically reduced both in the presence (Figure 32A) and absence (Figure 32B) of GEF, showing that any effect of electrostatic interaction facilitating spurious GDI-membrane interaction seems to be negated by the presence of lysate.

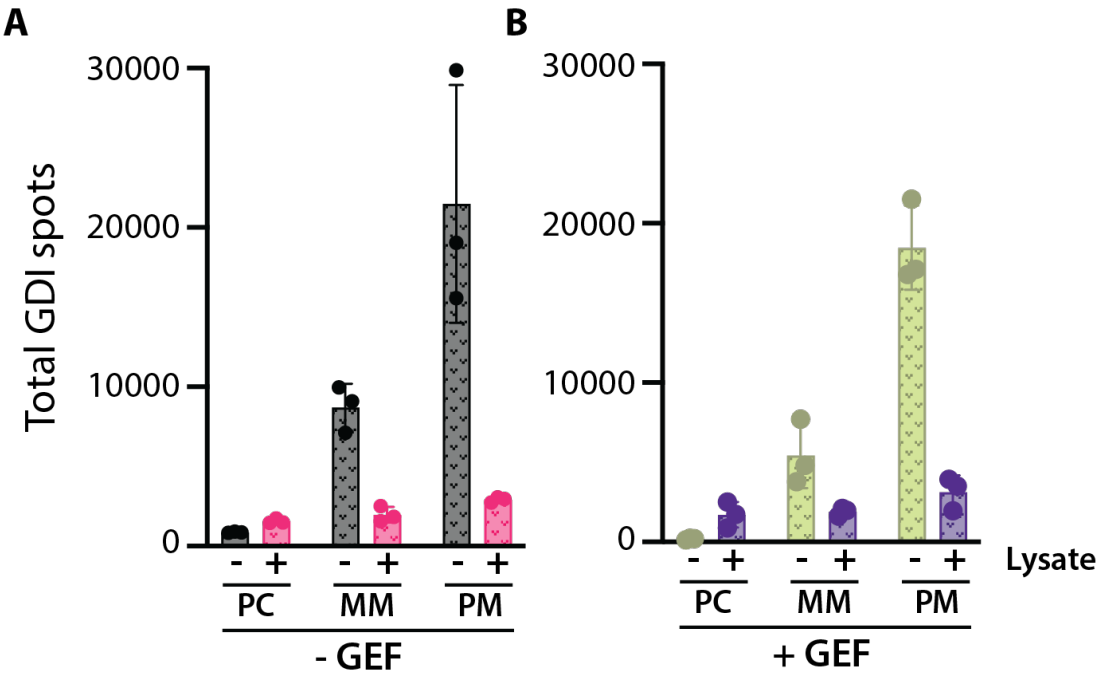

Figure 32. Impact of cell lysate on RhoGDI membrane interaction events. Number of GDI spots detected on PC, MM and PM lipid compositions in the presence and absence of cell lysate following the addition of 100 pM Cdc42:GDI complex. **(A)** Under GTP conditions in the absence of ITSN, GDI interaction was reduced in the presence of cell lysate. **(B)** Under GTP conditions in the presence of ITSN, GDI interaction was also reduced in the presence of cell lysate. All experiments used 100 pM Cy3-Cdc42:RhoGDI-AF647 complex. Colocalisation as a percentage of Cdc42 spots. Data presented from 1000 frames (22 s) N = 3. Error bars SD.

This suggests that the electrostatic interaction between the plasma membrane and RhoGDI in vivo is likely negligible, however in areas of high local membrane concentration, and in the absence of RhoGDI clients this phenomenon could arise.

To confirm that colocalisation is not only a rare event, but not a direct recruitment mechanism, probability of a GDI colocalisation event at each frame within a Cdc42 track was calculated. Should the negative charge act to recruit Cdc42 in complex with GDI, then it would be expected that there would be an increase in probability in

colocalisation at the time of recruitment as compared to the rest of the track. It can be seen however, that throughout the track probability of colocalisation with GDI remains comparable (Figure 33A). This supported the theory that the interaction between GDI and negative charge is transient and non-specific. This was compounded in the presence of lysate, where the probability across the entire track reduced (Figure 33 B).

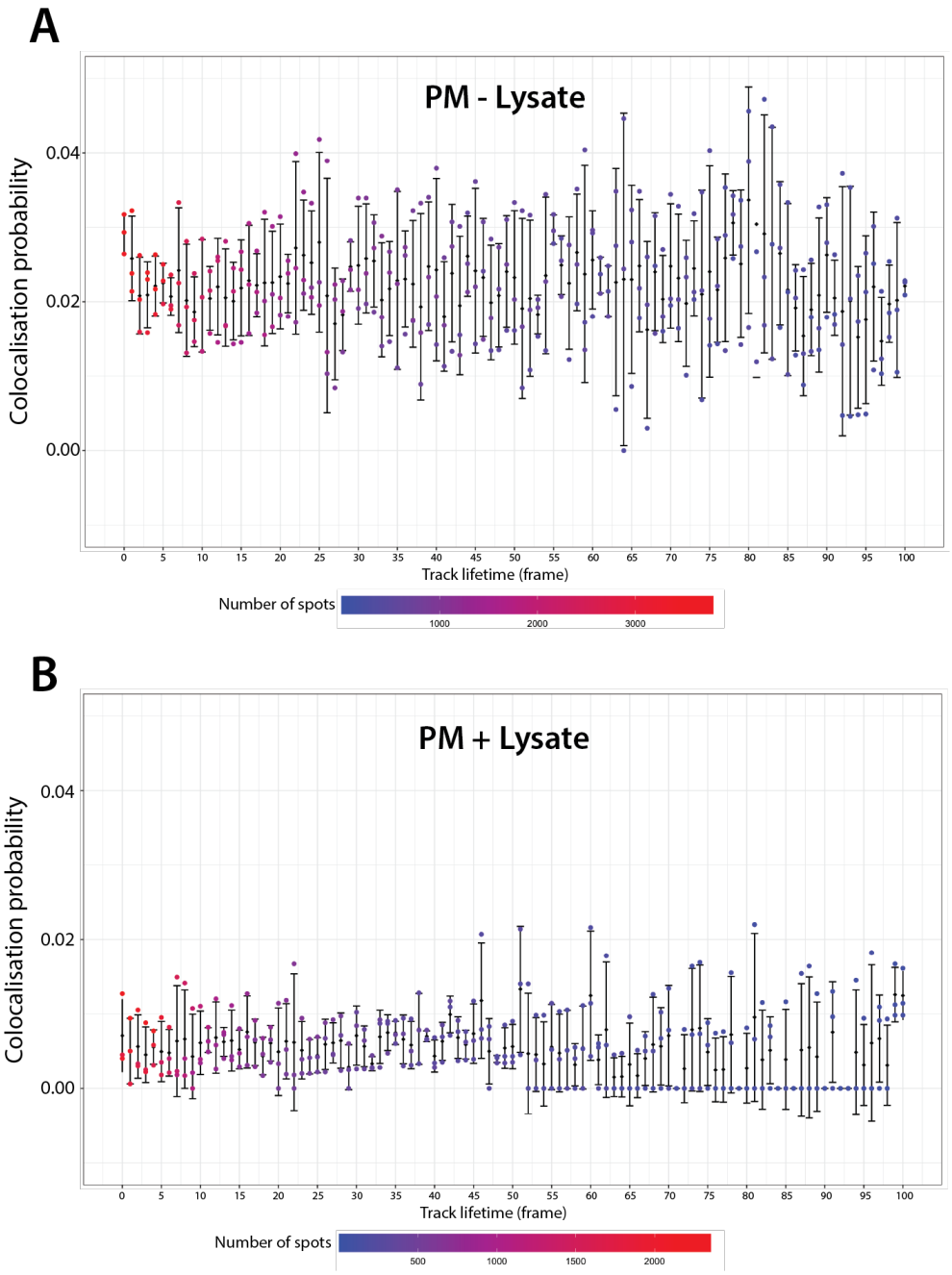

Figure 33. Probability of GDI colocalisation for Cdc42 throughout track lifetime. (A) A probability plot colocalisation with RhoGDI throughout the lifetime of a Cdc42 track on the PM SLB composition in GTP conditions, in the absence of GEF and cell lysate. **(B)** As in (A) however in the presence of cell lysate. Heat map indicative of number of spots in probability calculation at that frame number. Error bars SD.

This suggested that the minor increase in the colocalised Cdc42 fraction (Figure 28) is a result of this non-specific GDI membrane interaction immediately after complex dissociation, which then negated by the presence of lysate (Figures 31 and 32).

These data confirmed that as previously shown in buffer-based experiments, the inclusion of ITSN at the membrane did not influence the colocalising, once again supported by the lack of influence of the inclusion of GTP over GDP. The low levels of colocalisation under all conditions in these experiments suggested that within the cell, the likelihood of Cdc42 arriving to, and associating with the membrane in complex with RhoGDI is low, once again confirming that in a cellular like environment such as that used in this reconstitution, dissociation from GDI precedes membrane loading of RhoGTPases.

Discussion

Bacterially expressed, in vitro prenylated Cdc42 produces a stable RhoGTPase complex

In this work, we produced heterodimeric complexes, in vitro, of geranylgeranylated and fluorescently labelled Cdc42 and RhoGDI1. As bacteria lack the machinery to produce prenylated RhoGTPase, the majority of work on prenylated RhoGTPases has used expression in insect cells. However mass spectrometry data by our group and other laboratories shows a large fraction of unprenylated protein in the sample[236], which can confound the analysis of RhoGDI binding. Here we show that we can produce prenylated and labelled RhoGTPases using an in vitro prenylation approach (Figure 14), which when complexed with RhoGDI, shows comparable dissociation kinetics as seen in literature (Figure 16). Using this isolated complex, we confirmed that the RhoGDI binding prevents nucleotide exchange by RhoGEFs as anticipated from prior structural work (Figure 6)[13,114]. GEF assays utilising mant-GTP exchange confirmed that when the Cdc42 substrate was supplied in complex with RhoGDI, nucleotide exchange was not observed (Figure 17). These data are critical as any conclusions drawn regarding loading of Cdc42 to the membrane from its GDI complex assume full binding and inhibition of GEF activity as seen in vivo. The protocols outlined here in materials and methods are crucial for faithfully reconstituting RhoGTPase membrane dynamics.

Cdc42 localisation to membrane is not dependant on ITSN but on membrane composition

A main objective of this work was to investigate the nature of the coupling between the spatial and catalytic cycles of the RhoGTPases in the event of membrane loading. Here data was presented supporting the argument of indirect coupling, with the presence of RhoGEF not increasing RhoGTPase membrane binding. One of the larger biochemical conundrums in the RhoGTPase field is how do RhoGTPases overcome the high affinity interaction between themselves and their RhoGDI partner in the cytosol and make it to the membrane where they can exert their influence?[10] Due to the observation that recruitment of GEF to the plasma membrane in cells results in the corresponding activation of RhoGTPases[142], we asked whether GEF activates GTPases which are already localised at the plasma membrane, or alternatively actively recruits GTPases from solution in the process of activation? The fact that

activity sensors show a marked increase in active GTPases at the point of GEF recruitment[142] could have two interpretations. Firstly, that many GTPases can be found at the membrane in an inactive state, and the recruitment of GEF activates this pool. This interpretation would explain how polarisation of active RhoGTPases can occur on such a rapid timescale. However, this hypothesis is curious because RhoGDI preferentially extracts inactive RhoGTPases, making a stable pool of GDP-bound, inactive GTPases at the membrane unintuitive.

A second explanation could be that membrane bound GEFs directly recruit RhoGTPases from the GDI complex in solution. The suggestion that GEFs can liberate RhoGTPases from their RhoGDI partner and loaded onto the membrane has always been a contentious issue[68] as discussed in previous chapters. The hypothesis is based in the dual aspect nature of the interaction between RhoGTPases and GDI. The N-terminal arm and the globular domain interact with RhoGTPases independently, and therein lies the possibility to form a heterotrimeric complex. Should the N-terminal arm undock from its GTPase client, the complex would remain together via the globular domain interaction. A standout issue with this theory is that the N-terminal regulatory arm of RhoGDI blocks interaction with the switch regions of RhoGTPases[13], and therefore prohibits GEF interaction. However, literature has shown there is perhaps a dynamic property to this regulatory arm which may allow opportunistic GEF interaction[246] and reducing the affinity between RhoGDI and GTPase via N-terminal arm undocking. This opportunistic interaction could activate the GTPase whilst in complex with RhoGDI, further reducing affinity[84], destabilising the complex and allowing membrane association.

Data here showed that the RhoGEF ITSN is ineffective at activating Cdc42 whilst it is in complex with RhoGDI in solution (Figure 17), which would argue against the formation of a trimeric complex. However, it has been suggested that membrane association of the GEF may promote its ability to activate the GTPase whilst in complex with RhoGDI due to a more favourable geometry at the membrane[233].

The membrane binding geometry of Cdc42 is open to speculation as it is not possible to crystalise a membrane bound protein. We do, however, have structural information about Cdc42 in complex with RhoGDI[13]. Placing the C-terminus of GTPases in membrane can result in a state in which the switch regions are directed away from the plane of the membrane, amenable for GEF interaction[139]. Furthermore, there is a positively charged patch on the surface of RhoGDI (Figure 7), proximal to the

prenylation site[84] which is in the vicinity of the negatively charged membrane. Perhaps this geometry would provide a situation where the prenyl group of Cdc42 can interact with the membrane, made possible by the orientation of Cdc42 itself as well as interactions between the charged globular domain of GDI and the negatively charged lipids within the SLB.

Results presented here however show recruitment of Cdc42 is unaffected by the presence of ITSN on the SLB as compared to ITSN-free controls (Figure 27 B and E). When compared to samples in the absence of ITSN on PC bilayers, the landing rate is marginally decreased from 0.971 ± 0.052 to 0.521 ± 0.131 μm^{-2} s^{-1} (Table 3), suggesting that the presence of ITSN does not serve to increase RhoGTPase membrane recruitment. One consideration with the use of PC bilayers is the absence of PI(4,5)P_2 lipids and negative charge, both of which have been suggested to be involved in the geometry required to mediate this GEF-based mechanism as well as for activation of RhoGTPase signalling in reconstituted systems[164]. However, we show that changes in the lipid composition do not result in GEF-mediated RhoGTPase recruitment. Recruitment rates were slightly lowered in the presence of ITSN for MM and remaining about equal on PM bilayers (Table 3). These data show that ITSN is not responsible for facilitating direct recruitment of Cdc42.

Even in the absence of ITSN, Cdc42 bound to membranes at an appreciable rate. This showed that even in the most simple system of a PC bilayer and Cdc42:RhoGDI complex, Cdc42 recruitment to the membrane can be achieved.

Table 3. Landing rates of Cdc42 compared across all conditions in the absence of cell lysate

SLB composition	Cdc42 landing rates (μm^{-2} s^{-1})			
	GTP - ITSN	GTP + ITSN	GDP - ITSN	GDP + ITSN
PC	0.971 ± 0.052	0.521 ± 0.131	0.510 ± 0.123	0.508 ± 0.131
MM	2.073 ± 0.240	1.355 ± 0.414	1.371 ± 0.649	1.105 ± 0.162
PM	2.424 ± 0.155	2.814 ± 0.016	2.924 ± 0.483	2.714 ± 0.158

Our results showed that while recruitment did occur, very little Cdc42 was recruited via a GEF-mediated mechanism. It appears that the dominant mechanism of membrane recruitment is relying on the slow dissociation of the RhoGDI from Cdc42 and subsequent membrane binding of the latter. In line with this, Cdc42 recruitment was virtually unaffected by the identity of the guanosine nucleotide in solution (Table 3). One GEF-based mechanism proposed in literature relies on GEF-mediated nucleotide exchange of Cdc42 whilst remaining associated to GDI, exploiting the

reduced affinity between GTP-bound RhoGTPase and GDI. However, when looking at GTP against GDP data, not only were recruitment rates comparable, but the influence of ITSN was also minimal in both nucleotide cases.

Looking across the three lipid compositions used in this work, the lack of ITSN influence holds true, with no increase in landing rate in PC, MM or PM compositions. However, what is interesting is that the rate of Cdc42 landing increases across the lipid compositions, with PC being the lowest and PM showing the highest rate of Cdc42 recruitment (Table 3).

As mentioned above, the PC composition contains no $PI(4,5)P_2$ lipids or negative charge, meaning surface recruitment depended dominantly on the hydrophobic geranylgeranyl tail of Cdc42 for association. In the cases of MM and PM compositions, the inclusion of $PI(4,5)P_2$ as well as other lipid species results in a stronger negative charge on these bilayers. It was not simply the charge which differed, but the organisation of these bilayers varied with the separated phases in the MM preparation (Figure 23). Electrostatic interaction between the C-terminus of RhoGTPases and the plasma membrane have been suggested to be important in RhoGTPases recruitment[247]. Furthermore, charged patches on the globular domain of RhoGDI have also been implicated in membrane interactions[139]. The MM allowed for investigation of negative charge alone, as the sizable fraction of PI lipids (48%) provides a large amount of negative charge. Negative charge indeed appeared to moderately increase Cdc42 recruitment. Taking the rates in GTP experiments in the absences of ITSN as an example (all values in Table 3), the Cdc42 recruitment rate increased 2-fold with negative charge (MM).

The HVR of Cdc42 contains a large amount of positively charged residues close to the CAAX box (Figure 5). Should the Cdc42 be in proximity to the membrane then this large amount of positive charge along with the hydrophobic geranylgeranyl motif like drive recruitment to the membrane. However, negative charge appears to be not the sole property of the membrane required for increasing Cdc42 recruitment. The PM composition is much closer to mimicking the lipid composition of the inner leaflet of the PM in vivo[190,193]. Whist still containing negative charge and phosphoinositide ($PI(4,5)P_2$), it also contains components such as cholesterol, important for regulating membrane fluidity[248] as well lipid species such as DOPE and PI at molar ratios which, in vivo, identifies this membrane as the plasma membrane[190]. The PM SLBs increased Cdc42 recruitment rate by 2.5-fold over PC, suggesting that both the lipid composition

and the accompanying negative charge modulates the landing rate of Cdc42. The difference in influence on recruitment between MM and PM is less pronounced as MM over PC, suggesting that the negative charge may be dominant in affecting Cdc42 landing rate.

These data suggest that the catalytic cycle is not directly coupled to the spatial cycle of RhoGTPases in the process of membrane binding. The composition of the membrane rather than the presence of GEF controls the recruitment of Cdc42. This means that the GTPases are activated by GEFs after, and not upon, membrane loading. Such a mechanism implies the existence of inactive pools of RhoGTPase on the membrane, where activation via GEF is occurring after membrane recruitment. While the observations made in literature show an increase in active GTPases upon GEF recruitment[142], a likely explanation is that the increase in local GEF concentration allows a more rapid activation of this already-membrane-associated RhoGTPase pool, following GTPase membrane association. Due to the use of activity sensors for GTPases in such work, this manifests as the appearance of a large active GTPase signal, however data presented here would argue that there is not a corresponding increase in GTPase recruitment.

Dissociation from RhoGDI occurs before membrane association

As membrane composition, in particular negative charge seemed to influence the rate of Cdc42 recruitment, we investigated as to how many of the membrane association events of Cdc42 were colocalised with a RhoGDI molecule.

One of the suggested membrane-loading mechanisms of the Cdc42:GDI complex is electrostatic interactions between charged patches on the globular domain of RhoGDI facilitating Cdc42 release[139]. Potentially, this could destabilise the binding of the geranylgeranyl moiety in the charged pocket of the globular domain of GDI and allow for membrane association (Figure 7). Furthermore, Cdc42 also contains charged stretches of amino acids, found in its HVR perhaps further contributing to such a hand-over mechanism (Figure 5A).

Such a hand-over mechanism that a large fraction of the Cdc42 would be accompanied by RhoGDI at the moment when the complex encounters the membrane.

Results showed that the vast majority of Cdc42 arriving alone at the membrane (Figure 28). When compared to a positive control, colocalisation at the point of membrane

recruitment in experimental data is reduced by between 6.6 – 5000 fold. This suggests that in the vast majority of cases Cdc42 separates from GDI before membrane association.

This held true regardless of the specific membrane composition (Figure 27 B and E). Despite colocalisation increasing between PC, MM and PM compositions, the fraction of colocalised molecules when compared to the control remains low with no more than ≈ 5% of Cdc42 colocalised with a RhoGDI molecule upon membrane recruitment.

However, data supports, at least in part, the hypothesis that the charged patches of the globular domain of the RhoGDI can interact with the membrane. In the cases of the increased negative charge compositions, MM and PM, the number of GDI-membrane interaction events appears to grow, illustrated by the numbers of RhoGDI spots recruited (Figure 29).

Despite the large increase in the amount of short lived RhoGDI spots, the levels of localisation at the point of recruitment remains low with ≈ 5% of Cdc42 spots arriving colocalised. The suspected reasoning for this is that the RhoGDI is transiently interacting via electrostatics with the charged membrane, with the vast majority of these interactions in the absence of Cdc42. The GDI interactions appear transient in nature with tracking software showing the majority of spots last 1 frame (22 ms) (data not shown).

These data show that in addition to the recruitment of Cdc42 being uncoupled from activation via ITSN, the lack of colocalisation confirms that the separation of the RhoGDI is occurring prior to membrane recruitment. This would support the hypothesis that there is a kinetic bottleneck at the release of Cdc42 from RhoGDI. Once separated however, to modulate the recruitment of the RhoGTPase, cells rely predominantly on the negative charge and lipid composition of the membrane itself. This seems to provide a basal mechanism which is sufficient to result in Cdc42 association to the membrane. However, in the cell lysate, numerous potential mechanisms have been put forward (discussed in previous chapters), as to how this recruitment may be manipulated, including phosphorylation, or protein interaction which serves to function as a GDF. The data discussed above is in the absence of such potential influences due to the use of buffer in these experiments, therefore can only be interpreted as a basal mechanism of RhoGTPase recruitment. By exchanging the buffer for a functional cell lysate, it was possible to investigate effects of these potential GEF-like behaviours on Cdc42 recruitment.

Cell lysate does not provide a mechanism of enhanced Cdc42 membrane recruitment

Cell lysate provided no mechanism of increased Cdc42 loading on the membrane. Cell lysate contains many, if not all, of the endogenous soluble protein pool as shown by the formation of an actin network around lipid coated beads (Figure 18). Should the cell lysate have provided a GDF-like mechanism then it would be expected that the landing rate of Cdc42 would increase. However, what is interesting is that the rate with which Cdc42 is landing on the membrane is reduced when compared to buffer experiments, both in the presence and absence of localised ITSN (Table 3 compared to Table 4, Figure 34), contrary to what would be expected by a GDF-like mechanism provided by the inclusion of cell lysate.

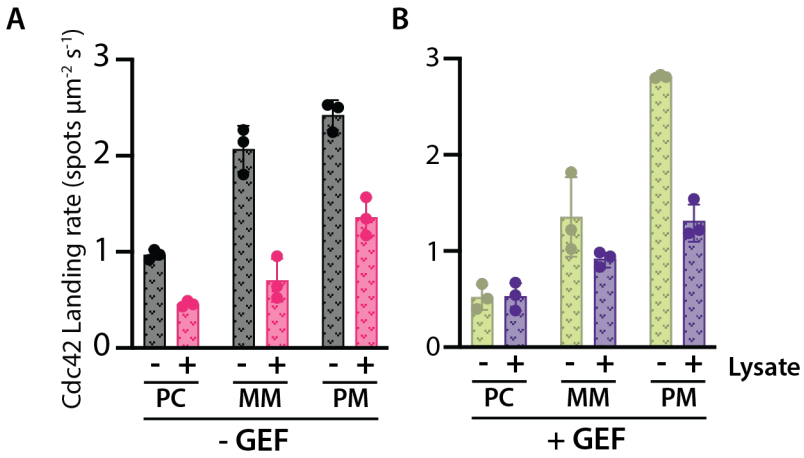

Figure 34. Influence of cell lysate on Cdc42 landing rates. (A) The presence of cell lysate reduces the landing rate marginally when compared to buffer-based experiments in the absence of ITSN. **(B)** The comparable results in the presence of ITSN show that the landing rate is not dependent on the presence of a localised RhoGEF. Once again, the presence of lysate reduces the landing rate, however the increase in landing rate in the presence of negative charge (MM) and a plasma membrane-mimicking environment (PM) holds true.

The lipid influence discussed in buffer-based experiments is still apparent, with an increase from PC to MM and again to PM. This shows that trend observed because of membrane composition holds true in lysate-based experiments, despite reduced Cdc42 landing rates when compared to buffer-based experiments (Figure 34).

Regarding the effect of ITSN localisation, results mirrored those seen in the buffer experiments, with once again no influence of Cdc42 landing rates in the presence of localised GEF (Table 4).

Table 4. Cdc42 landing rates compared across all conditions in the presence of cell lysate

SLB composition	Cdc42 landing rates ($\mu m^{-2} s^{-1}$)			
	GTP – ITSN + Lysate	GTP + ITSN +Lysate	GDP – ITSN + Lysate	GDP + ITSN +Lysate
PC	0.458 ± 0.030	0.532 ± 0.145	0.414 ± 0.098	0.452 ± 0.237
MM	0.706 ± 0.223	0.923 ± 0.078	0.527 ± 0.105	0.639 ± 0.030
PM	1.362 ± 0.198	1.315 ± 0.196	1.402 ± 0.413	1.326 ± 0.633

While the lack of increase in Cdc42 recruitment rates suggests the lack of a mechanism provided by the lysate which acts in a GDF-like manor, the reduction in landing is curious.

The inclusion of lysate does not only contain any potential GDFs, but also an influx of the regulators involved in the RhoGTPase catalytic and spatial cycles. Many of these could be responsible for the reduction in the landing rate observed in experiments. One explanation would be the presence of endogenous RhoGDI. In buffer-based experiments, concentrations of 100 pM complex are used. As discussed previously, cellular concentrations of RhoGDI are expected to be much higher, in the micromolar regime[54]. The inclusion of cell lysate with high RhoGDI concentrations results in an influx of dark (unlabelled) RhoGDI from the lysate, binding to not only to RhoGTPases found in the lysate but also labelled Cdc42 which has been liberated of its RhoGDI. In a model where separation of Cdc42 from RhoGDI occurs prior to membrane association, any Cdc42 which does dissociate, would have a large availability of RhoGDI to which it can re-bind rather than associate to the membrane resulting in a reduction in landing rate.

An addition explanation may be that despite the hard spinning of lysates prior to use, however, small amounts of plasma- and endomembranes are likely retained. It could be that labelled Cdc42 which is liberated from the exogenously added complex is not only associating to the SLB, but also to this endogenous lipid-membrane residue. As these lipids are likely floating in the cytosol and out of the TIRF field, they cannot be tracked and recorded as landing events.

It is probably the case that both explanations are at play, there is dissociation of Cdc42 from GDI prior to membrane binding, however rather than rebinding to the stochiometric amounts of RhoGDI or the SLB provided in buffer experiments, a large amount of RhoGDI and extra membrane surfaces act as binding competition with the SLB for the liberated Cdc42, reducing landing rates. Despite this, the influence of membrane composition and negative charge remains.

The effect of an influx of potential GTPase interaction partners from cell lysate is supported by the reduction in the amount of colocalisation in lysate experiments when compared to buffer-based experiments, with the highest colocalisation measured being < 1.2% ± 0.252 (compared to 5% in buffer-based experiments). Interestingly this corresponded with a loss of the spurious interaction between RhoGDI and the membrane observed in buffer-based experiments (Figure 32). The reduction in spurious interactions between negatively charged lipids and RhoGDI is likely due to the presence of many interaction partners for GDI in cell lysate. This suggests that the interaction between RhoGDI and negatively charged membranes may only be relevant under circumstances where there is a large excess of GDI over interaction partners, or where negative membrane concentrations are high, such as in areas of high surface to volume ratios. Furthermore, there are likely many other proteins interacting with these negatively charged lipids, as evident by pulldown assays utilising PIP lipids[199], which may prevent electrostatic interactions between the membrane and GDI, perhaps between Cdc42 and the membrane, resulting in the observed reduced recruitment.

These results suggest that under the geometry of experiments used in this work, the vast majority of GDI remains in the solution above the bilayer in the presence of cell lysate, and that the non-specific interactions between the GDI and the bilayer likely do not play a major role in the membrane loading of Cdc42 in these experiments.

Combined these data show that in the presence of cell lysate, Cdc42 landing rate is influenced predominately by the membrane composition. There is no apparent increase in Cdc42 recruitment, in fact, in this work, the recruitment rate is marginally reduced using cell lysate in the place of buffer. This suggests that the presence of endogenous regulators present in cell lysate does not provide a GDF-like mechanism.

Quantitative interpretation of an uncoupled mechanism based on dissociation of GDI

The inclusion of a membrane-associated GEF as well as cell lysate did not provide an increased rate in the observed recruitment of Cdc42 from the RhoGDI complex. In conditions most closely representing the physiological environment (PM lipid composition with cell lysate supplemented with GTP), the observed Cdc42 landing rate was around 1 s^{-1}. Is this observed rate sufficient to sustain RhoGTPase activity in cells? Answering this question is not straightforward, as several assumptions must be made as described below.

First, I estimate the theoretical equilibrium concentration of free Cdc42 from the equilibrium dissociation constant (K_d) of the Cdc42:RhoGDI complex (5.4 $x10^{-12}$ M[84]) though mass action. At cellular concentrations of Cdc42 of around 3 μM and equimolar RhoGDI concentrations[54], this should yield a low, but appreciable concentration of 4 nM free Cdc42 at equilibrium. To estimate the landing rate at this equilibrium concentration, we can scale the observed landing at in our reconstitution experiments by simply assuming linear, concentration-dependent scaling. This would result in a landing rate of around 260 molecules μm^{-2} s^{-1} at 4 nM free Cdc42. This value serves as a potential upper bound of Cdc42 recruitment, at which time free GTPases are yet to bind to the membrane, akin to an instantaneous recruitment rate.

Orthogonally, from the dissociation rate of Cdc42 from GDI (k_{off}) of 2.0 $x10^{-4}$ s^{-1} [84] and an average cell volume of 2000 fL, one can estimate how many free Cdc42 molecules per second can be generated from the total soluble GTPase:GDI pool. Dividing this dissociation rate by the total surface area of the inner leaflet of the plasma membrane (4000 μm^2 [212]) would result in a landing rate of 0.72 molecules μm^{-2} s^{-1}, considerably lower than what can be estimated from membrane recruitment of free GTPases at equilibrium (see above). This rate therefore likely represents a lower bound of membrane recruitment in a circumstance where all Cdc42 is bound to the membrane or GDI. This potentially serves as a rate for generation of recruitable GTPase molecules perhaps to replenish degraded RhoGTPase molecules.

With these upper and lower bounds estimated, a comparison can be made to literature values of RhoGTPase recruitment rates.

With cellular concentrations of Cdc42 around 3 μM[54] and between 1 – 10% being localised to the plasma membrane[32], one can estimate a concentration of 150 nM (assuming 5% of total) Cdc42 at the plasma membrane at steady state. With a cellular volume of 2000 fL, and a plasma membrane area of 4000 μm^2 this, yields a steady-state density of 45 molecules μm^{-2} of plasma membrane. Recruitment and polarisation of RhoGTPases in response to signalling in vivo occurs on the minute timescale. This means that a recruitment rate of 0.75 molecules μm^{-2} s^{-1} would be sufficient to for membrane turnover at these densities and time scales. Of course, this rate suggests a uniform recruitment across the whole plasma membrane area. In reality, the polar site constitutes only about 10 – 25% of the total plasma membrane area[92] meaning that should the majority of Cdc42 recruitment events be limited to this region, via lipid composition for example, the potential landing rate would increase to around 7.5

molecules μm^{-2} s^{-1}. These estimates suggest that the landing rates measured in our reconstitutions might suffice to explain turnover of RhoGTases at the plasma membrane without invoking additional unknown factors such as GDF-like activities.
One should however note that these calculations make several experimentally untested assumptions, crucially that recruitment rate of Cdc42 scales linearly with free Cdc42 concentration. Further assumptions include cellular concentration of GTPases, which likely varies across cell types, ignoring Cdc42 extraction rates from the membrane. One fundamental limitation in these estimations is that RhoGTPases are assumed to only bind to the plasma membrane and/or RhoGDI. However, in cells other binding partners such as effectors or other GDI family members such as RhoGDI2 likely interact with Cdc42. More importantly, the endomembrane surface area is likely much large than plasma membrane area[249], acting potentially as a large sink for GTPase localisation.

Conclusions and future directions

Membrane-based mechanism to modulate RhoGTPase recruitment

The data presented and discussed above sheds new light onto several questions in the RhoGTPase field. We show that dissociation of the RhoGTPase:RhoGDI complex occurs prior to the association of the GTPase to the membrane. Furthermore, there is no active mechanism mediated by GEF interaction which facilitates increase RhoGTPase recruitment. GEF interaction and subsequent GTPase activation occurs post membrane association. This suggests that the spatial and catalytic cycles are not coupled in the process of membrane recruitment. Furthermore, the inclusion of cell lysate seems to provide no GDF-like activity which would manifest in an increased RhoGTPase membrane recruitment rate. The conclusions drawn from this data support the proposed two step model, whereby the GTPase dissociates from RhoGDI, and GEF subsequently catalyses the exchange of nucleotide on the membrane surface[229].
One intriguing result of this work was that the inclusion of negative charge and lipid compositions mimicking the plasma membrane increase the loading rate of Cdc42. This suggests that manipulation of the plasma membrane in terms of composition, charge and local lipid concentration is a mechanism by which the cell can modulate RhoGTPase recruitment. As discussed in Figure 13 the interconversion of phosphoinositides is coupled to the presence of active Rho GTPases on the

membrane, via activation of lipid regulators[200–202]. Furthermore, phosphoinositides have been shown to phase separate in the plasma membrane[250–252] which could result in patches on the membrane of predominantly negatively charge lipids, which themselves can also recruit RhoGEFs[97,119,253]. This could be an interesting mechanism of positive feedback. As GTPases are recruited at an increased rate to regions of negative charge and phosphoinositides, along with GEFs, via their PH domains (discussed above), a pool of active GTPase could develop. These active GTPases could promote the production of specific phosphoinositide species via interaction with lipid regulators[201,202,254], in turn increasing GTPase recruitment further.

As discussed, RhoGTPases are a central regulator for the assembly of distinct actin networks. In the leading edge of the cell, one of the most distinctive features of the actin cytoskeleton is the development of large, flat lamellipodia (Figure 2). A feature of lamellipodia, indeed filopodia also, is a high surface to volume ratio. A mechanism based on intrinsic dissociation rates, such as the one proposed here, relies on where the thermodynamic balance regarding RhoGTPase association lies. Taking a sphere with an internal volume of that of a cell and corresponding RhoGTPase, GDI and lipid concentrations, the balance as discussed likely lies towards the association with GDI in the cytosol. However, by increasing the surface to volume ratio, such as that seen in lamellipodia, it is possible to raise the local concentration of lipids relative to RhoGDI, perhaps tipping the balance in favour of binding to the membrane, rather than re-binding to a GDI molecule (Figure 35).

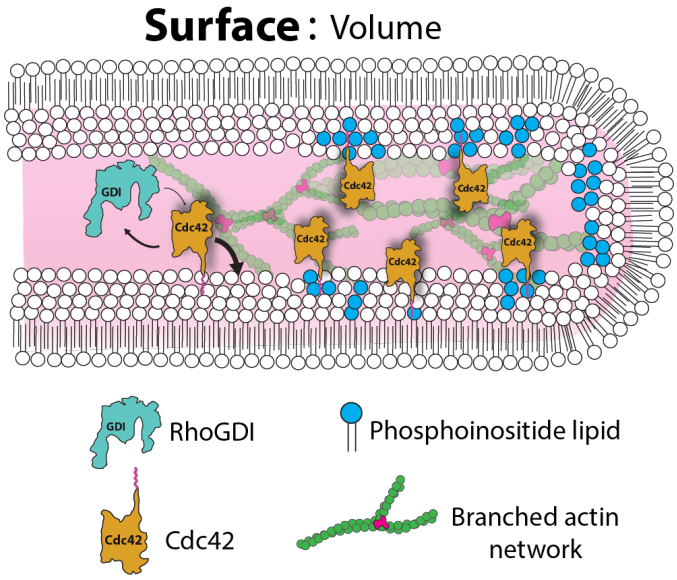

Figure 35. A dissociation limited loading model. In regions of increased local membrane concentration, such as seen in lamellipodial protrusions, this may tip the thermodynamic balance towards binding to the membrane rather than re-binding to RhoGDI (indicated by arrows) following complex dissociation. Increases in local concentrations in phosphoinositides (blue lipid), may provide the environment to increase recruit more GTPase due to increased negative charge. The presence of a protrusive actin network, as well as RhoGTPase effectors may serve to stabilise these recruited GTPases as well as rapid activation of the GTPase following membrane recruitment due to high local concentration of RhoGEF.

However, the increase in local membrane concentration may be much higher than the corresponding increase in GTPase landing rate, resulting in a reduction in the number of GTPase molecules per unit area. How can this be reconciled? It could be that the charge, and presence of specific phosphoinositides can indeed modulate the recruitment of RhoGTPases following dissociation from RhoGDI, in particular when in proximity to a membrane, in an area of high surface to volume ratio. Subsequently factors such as GEF-mediated activation, reduction in diffusion, interaction with actin cytoskeleton associated proteins or interaction with curvature sensing proteins then serve to stabilise the newly recruited GTPases, allowing for development of a polar site.

Probing GTPase recruitment in cellular environments

In addition to the methods described here, we have also developed sensors capable of detecting the activity state of the GTPase. Critically these sensors can detect the moment of nucleotide exchange, as well as visualising the inactive pool of RhoGTPases (unpublished data). Reconstitutions of the self-organising nature of the plasma membrane in literature[255] have also been established in the lab. The combination of these reconstituted systems provides an incredibly powerful and

dynamic toolkit to answer several unanswered questions. Firstly, data presented in this thesis suggests the existence of an inactive GTPase pool at the membrane. But how long do inactive RhoGTPases dwell at the membrane? It has been shown that RhoGDI can extract both inactive and active RhoGTPases from the membrane with remarkable little preference[38]. This suggests that inactive RhoGTPases could reside on the membrane prior to GEF-mediated activation or GAP-catalysed hydrolysis acting as a rapidly activatable pool. In reconstituting these loading events as presented in this work, along with activity sensors, it would be possible to visualise the populations of active and inactive RhoGTPases at the point of light mediated GEF recruitment.

Secondly, the use of such sensors under these reconstitutive conditions would allow visualisation of the catalytic progression of RhoGTPases. Do RhoGTPases undergo a single activation followed by inactivation and extraction? Or does the existence of an inactive pool at the membrane allow for multiple turnovers between active and inactive states?

Third, through the advanced single molecule tracking scripts utilised here, it is possible to understand the dynamics of individual RhoGTPases, or populations of RhoGTPases at the membrane. When combined with a self-organising membrane reconstitution, producing patches of different phosphoinositide species, it would be possible to understand recruitment dynamics spatially on a supported lipid bilayer and how they correspond with distinct phosphoinositide patterns.

Finally, by using the tools presented here, it is possible to test these in vitro observations in vivo. Pilot experiments utilising micro-injection of the complexes presented in this work have been visualised and tracked inside living cells. This will allow the probing of the recruitment dynamics not only in an in vivo environment, but will allow characterisation of landing events in distinct local within the cell such as lamellipodia or trailing edges.

Materials and Methods

Commercially available proteins and chemicals

Table 5. Commercially available proteins and chemicals

Protein / Chemical	Manufacturer / Supplier
1,2-dioleoyl-sn-glycero-3-[(N-(5-amino-1-carboxypentyl)iminodiacetic acid)succinyl] 18:1 DGS-NTA(Ni)	Avanti Polar lipids (Sigma-Aldrich (München))
1,2-dioleoyl-sn-glycero-3-phospho-L-serine 18:1 PS (DOPS)	Avanti Polar lipids (Sigma-Aldrich (München)
1,2-dioleoyl-sn-glycero-3-phosphoethanolamine 18:1 (Δ9-Cis) PE (DOPE)	Avanti Polar lipids (Sigma-Aldrich (München)
1,2-dioleoyl-sn-glycero-3-phosphoethanolamine-N-[methoxy(polyethylene glycol)-5000] 18:1 PEG5000 PE	Avanti Polar lipids (Sigma-Aldrich (München)
1,4 Dithiothreitol (DTT)	Gerbu biotechnik (Heidelberg)
2-Mercaptoethanol	Serva (Heidelberg)
2-propanol (for spectroscopy Uvasol)	Sigma-Aldrich (München)
3-phosphoglycerate	Sigma-Aldrich (München)
AccuPrimeTM Taq Polymerase	Thermo Fisher Scientific (München)
Adenosine 5' triphosphate disodium salt (ATP)	Sigma-Aldrich (München)
Alexa Fluor® 647-Maleimide (AF647)	Jena Bioscience (Jena)
Benzamidine	Thermo Fisher Scientific (München)
Blocker Casein (β-Casein)	Thermo Fisher Scientific (München)
Catalase	Sigma-Aldrich (München)
Chloroform	Sigma-Aldrich (München)
Cholesterol (ovine)	Avanti Polar lipids (Sigma-Aldrich (München))
Chymostatin	Sigma-Aldrich (München)
DMSO	Invitrogen ((Thermo Fisher Scientific (München))
EDTA	Gerbu (Heidelberg)
EDTA-Free cOmplete^{TM} protease inhibitor tablets	Roche (Basel)
EGTA	VWR (Solon, Ohio, USA)
Geranylgeranyl pyrophosphate ammonium salt	Sigma-Aldrich (München)
Glucose oxidase	Serva (Heidelberg)
Glucose	Sigma-Aldrich (München)
Glycerol	Gerbu (Heidelberg)
Guanosine 5′-triphosphate sodium salt hydrate (GTP)	Sigma-Aldrich (München)
Hellmanex III	Hellma GmbH (Müllheim)
Hydrogen peroxide	Roth (Gosen, IN, USA)
Imidazole	Fisher Scientifc (Schwerte)
L-α-phosphatidylcholine (PC, soy)	Avanti Polar lipids (Sigma-Aldrich (München)
L-α-phosphatidylinositol (Soy) (PI)	Avanti Polar lipids (Sigma-Aldrich (München)
L-α-phosphatidylinositol-4,5-bisphosphate (Brain, Porcine) (PI(4,5)P_2	Avanti Polar lipids (Sigma-Aldrich (München))
Leupeptin	Serva (Heidelberg)
PBS	Corning (Manassas, VA, USA)
PEG2000	Rapp Polymere GmbH (Tübingen)
Pepstatin	Roth (Gosen, IN, USA)
Peptides (general)	GenScript (Piscataway, NJ, USA)
Phosphatase inhibitor cocktail 2	Sigma-Aldrich (München)
Phosphatase inhibitor cocktail 3	Sigma-Aldrich (München)

Phosphocreatine	Sigma-Aldrich (München)
Sulpho-Cy3-NHS	Lumiprobe (Hannover)
Sulphuric acid	Sigma-Aldrich (München)
TCEP	Sigma-Aldrich (München)
Triethylamine	Sigma-Aldrich (München)

Material and Equipment

Table 6. Material and Equipment

3000 dionex Microfluidizer	Hyland Scientfic
AKTA pure system	GE Healthcare
AKTA purifier system	GE Healthcare
Centrifugal concentrator	Amicon
Detergent removal columns	Pierce
Diaphragm pump	KNF
HiPrep 26/10 column	GE Healthcare
HiTrap chelating column	GE Healthcare
Plasma cleaner	Plasma technology
Rotary evaporator	KNF
Superdex 75 10/300 GL increase	GE Healthcare
Superdex 75 XK 16/60	GE Healthcare
Superdex 200 XK 16/60	GE Healthcare
Superdex 200 XK 26/60	GE Healthcare
Tecan Spark plate reader	Tecan
Zeba Spin column	Thermo Fisher

Software, tools and databases

Table 7. Software, tools and databases

Adobe Illustrator	Adobe
ApE	M. Wayne Davis
CodonCode aligner	CodonCode corporation
Expasy-ProtParam	SIB, Swiss
ImageJ (Fiji)	Wayne Rasband, NIH-USA
Origin	Origin corporation
PDB	RSCB
Prism	Graphpad Software
PyMol	Schrödinger, LLC
Python	Python software foundation
R	R Core Team
Snapgene viewer	Insightful science
Trackmate	Jean-Yves Tinevez
UniProt	EMBL-EBI

Cell strains

Escherichia coli strains

XL10 Gold	Stratagene (San Diego, USA)
BL21 (DE3)	Thermo Fisher Scientific (München)
Rosetta	Novagen (Sigma-Aldrich (München))

Culture media

Table 8. Culture media

SOC	20 g/L BactoTrypton 5 g/L yeast extract 0.58 g/L NaCl 0.19 g KCl 2.03 g/L MgCl2x 6 H_2O 2.46 g/L MgSO4 x 7 H_2O 2 % Glucose
LB	10 g/L BactoTrypton 5 g/L yeast extract 10 g/L NaCl pH 7.4
TB	12 g/L BactoTrypton 24 g/L yeast extract 4 ml/L glycerin 2.31 g/L KH_2PO_4 12.54 g/L K_2HPO_4

Cloning and plasmids

Gibson assembly

Gibson assembly[256,257] was used to incorporate DNA fragments into the expression vector. Primers were designed with an overlap of 20-30 bp of adjacent DNA fragments to be combined, (DNA fragments generated from codon optimised sequences for bacterial expression, protein amino acid sequences from UniProt). Following PCR amplification of the plasmid backbone and Gibson-assembled insert, the DNA fragments, the backbone and primers (5 μL final volume) were mixed with 15 μL Gibson assembly mix (150 μL ISO buffer (100 mM Tris-HCl pH 7.5, 10 mM $MgCl_2$, 5 mM dNTP mix, 10 mM DTT, 6.25 mM PEG-8000, 1 mM NAD), 0.32 μL 10U/mL T5 exonuclease, 10 μL 2U/mL Phusion polymerase, 10 2U) and incubated for 1 h at 50 °C.

Table 9. Construct information

Construct	Source
pETMZ2-His6-zTag-TEV-Cdc42	P. Bieling
pETMZ2-RhoGDI1wt	P. Bieling
pETMSumoH10-His10-Sumo3-GGGGG-ITSN(DHPH 1229-1577)	P. Bieling
pETM66-NusA-His-TEV-SortaseA(delta59)	P. Bieling
pMal-C2-MBP-TEV-His6-TEV(Protein,S129V)-Arg6	S. Hansen

Table 10. Primer information

pETMZ2 Fwd	GCCTTCATCCAAAGTTTAAAAGA
pETMZ2 Rev	CAACTCAGCTTCCTTTCGGGC
pETM66SumoH10 Fwd	GGAAGTTCTGTTCCAGGGGCCCATGCAAGCTAAACCTCAAATTCC
pETM66SumoH10 Rev	GGTGGTGCTCGAGTGCGGCCGCTTATTTGACTTCTGTAGC
pMal Fwd	TCTTTATTTTCAGGGCCAT
pMal Rev	GCATCTAGAGGGCCCGGATCCTTA
T7 Promoter	TAATACGACTCACTATAGGG
T7 Terminator	GCTAGTTATTGCTCAGCGG

Agarose gel electrophoresis

Agarose gel electrophoresis was used to separate DNA strands based upon their size. An agarose gel of 1.5% (w/v) with TAE-buffer (40 mM Tris-acetate, 1 mM EDTA, 20 mM NaOAc), supplemented with RedSafe nucleic acid stain (50 μL/L) was prepared. All DNA samples were prepared in DNA loading buffer (5% Glycerol (w/v) 0.01% Bromophenol blue (w/v), 0.03% xylene cyanol, 10 mM EDTA) and loaded into the wells of the gel. The gel electrophoresis was run at 120 V. To determine fragment size, a 2-log DNA profile ladder was used as a reference and an image taken using a GelDoc XR system (Bio-Rad, Hurcules CA, USA). Bands of the desired size were excised from the gel with a scalpel and DNA recovered using the Zymoclean Gel DNA Recovery Kit (Zymo Research, Freiburg).

Bacterial transformations

Bacteria were transformed with plasmids via heat shock. Aliquots of culture to be transformed were thawed slowly on ice. DTT (70 mM) was added to the cells along with 1 μL of plasmid from mini prep (around 50 ng/μL) added and incubated on for 30 min. Cells were placed in a heat block at 42 °C for 45 – 60 s to heat shock the cells. Cells were then removed and placed back on ice for 3 min. 400 μL of SOC media (free from antibiotic) was added and incubated at 37 °C, 180 rpm for 1 hr. Cells were spun at max speed in a benchtop centrifuge for 30s to pellet the cells. 250 μL of media was removed and the cells resuspended in the remaining 150 μL which was spread-plated onto LB plates containing the appropriate antibiotics. Plates were incubated at 37 °C overnight. Plates were either stored at 4 °C.

Preparation of plasmids and measuring of DNA concentration.

To isolate DNA, single clones were selected from the agar plate and inoculated in 10 mL of LB medium, containing appropriated antibiotics, and incubated at 37 °C of 16 hours / over night. Following incubation, cultures were centrifuged at 4000 x g for 5 minutes and the pellet was processed to extract plasmid DNA using the NucleoSpin plasmid kit from Machery-Nagel. DNA concentration was measured by taking 260 nm absorbance values using the Nanodrop (Nanodrop ND1000).

DNA sequencing

DNA sequencing was performed by the Eurofins GATC sequencing service. The sequencing reaction was 2.5 μL DNA (50 – 200 ng/μL), 5 μL nuclease free water, and 2.5 μL primer (specific to sequencing, in this case T7 Reverse, see Table 10).

Expression from bacteria

For expression, a plate scrape was taken and added to 50 mL of TB media (including antibiotics where appropriate) in a baffled flask and incubated at 37 °C at 180 rpm. Once cell density had increase sufficiently (assessed by eye), media volume was expanded 3 – 5 times. This was repeated until desired volume was reached. At this point OD_{600} measurements were taken to ensure correct density prior to IPTG induction.

Protein purifications

Purification of Cdc42

BL21(DE) cells were transformed (as above) with WT Cdc42, grown to an OD_{600} of 1.0 – 1.2 and were induced with 1 mM IPTG at 37 °C for 4 hr. Cells were centrifuged at 4000 x g for 20 min, supernatant removed and the pellet was flash frozen in liquid nitrogen and stored at -80 °C. Three times pellet volume of lysis buffer (100 mM KPi pH 7.4, 400 mM NaCl, 5 mM $MgCl_2$, 0.1 mM GDP, 0.5 mM β-mercaptoethanol, 1 mM PMSF and 0.1 – 1 g of DNAse) was added and the pellets were placed in warm water ~ 20 °C until thawed. Once thawed the pellet was resuspended and homogenised using the EmulsiFlex-C5 (1 cycle between 5000 and 15000 psi). The homogenised lysate was spun at 35000 x g for 60 min at 4 °C following which the supernatant was removed and filtered through a 0.45 μm filter. The filtered supernatant was recirculated

at 4 °C over a HiTrap chelating column loaded with 200 mM cobalt chloride and equilibrated in wash buffer (100 mM KPi pH 7.4, 400 mM NaCl, 5 mM $MgCl_2$, 0.1 mM GDP and 0.5 mM β-mercaptoethanol). After 2 hours of recirculation, the column was removed and attached to the Akta pure purification system. The column was washed using wash buffer until baseline mAU was reached (around 5 column volumes). A gradient elution was run with increasing % of elution buffer (100 mM KPi pH 7.4, 400 mM NaCl, 5 mM $MgCl_2$, 500 mM Imidazole, 0.1 mM GDP and 0.5 mM β-mercaptoethanol) resulting in a 0 – 500mM gradient of imidazole over 6 column volumes. Peak fractions were pooled and TEV protease (1:30 TEV:Cdc42) was added to cleave the affinity tag and incubated overnight at 4 °C. Lysate was concentrated using a Vivaspin 10kDa MWCO concentration system and desalted into wash buffer using a HiPrep26/10 desalting column. The HiTrap chelating column was re-equilibrated into wash buffer and the lysate once again re-circulated over the column to remove the tag leaving only cleaved protein in the flow through. The recirculated lysate was then gel filtered using the Superdex 75 16/60, pre equilibrated in gel filtration buffer (100 mM KPi pH 7.4, 150 mM NaCl, 2 mM $MgCl_2$, 0.5 mM TCEP) and the Cdc42 peak was collected, pooled and concentrated as above. Glycerol was added to a final concentration of 20% v/v and the protein aliquoted, snap frozen using liquid nitrogen and stored at -80 °C.

Purification of GDI

Rosetta cells were transformed as above and grown to an OD_{600} of 1.0 and induced using 0.25 mM IPTG overnight at 16°C. GDI was purified much the same as Cdc42 above, however with the following changes. The lysis buffer used was altered to 50 mM KPi pH 8.0, 400 mM KCl, 1 mM EDTA, 1 mM benzamidine, 5 mM β-mercaptoethanol and 1 mM PMSF and 0.1 – 1 g of DNAse. Rather than HiTrap chelating columns, supernatants were recirculated on a GST column equilibrated in GDI wash buffer (50 mM KPi pH 8.0, 400 mM KCl, 1 mM EDTA, 5 mM β-mercaptoethanol, 1 mM benzamidine). Elution from the GST column was completed via a single step elution rather than a gradient using GDI elution buffer (50 mM KPi pH 8.0, 400 mM KCl, 1 mM EDTA, 10 mM reduced glutathione, 1 mM benzamidine and 5 mM β-mercaptoethanol). Cleaving of the GST tag was achieved using PreScission protease (1:30 as previous) overnight in 10000 MWCO dialysis tubing, dialysing against dialysis buffer (50 mM KPi pH 8.0, 400 mM KCl, 1 mM EDTA, 5 mM β-

mercaptoethanol, 1 mM benzamidine). The protein was then recirculated over a GST Sepharose column equilibrated in wash buffer (50 mM KPi pH 8.0, 400 mM KCl, 1 mM EDTA, 5 mM β-mercaptoethanol, 1 mM benzamidine) and the flow through was concentrated as previously described and gel filtered using a SD75 16/60 column equilibrated in GDI storage buffer (20 mM KPi pH 8.0, 150 mM KCl, 0.5 mM TCEP, 20% v/v glycerol). Concentration and storage was completed as described preciously.

Purification of Intersectin

BL21 (DE3) cells were transformed with Intersectin (ITSN-DH-PH-HIS_{10}) and cultured at 37 °C, 180 rpm to an OD_{600} of 1.0 was reached. Cells were induced with 0.25 mM IPTG and left shaking overnight at 18 °C. Cultures were centrifuged at 4000 x g for 20 min, supernatant removed, pellets flash frozen with liquid nitrogen and stored at -80°C. Purification was as outlined in Cdc42 with the following changes. For cell lysis (lysis buffer (50 mM Kpi pH 7.3, 400 mM NaCl, 0.5 mM β-mercaptoethanol, 2 mM PMSF, 15 mM benzamidine and 0.1 – 1 g DNAse)), 2 passes on the Emulsiflex were used. Recirculation was completed with wash buffer (50 mM Kpi pH 7.3, 400 mM NaCl, 0.5 mM β-mercaptoethanol, 15 mM benzamidine). In elution, a gradient of 0 – 45% elution buffer (50 mM Kpi pH 7.3, 400 mM NaCl, 500 mM imidazole, 0.75 mM β-mercaptoethanol, 15 mM benzamidine) was used, over 8 column volumes. Peak fractions were pooled and TEV protease (1:10 SenP2:ITSN) was added to cleave the affinity tag and incubated overnight at 4 °C. Lysate was concentrated using a Vivaspin 10kDa MWCO concentration system and desalted into wash buffer (50 mM Kpi pH 7.3, 400 mM NaCl, 0.5 mM β-mercaptoethanol, 15 mM benzamidine) using a HiPrep26/10 desalting column. The lysate was then gel filtered using the Superdex 200 16/60, pre equilibrated in gel filtration buffer (20 mM HEPES 7.5, 150 mM NaCl, 0.5 mM TCEP) and the Cdc42 peak was collected, pooled and concentrated as above. The ITSN peak was collected, pooled and concentrated as above. Glycerol was added to a final concentration of 20% v/v and the protein aliquoted, snap frozen using liquid nitrogen and stored at -80 °C.

Purification of Sortase

BL21(DE3) cells were transformed with NusA-Sortase and cultured at 37 °C and 180 rpm until and OD_{600} 0.8. Cells were induced with 0.25 mM IPTG for 6 hr at 30 °C 180 rpm. Cells were harvested by centrifugation at 4000 x g, supernatant removed and

pellets snap frozen in liquid nitrogen. Sortase was purified as outlined for Cdc42 with the following changes. The buffer used for cell lysis was 50mM KPO_4 pH 7.5, 400 mM NaCl, 0.75 mM β-mercaptoethanol a 0.1 – 1 g DNase, 1mM PMSF. A one step elution of 100% elution buffer (was used 50mM KPO_4 pH 7.5, 400 mM imidazole, 400 mM NaCl, 0.75 mM β-mercaptoethanol). Concentration of the lysate was achieved using a 50000 Da MWCO centrifugal concentrator. Gel filtration used the Superdex 200 XK26/60 column. The peak fraction was pooled and concentrated as described in Cdc42 purification methods however using sortase storage buffer (20 mM HEPES, pH 7.5, 150 mM KCl, 0.5 mM DTT 20% v/v glycerol.

Purification of GGTase1

BL21(DE3) cells were transformed and cultured at 37 °C and 180 rpm until and OD_{600} 0.8. Cells were induced with 0.25 mM IPTG overnight at 18 °C 180 rpm. Cells were centrifuged at 4000 x g for 20 min, supernatant removed, and the pellet was flash frozen in liquid nitrogen and stored at -80 °C. Three times pellet volume of lysis buffer (50 mM KPi pH 8.0, 300 mM NaCl, 2 mM $MgCl_2$, 0.1 mM β-mercaptoethanol, 1 mM PMSF and 0.1 – 1 g of DNAse, and cOmplete protease inhibitor tablets (1 per 50 mL)) was added and the pellets were placed in warm water ~ 20 °C until thawed. Once thawed the pellet was resuspended and homogenised using the EmulsiFlex-C5 (1 cycle between 5000 and 15000 psi). The homogenised lysate was spun at 35000 x g for 60 min at 4 °C following which the supernatant was removed and filtered through a 0.45 μm filter. The filtered supernatant was recirculated at 4 °C over a HiTrap chelating column loaded with 200 mM cobalt chloride and equilibrated in wash buffer (50 mM KPi pH 8.0, 300 mM NaCl, 2 mM $MgCl_2$, 0.1 mM β-mercaptoethanol, 10 mM imidazole). After 2 hours of recirculation, the column was removed and attached to the Akta pure purification system. The column was washed using wash buffer until baseline mAU was reached (around 5 column volumes). A gradient elution was run with increasing % of elution buffer (50 mM KPi pH 8.0, 300 mM NaCl, 2 mM $MgCl_2$, 0.1 mM β-mercaptoethanol, 500 mM imidazole) resulting in a 10 – 500mM gradient of imidazole over 6 column volumes. The peak fractions were pooled and incubated with 30 mM $ZnCl_2$ overnight, on ice. Lysate was concentrated using a Vivaspin 10kDa MWCO concentration system and ran over a size exclusion chromatography column (S200 26/60) equilibrated in SEC buffer (50 mM HEPES pH 7.5, 200 mM NaCl, 2 mM $MgCl_2$, 2 mM DTT), peak fractions were pooled and the protein was recirculated on a

GST column (equilibrated in SEC buffer) overnight at 4 °C. The GSH column was washed until baseline on the Akta system, then the protein eluted with GST elution buffer (50 mM HEPES pH 7.5, 200 mM NaCl, 200 mM Glutathion, 2 mM $MgCl_2$, 2 mM DTT) and the peak fractions were pooled and concentrated as above. A final gel filtration step using a HiPrep 26/10 column facilitated buffer exchange into storage buffer (50 mM HEPES pH 7.5, 200 mM NaCl, 2 mM $MgCl_2$, 0.5 mM TCEP, 20 % (v/v) glycerol) an alliquotes were snap frozen in liquid nitrogen and stored at -80 °C.

Production of a labelled Cdc42:RhoGDI complex

In vitro prenylation of Cdc42

Cdc42 was purified from bacterial expression, therefore required prenylation of the C-terminus to be completed in vitro as bacteria lack the machinery to complete this in vivo. Reactants were added to prenylation reaction buffer (50 mM HEPES pH 7.5, 50 mM NaCl, 2 mM $MgCl_2$, 2% w/v CHAPS and 2 mM DTT) in the following order. $ZnSO_4$ (10 μM) Glycerol (10% v/v) Cdc42 (57.9 μM) GGTase1 (9 μM) Geranylgeranyl pyrophosphate (GGPP) (148 μM). Concentrations of the Cdc42, GGPP and GGTase1 can be varied, but the ratio was kept constant between these three components. The reaction was rotated in a glass bottle, on a disc rotator at 4 °C overnight. Following incubation, the prenylation reaction was gel filtered using the Superdex 75 16/60 column pre-equilibrated in prenylation buffer (50 mM HEPES pH 7.5, 50 mM NaCl, 2 mM $MgCl_2$, 0.5% w/v CHAPS and 2 mM DTT). The peak fractions were collected, pooled and concentrated using a 5 kDa MWKO centrifugal concentrator to < 250 μL.

Dye conjugate formation

Prior to sortase mediated peptide ligation, SulphoCy3 dye with an NHS ester reactive group was conjugated to the primary amine of an LPETGG peptide. Dye was dissolved in DMSO to a final concentration of 80 mM. Peptide was also dissolved into DMSO at a final concentration of 40 mM. Triethylamine was added to the peptide stock at a final concentration of 60 mM. Dye and peptide was combined at a 2:1 ratio respectively and incubated at 42 °C in a heat block, shaking at 750 rpm. The reaction was quenched with a final concentration of 100 mM TRIS (pH 8.0) and incubated as above for a further 5 hours. After incubation, the dye conjugated was stored at -20 °C.

Note: In single molecule control experiments, the biotin handle was incorporated at this point, with the use of a CLPETGG peptide. This allows for maleimide labelling of

the Cy3-peptide with Biotin-PEG11-maleimide at the reactive Cys. Maleimide labelling conditions outlined below for GDI, but briefly, Peptide was mixed with a 6 fold molar excess biotin-Peg11-maleimide in labelling buffer (50 mM HEPES pH 7.5, 50 mM NaCl and 2 mM MgCl2). The reaction was incubated at 16 °C in a heat block while shaking at 750 rpm. To quench the reaction, DTT was added to a final concentration of 10 mM.

Sortase mediated peptide ligation to N terminus of Cdc42

Prenylated Cdc42 was labelled with Sulpho-Cy3-LPETGG at its N-terminus using sortase. It was found that increasing the concentrations of these components maximised labelling ratio. But as a rule, concentration of sortase should be 1/3 of substrate (Cdc42) concentration (minimum 10 μM). The Dye-peptide should be 4 – 10 fold excess over substrate (minimum of 500 μM), in these experiments, 6 fold excess was used. For gel filtration a final target volume of 500 μL was used. The reaction was mixed as follows. Cdc42 (440 μM), Sulpho-Cy3-LPETGG (2640 μM), $CaCl_2$ (6 μM), Tris pH 8 (126.5 μM) were mixed in labelling buffer (150 mM KCl pH 8.0, 0.5 mM TCEP). Finally, sortase (146.7 μM) was added and the reaction incubated overnight at 16 °C spinning at 16000 x g. Following centrifugation, the labelling reaction was gel filtered using a Superdex 75 10/300 column equilibrated in prenylation buffer (50 mM HEPES pH 7.5, 50 mM NaCl, 2 mM $MgCl_2$, 0.5% w/v CHAPS and 2 mM DTT). Labelled protein was tracked using 280 nm and 555 nm absorbance, this gives three peaks; labelled sortase, labelled Cdc42 and residual labelled peptide. The Cdc42 peak was separated, pooled and concentrated using a 5000 Da MWCO centrifugal concentrator to a volume of 150 – 250 μL.

Maleimide labelling of RhoGDI

RhoGDI was labelled by exploiting the exposed reactive cystine (Cys78) to attach maleimide AF647. GDI was mixed with a 6 fold molar excess dye in labelling buffer (50 mM HEPES pH 7.5, 50 mM NaCl and 2 mM $MgCl_2$). The reaction was incubated at 16 °C in a heat block while shaking at 750 rpm. To quench the reaction, DTT was added to a final concentration of 10 mM. The reaction mix was gel filtered over a Superdex 75 10/300 column pre-equilibrated in GDI gel filtration buffer (50 mM HEPES pH 7.5, 50 mM NaCl, 2 mM $MgCl_2$, and 2 mM DTT). Labelled GDI peak was selected by monitoring of absorbance of 280 and 650 nm, pooled and concentrated using a 5000 Da MWCO centrifugal concentrator to a final volume of 150 – 250 μL.

Assembly of the Cdc42 and RhoGDI complex

To produce the dual labelled complex the Cy3-Cdc42:RhoGDI-AF647, the complex was mixed at a 1:1 molar ratio and gel filtered using a Superdex 75 10/300 column pre-equilibrated in gel filtration buffer (50 mM HEPES pH 7.5, 50 mM NaCl, 2 mM $MgCl_2$, and 2 mM DTT). The lack of detergent in the buffer combined with the hydrophobicity of the prenyl tail of the Cdc42 drives complex formation with RhoGDI. Peak fraction was detected by monitoring 280, 555 and 650 nm. The peak was pooled and concentrated using a 5000 Da MWKO centrifugal concentrator to 200 – 400 μL. To ensure complete detergent removal, the complex was passed over detergent removal columns (Pierce). To prepare the columns they were spun at 1500 x g for 60 s to remove storage buffer. 300 uL of gel filtration buffer (50 mM HEPES pH 7.5, 50 mM NaCl, 2 mM $MgCl_2$, and 2 mM DTT) containing 20% glycerol was added and spun as above. This was repeated a total of 3 times. 300 μL gel filtration buffer 20% glycerol was added with additional 0.5 mg/mL beta casein was added to saturate the column to prevent non-specific protein binding. Beta casein was incubated at RT for 1 min then spun at 1500 x g for 2 min. Following this, washing was repeated 3 times as above. Complex (100 μL maximum) per column was added and incubated for 1 min. Columns were then spun at 1500 x g for 2 min. The sample was added to a second column (prepared as above) and spun once more ensuring total detergent removal. Finally, concentration and labelling ratio was calculated by absorbance measurements using the Nanodrop (Nanodrop ND-1000) using the equations below. Samples were snap frozen in liquid nitrogen and stored at -80 °C.

Eq.1

$$Total\ protein\ concetration\ (M) = \frac{(Abs_{280} - Abs_{650} * C.F._{AF647} - Abs_{555} * C.F._{sulfoCy3})}{\varepsilon_{280}}$$

Eq. 2

$$SulphoCy3\ concetration\ (M) = \frac{Abs_{555}}{\varepsilon_{sulphoCy3}}$$

Eq. 3

$$AF647\ concetration\ (M) = \frac{Abs_{647}}{\varepsilon_{AF647}}$$

SDS-PAGE gel

12% SDS-PAGE gels were cast and samples loaded in SDS loading buffer (50 mM Tris pH6.8, 2% (w/v) SDS, 1 mM EDTA, 0.1 mM DTT, 0.1% (w/v) Bromophenol Blue,

10% (v/v) glycercol). The sample was incubated ay 97 °C for 2 mins and spun at max speed in a benchtop centrifuge for 3 min at room temperature before being added to the wells of the gel. Gels were run in MES or MOPS running buffer (50 mM MES/MOPS, 50 mM Tris base, 1 mM EDTA, 0.01% (w/v) SDS, 5 $NaHSO_3$) depending on MW. In addition to samples, Precision Plus MW marker (BioRad) was run to serve as a molecular weight reference. SDS-PAGE was run at 180 V for around 1 hour using a Mini-PROTEAN Tetra Cell System (BioRad).

Preparation of cell lysate

Pig brains were collected fresh from the slaughterhouse on the day of preparation, this is essential for the best results. As quickly as possible they were placed in ice cold PBS and stored on ice. Brains were peeled to remove Meninges membrane and attached blood vessels of both the brain hemispheres as well as the cerebellum. Once peeled, the brains (around 200 g was used in this prep) were placed into a blender along with 200 mL of extraction buffer (20 mM HEPES pH 7.4, 100 mM KCl, 1 mM EGTA, 0.1 mM EDTA, 2 mM $MgCl_2$ 2.5 mM DTT, 0.5 mM ATP, 10 mM Leupetin, 10 mM Pepstatin, 10 mM Chymostatin, cOmplete protease inhibitor tablets (1 per 50 mL) and phosphatase inhibitor cocktail 2 + 3, 4μL per mL). The brains were blended on the lowest setting for 1 min and then the blender container was placed in ice for 3 min. Following this, the container was placed back on the blender and switched to high powers for 40 s then quickly placed back on ice for 3 min. This was repeated two more times.

Note: The blending process generates a lot of heat, but it is important that the blended brain slurry does not get hot. To assist in this all work was carried out in the cold lab (4 °C) and a thermometer was used to measure the slurry temperature as the container was placed on ice. Ideally the slurry should be as cold as possible but a target of <30 °C was used.

Following blending, fresh DTT was added to a final concentration of 2.5 mM and the slurry was spun at 20000 x g, 4 °C for 30 min. The SN was decanted through a nylon cheesecloth filter into a clean beaker (on ice). The SN was then spun once more at 142000 x g at 4°C for 45 min. The SN was then added to 10000 MWCO dialysis tubing and dialysed against extraction buffer (20 mM HEPES pH 7.4, 100 mM KCl, 1 mM EGTA, 0.1 mM EGTA, 2 mM $MgCl_2$ 2.5 mM DTT, 0.5 mM ATP) containing 50% glycerol while stirring continuously at 4 °C to a final volume of around 50 mL.

Note: during the dialysis process, due to the high concentration of glycerol, mixing via inversion was also required. This was achieved by placing parafilm over the cylinder used for dialysis and inverting 3 – 5 times. This was repeated every 10 – 15 min.
Once at the desired concentration, the lysate was aliquoted and snap frozen in liquid nitrogen and stored at -80 °C.

FRET based dissociation assays

FRET based dissociation assays were completed taking a dark chase strategy. 80 nM of Cy3-Cdc42 was complexed in situ with 120 nM of AF647-RhoGDI in GEF buffer (50 mM HEPES pH 7.5, 50 mM NaCl, 2 mM $MgCl_2$, 10 mg/mL blocker casein, 1 mM β-mercaptoethanol) in a quartz cuvette (previously washing in nitric acid, rinsed in water, and dried with nitrogen). Ratiometric FRET was measured by exciting Cy3 (550 nm) and measuring Cy3 emission (563 nm) and AF647 emission (665 nm) using the PTI photospectrophotometer (Photon Technology International, Birmingham NJ, USA). Once a baseline was established, 5000 nM unlabelled RhoGDI was added and the FRET signal was measured at intervals of 2 s for 20000 s. Data was fit with a two-component decay fit in Prism (GraphPad software).

Nucleotide exchange and GEF assays

Cdc42 was mixed with a 5 X molar excess of Mant nucleotide (Jena Bioscience, Jena) in nucleotide exchange buffer (20 mM HEPES pH 7.5, 50 mM NaCl) (- Mg). To this EDTA was added to an equimolar concentration of the magnesium present in the storage buffer of Cdc42. The reaction was then incubated at RT for 1 hour after which $MgCl_2$ was added to a final concentration matching the EDTA added in the previous step. The reaction was then passed over two Zeba 5kDa MWCO columns equilibrated in the desired GTPase storage buffer, (20 mM HEPES pH 7.5, 50 mM NaCl, 2 mM $MgCl_2$, 0.5 mM β-mercaptoethanol) to remove excess unbound nucleotide. Cdc42 was then concentrated using Amicon 5 kDa MWCO centrifugal concentrators to the desired volume, 20% glycerol was added and then aliquots were snap frozen and stored at –80 °C.
To perform GEF assays, 120 nM of Cdc42 alone, or in complex with RhoGDI was added along with a final concentration of 1.167 μM Mant GTP in GEF buffer (50 mM HEPES pH 7.5, 50 mM NaCl, 2 mM $MgCl_2$, 1 mM β-mercaptoethanol) . The nucleotide exchange was stimulated by the addition of 1.6 nM of ITSN-DH-PH and mant

fluorescence measured (365 nm Ex, 440 nm Em) every 5 s for 5000 s using the TECAN plate reader (Tecan life sciences Männedorf, Switzerland).

Glass preparation for single molecule

Water source

To prevent contamination in the lipid preparation it is imperative that all glass which comes into contact with lipids is extremely clean. This begins with the water source used throughout this process. Here a Millipore IQ7003 is with a LC-Pak UHPLC grade filter is used to produce ultra-pure water from a lab water source. It should be noted that many water purification systems draw from deionised water supplies. In this work, this was found to be a source of auto-fluorescent contamination as the cleanliness of the pipes and lines of the deionised water source could not be determined. Once a clean water source was identified, this source was used for any rinsing steps and to prepare buffers and cleaning reagents.

General glassware

All general glassware such as beakers, measuring cylinders, slide holders, round bottom flasks and rotary evaporator tips were treated in the same way for washing. Glass was washed extensively (at least five times) in ultrapure water from the milipore system outlined above. Then glass was submerged (or filled in the case of beakers) in 5% Helmenex III for 45 mins at 60 °C in a dry oven. Once removed from the oven, glass was rinsed once again, five times more in ultrapure water. Next, glass was submerged or filled with 50% 2-propanol 50% ultrapure water and sonicated for 30 min. After sonication, glass was removed and rinsed a final five times with ultrapure water and place back in the dry oven at 60 °C to completely dry.

Lipid glassware

Lipid glassware is glass which comes into direct contact with lipids, this includes round bottomed flasks, glass coverslips, extruder needles (glass parts only for the needles, tips are removed, however Teflon parts are included). Round bottom flasks are washed as described in general glassware above, however, once rinsed and dried, both the flask and stoppers are filled and submerged in piranha solution (5 parts sulphuric acid to 3 parts hydrogen peroxide 30%)) for 90 min. Carefully remove the flasks using clean forceps and submerge in a clean beaker containing ultrapure water.

Rinse the flasks and stoppers five times with ultrapure water and place in a clean beaker in the 60 °C dry oven to dry overnight. The extruder parts were rinsed in ultrapure water five times then placed in 50% 2-propanol 50% ultrapure water and sonicated for 30 min then rinsed five times in ultrapure water prior to use. Prior to their first use, extruder parts were washed as described, however, the glass parts of the cylinder and the Teflon parts of the extruder were placed in piranha solution (5 parts sulphuric acid to 3 parts H_20_2) for 30 minutes being careful to avoid the metal collar touching the piranha solution as this will corrode. After 30 min the parts were removed and submerged in a clean beaker of ultrapure water and rinsed five more times with ultrapure water. It should be noted that all glassware that is used here should not have been in contact with any fluorescent labels or fluorescently tagged protein. Separate glass stocks are kept for labelled lipid and/or protein work as any trace contamination makes identifying single molecules from fluorescing dirt contamination incredible difficult.

Preparation of supported lipid bilayers

Lipid preparation

All lipids used in this work were supplied by Avanti lipids product numbers are provided where possible however, in some cases special orders were made of high-grade lipids, this will be made clear where appropriate. The composition of the lipid mixtures is outlined in Table 11, however in all cases preparation is the same. 1 mL of chloroform is used to rinse the inside of the cleaned round bottomed flask and then removed. Fresh chloroform is added (volume dependent on lipid mixture and final desired volume. Once all the desired lipid species are added, the flask is gently swirled for a few seconds and then attached to the tip of the rotary evaporator (KNF RC900). The water bath of the evaporator was set to 42 °C, and the flask was set to rotate at 110 rpm just above (around 5 – 10 mm) the water. A vacuum was drawn as the flask is rotating, whilst carefully watching the lipids in the flask. As soon as the lipids turn milky, the flask was lowered into the water, keeping the waterline level with the lipid watermark. This rotary evaporator has an automatic setting which detects the boil point of the chloroform during evaporation and holds the pressure as the evaporation takes place. If the evaporator doesn't have this function then one should watch the lipids to ensure they do not over boil. If boiling begins, lift the flask out of the water bath. If this does not eradicate the boil, gently release some pressure using the pressure release

valve or pause the pump (system dependent). It was found that using a diaphragm pump (KNF RC920 G) (yields the best results as this prevents any air reflux during the process. Once all the chloroform was evaporated, the vacuum was released slowly whilst still rotating the flask at a rate of around 10 mbar s^{-1}. Once removed from the rotary evaporator, the flask was placed in the desiccator for 20 min, using the full power of the pump. Once again the pressure was released slowly and the lipid resuspended in PBS and gently vortexed (lowest setting) for 2 min. During Vortexing, the flask is gently rotated ensuing that all of the lipids were rehydrated in PBS. After 2 min the lipids appeared cloudy and were ready to extrude. Prior to extrusion, the extruder needles were rinsed three times with PBS. The filter supports and the 30 nm filter were also rinsed with PBS. Once assembled, 5 passes of PBS were made to ensure the filter and its supports are saturated. The lipid was pushed through the extruder 11 times. It is important to keep one syringe for crude lipid uptake and the other for the clarified lipid (hence the odd number of extrusion passes) as this prevents larger, non-clarified lipid vesicle contamination. Once extruded lipids are transferred to small brown glass bottles (Roth), screwed tightly closed and stored at 4 °C for 2 – 7 days depending on the lipid, PC compositions are stable for < 7 days, MM and PM 3 – 4 days maximum.

Table 11. Supported lipid bilayer composition

Lipid mix	Lipid	Molar fraction (%)
Neutral charge	L-α-phosphatidylcholine (PC, soy)	99.75
	1,2-dioleoyl-sn-glycero-3-[(N-(5-amino-1-carboxypentyl)iminodiacetic acid)succinyl] 18:1 DGS-NTA(Ni)	0.25
Strong negative charge	L-α-phosphatidylcholine (PC, soy)	47.25
	1,2-dioleoyl-sn-glycero-3-[(N-(5-amino-1-carboxypentyl)iminodiacetic acid)succinyl] 18:1 DGS-NTA(Ni)	0.25
	L-α-phosphatidylinositol (Soy) (PI)	48.0
	L-α-phosphatidylinositol-4,5-bisphosphate (Brain, Porcine) ($PI(4,5)P_2$)	4.0
	1,2-dioleoyl-sn-glycero-3-phosphoethanolamine-N-[methoxy(polyethylene glycol)-5000] 18:1 PEG5000 PE	0.5
Plasma membrane mimic	L-α-phosphatidylcholine (PC, soy)	26.25
	1,2-dioleoyl-sn-glycero-3-[(N-(5-amino-1-carboxypentyl)iminodiacetic acid)succinyl] 18:1 DGS-NTA(Ni)	0.25
	L-α-phosphatidylinositol-4,5-bisphosphate (Brain, Porcine) ($PI(4,5)P_2$)	4.0
	1,2-dioleoyl-sn-glycero-3-phosphoethanolamine-N-[methoxy(polyethylene glycol)-5000] 18:1 PEG5000 PE	0.5

	1,2-dioleoyl-sn-glycero-3-phospho-L-serine 18:1 PS (DOPS)	22.5
	1,2-dioleoyl-sn-glycero-3-phosphoethanolamine 18:1 (Δ9-Cis) PE (DOPE)	26.5
	Cholesterol (ovine)	20
Note: All compositions to a final concentration of 1 mM in chloroform.		

SLB chamber preparation

Coverslips were prepared by submerged in 5% Hellmenex III for 45 min at 60 °C. After heating the slides were removed from the dry oven and rinsed five times with ultrapure water. Slides were then placed in piranha solution (5 parts sulphuric acid to 3 parts H_20_2) and left overnight. The following day, slides were removed and submerged in ultrapure water and rinsed five times. Once rinsed, coverslips were dried with a gentle flow of argon, the water should run off in a film leaving behind the clean glass. Imbdi chambers (sticky slides IV) were placed in a plasma cleaner (Flecto 10, Plasma technology), cleaned for 3 min and attached to the clean coverslip, adhesion was ensured by using a cotton bud to gently apply pressure to the adhesive.

SLB formation

Once the chambers are assembled and the lipids are prepared SLB formation could begin. Lipids were diluted to a final concentration of 250 μM (1/4 from a 1 mM stock) in PBS. Chambers were placed on a pre-heated metal block at 45 °C for 2.5 min. Lipids were added to the chambers and incubated for 2.5 min. 500 mM NaCl was added to the chamber and pipetted gently from each end to ensure mixing. Chambers were then incubated for 30 min at 45 °C. Following incubation, chambers were washed, each with 5 mL of PBS followed by 1 mL of GEF buffer (50 mM HEPES pH 7.5, 50 mM NaCl and 2 mM $MgCl_2$). The heat block was then turned off however, critically, the chambers were not removed, they are left until the heat block has cooled to RT. This slow decrease in temperature is critical to ensure fluid bilayer formation. The heat shock of removing the chamber too early will cause disintegration of the bilayer.

Lipid coated bead preparation

150 μL of 3 μm bead slurry (Bangs Laboratory, Indiana, USA) was added to 1 mL of nitric acid in a glass vial and incubated overnight. The vial was placed inside of a 50 mL falcon and spun at 200 x g for 4 min at RT. Nitric acid was apricated, being careful

not to disturb the bead pellet. Beads were resuspended in 1 mL MilliQ water, vortexed at full speed for 10 s and transferred to a 1.5 mL epi. Beads were spun in a tabletop microcentrifuge at 200 x g for 2 min at RT. SN was aspirated, 1 mL of MilliQ added and resuspended by vortex, max speed, 10 s. Centrifugation, SN aspiration and resuspension were repeated a further two times, however on the final resuspension, beads were resuspended in 500 μL of 20 mM HEPES (pH 7.0) prior to the final vortex step, after which, the resuspension was transferred to a new 1.5 mL epi. Suspension was spun in a tabletop microcentrifuge at 200 x g for 2 min at RT, SN aspirated, and beads were resuspended in 150 μL of MilliQ water. 50 μL of PBS was added, and the beads were sonicated for 10 mins in the sonicator bath. 400 mL of lipid mix was added, and tubes rotated using an epi rotator for 30 min.

Note: The total volume at this point is 600 μL, in a 1.5 mL epi this will cause the solution to move up and down as the epi inverts. This should be avoided as it will cause the beads to clump. Therefore, the bead suspension should be split over more epis with a maximal volume of 150 μL.

Following rotation, 750 μL MilliQ water was added gently and beads were resuspended using cut tips. Beads were spun in a tabletop microcentrifuge at 200 x g for 1 min at RT, SN was aspirated and the resuspension and centrifuging steps were repeated a further 4 times. On the final resuspension step, beads were resuspended in 200 μL PBS (as the reactions were split into multiple tubes earlier, at this stage all beads (of the same lipid composition) should be recombined into the final 200 μL volume).

Optional step: If the experiment required GEF localisation to the bead then GEF at the desired concentration was incubated with the beads while rotating (max 150 μL per epi) for 1 h. Following incubation, beads were spun slowly (50 x g, for 60 s at RT) and SN was carefully removed. Any reactions that were split were re-combined and resuspended in 200 μL of assay buffer using cut tips.

Preparation of PEG glass slides

Cleaning

Coverslip glass was marked using a diamond knife in such a way that the functionalised side could be identified, in this case a small, asymmetric corner was removed with a diamond knife and any dust was removed using a Kimtech tissue. Coverslips were submerged in 3M NaOH and sonicated for 5 min using an ultrasound

water bath. Coverslips were carefully removed and submerged in ultrapure water and rinsed 5 – 6 times with ultrapure water. Once rinsed the coverslips were arranged in a Teflon rack and placed in a beaker. Freshly prepared "Piranha solution" (5 parts sulphuric acid to 3 parts hydrogen peroxide 30%) was added to the beaker ensuring to completely submerge the coverslips and incubated in the fume hood for 40 min.

Note: It should be noted that Piranha solution is incredibly corrosive, hot, volatile and potentially explosive. Work should always be carried out under the fume hood with lab coat, eye protection, face shield, acid apron and acid gauntlets. Handling of glass should be achieved with long forceps. All beakers should have redundancy in place so if cracking of the glass should occur, there is a system whereby large spills are prevented.

Coverslips were carefully removed from the Piranha solution and placed in ultrapure water and were washed with ultrapure water 3 times, sonicated in ultrapure water in the water bath for and rinsed 3 more times with ultrapure water. To dry the coverslips, they were spun for a few seconds at maximum speed in the spin drier and placed functionalised side up on KimTech tissues. Avoid dust by covering the coverslips with a Petri dish or alternative covering.

Salinisation

Coverslips were placed in a pre-warmed glass Petri dish with the functionalised side up. A few drops of GOPTS were added using a Hamilton syringe and a second coverslip was added, functionalised side down to make a "sandwich".

Note: avoid any traces of water at this step as this will induce polymerisation of the silane.

The lids were placed on the Petri dishes and the dishes placed in the dry oven at 75 °C for 15 min. After incubation, allow the Petri dish to cool down for 15 min before continuing.

PEG coupling

Two beakers 250 mL acetone were prepared and the glass coverslip "sandwiches" were submerged in the first beaker and separated. The single coverslips were then submerged in the second beaker to further rinse. Dry the coverslips using a gentle flow of nitrogen and place them functionalised side up into a prewarmed (75 °C) glass Petri dish. PEG 2000 powder was added to the coverslip (completely covering the

surface) and coverslip sandwiches were made as before. Place the dishes containing the sandwiches back into the dry oven at 75 °C for 15 min. If there are any bubbles, remove them from the sandwiches by pressing down gently. Once bubbles have been removed, place back in the oven at 75 °C overnight.

Note: avoid any traces of water and minimise exposure to cold air. To minimise cold air, transfer to the hot Petri dishes quickly and move them back to the oven as quickly as possible.

Following incubation, while still warm, quickly and carefully separate the sandwiches and rinse by submerging with ultrapure water. The slides were finally dried using a gentle flow of nitrogen.

Note: If the sandwiches get cool, they will stick firmly together and will be very difficult to separate. Should this happen, simply place them back in the Petri dish and back in the oven for a few minutes to re-warm. The slides can be stored at RT, or 4 °C.

Attachment of NHS-Biotin

NHS biotin was dissolved in DMF at a final concentration of ~35 mg/mL. PEG coverslips were placed with functionalised side up in pre-warmed glass Petri dishes (75 °C) and ~80 μL of NHS-Biotin was added on top of the slide and second coverslip was made into a sandwich as above. The Petri dish was closed and placed in the dry oven at 75 °C for 1 h.

Note: The concentration of NHS biotin used and the incubation time are what regulate the density of binding.

Following incubation, the sandwiches were separated and rinsed twice in DMF then rinsed 5-6 times in ultrapure water. The coverslips were dried with a gentle flow of nitrogen and stored in a slide box at RT for 1 month.

Assembly and preparation of flow chambers

Flow chambers were assembled as shown in Figure. 36. Counter sliders were plasma cleaned for 3 min using plasma cleaner (Flecto 10, Plasma technology). Pieces of double-sided tape were cut to length and stuck to the cleaned counter slide using forceps. The coverslip was placed functionalised side down and secured by gently rubbing the taped areas with a cotton bud.

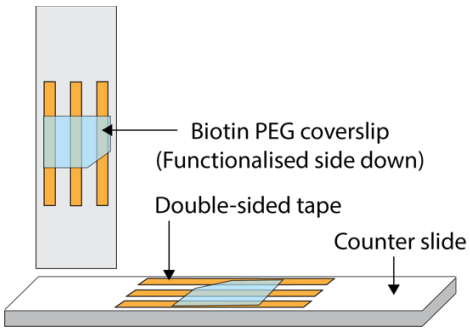

Figure 36. Functionalised glass imaging chamber. Assembly of the flow chambers was completed prior to each experiment.

The chambers were then passivated by using PLL-PEG with a grafting ratio of 3.5. Grafting ratio refers to the number of PEG chains grafted to a lysine group[258]. This was prepared by dissolving PLL-HBr in 50 mM sodium tetraborate solution, pH 8.5 (25 mL pre mg of PLL-HBr) and filtering with a 0.22 μm Seritop. The required stochiometric amount of methoxy-PEG 2000-NHS was added for a 3.5 grafting ratio and the left to react of 6 h, 25 °C whilst stirring. This was dialysed against PBS for 12 h at which point the PBS was replaced for the next 12 h of dialysis. Two more 12 h dialysis steps were completed this time dialysing against MilliQ water. The final concentration of stocks was ~25 mg/mL which was stored at – 20 °C.

The PLL-PEG passivation agent was diluted 10 fold in MilliQ water and flowed into the chamber, using Whatmann paper on the opposing side and capillary action to draw liquid through. Once full this was incubated at room temperature for 3 min and washed with 100 μL MilliQ water. Following washing the slides are ready to use.

Note: The wash volume of water will vary depending on the number of lanes on the slide, be sure to rinse thoroughly to remove any residual PLL-PEG.

TIRF microscopy

Biotin-mediated recruitment controls

Biotinylated slides were prepared as described above. 1 nM of Neutravidin in GEF buffer (50 mM HEPES pH 7.5, 50 mM NaCl, 2 mM $MgCl_2$, 0.5 mg/mL blocker casein, 0.5 mM β-mercaptoethanol) was flushed into the chamber and incubated at room temperature for 2 min. Chambers were washed with GEF buffer once more and a reaction mix was prepared. The reaction mix, prepared in GEF buffer, contained 100 pM Cy3-Cdc42:RhoGDI-AF647, 200 μM nucleotide (GDP or GTP), 10 % (v/v) oxygen

scavenger system (3.75 mg/mL glucose oxidase, 3.75 mg/mL catalase, 40 mg/mL glucose) as made fresh and added to the chamber. Imaging (laser power 35%, exposure 1 frame (continuous illumination), gain stage 3, gain 200) and lasted 40 s. All dual colour single molecule recruitment experiments were performed at RT using the Nikon Ti2 microscope utilising the Nikon NIS-Elements software for control and image acquisition. Essential to single molecule TIRF imaging such as this was the perfect focus system from Nikon also fitted to this system. The dual colour TIRF system used was from Cairn Research, Kent, UK. This setup allows for dual colour images to be acquired simultaneously by means of a quad splitter in the turret of the microscope and a beam splitter cube downstream of the Apo TIRF 60x oil DIC N2 objective and upstream of the cameras. The cube used in this work had a splitting wavelength of 635 nm, meaning light of a wavelength < 635 nm are sent to one camera and > 635 nm go to the other. The laser system used for this work was a custom multi-laser system from AcalBFi LC which was set up to be hardware triggered by the shutter allowing for maximum time resolution, resulting in 22 ms per frame. The cameras used to acquire images were EM CCD Andor iXon cameras.

Supported lipid bilayer integrity FRAP

Single colour bulk experiments such as those used to determine SLB integrity were performed at RT using a Nikon Ti1 microscope controlled by the Visiview software. Images for were collected a 1 s intervals prior to FRAP. A FRAP region was set to allow for a 3 second photobleaching time, after which images were once again collected at 1 s interval. FRAP was realised using the Visitron system from Visitron systems. Images were captured through a Nikon 60X Oil 1.4 NA objective using Evolve Delta cameras from Photometrics (AZ, USA).

Flow-out experiments

Single colour bulk flow-out experiments such as those used to determine SLB integrity were performed at RT using a Nikon Ti1 microscope controlled by the Visiview software (Visitron Systems, Puchheim). Following incubation of 1 μM ITSN-DHPH-His_{10} for > 45 min, a flow of GEF buffer (50 mM HEPES pH 7.5, 50 mM NaCl, 2 mM $MgCl_2$, 0.5 mM β-mercaptoethanol) was pumped across the SLB at a rate of 10 μL/min using Pump11 Elite pumps (Harvard apparatus, Holliston MA, USA). FRAP was realised using the Visitron system from Visitron systems. Images were through a Nikon

TIRF 60x oil NA1.49 objective at time intervals of 10 s using Evolve Delta cameras from Photometrics (AZ, USA) using a 488 nm laser (Visitron Systems, Puchheim).

Dual colour single molecule TIRF data acquisition

SLB chambers (assembled as described above) were placed on the stage of the microscope and washed with 1 mL of GEF buffer (50 mM HEPES pH 7.5, 50 mM NaCl, 2 mM $MgCl_2$, 0.5 mM β-mercaptoethanol). Lasers were line placed at their "centre" allowing for illumination in epifluorescence at 100% laser power to bleach and dirt on the SLB or in the buffers. Following 2 min of bleaching lasers were orientated back into TIRF angles and bleaching continued for 30 s. Once bleached, in the case of + GEF experiments, 400 nM of ITSN-DHPH-His_{10} was added and incubated for 45 mins to bind to NTA(Ni), after which unbound GEF was washed out with 1 mL GEF buffer. 100 pM of freshly diluted complex was mixed in GEF buffer with 10 % (v/v) oxygen scavenger system and nucleotide (3.75 mg/mL glucose oxidase, 3.75 mg/mL catalase, 40 mg/mL glucose, 200 μM nucleotide) and 200 μL was added to the SLB chamber and imaging started immediately (laser power 35%, exposure 1 frame (continuous illumination), gain stage 3, gain 200) and lasted 40 s. All dual colour single molecule recruitment experiments were performed at RT using the Nikon Ti2 microscope utilising the Nikon NIS-Elements software for control and image acquisition. Essential to single molecule TIRF imaging such as this was the perfect focus system from Nikon also fitted to this system. The dual colour TIRF system used was from Cairn Research, Kent, UK. This setup allows for dual colour images to be acquired simultaneously by means of a quad splitter in the turret of the microscope and a beam splitter cube downstream of the Apo TIRF 60x oil DIC N2 objective and upstream of the cameras. The cube used in this work had a splitting wavelength of 635 nm, meaning light of a wavelength < 635 nm are sent to one camera and > 635 nm go to the other. The laser system used for this work was a custom multi-laser system from AcalBFi LC which was set up to be hardware triggered by the shutter allowing for maximum time resolution, resulting in 22 ms per frame. The cameras used to acquire images were EM CCD Andor iXon cameras.

Widefield microscopy

Imaging of lipid coated beads

Beads assays were carried out in either GEF buffer (50 mM HEPES pH 7.5, 50 mM NaCl, 2 mM $MgCl_2$, 0.5 mM β-mercaptoethanol) or activated cell lysate (activated with energy mix (30 mM phosphocreatine, 4 mM ATP, 4 mM MgCl2, pH 7.4) and salt mix (120 mM KCl, 10 mM EGTA, 40 mM 3-phosphoglycerate) prior to use in experiments). To this 5 mM DTT, 1 mM GDP or GTP and 500 nM Cdc42:GDI complex was added along with 2 uL of 1X lipid coated beads to a final volume of 20 μL. This was flowed into passivated chambers assembled as in Figure 36. Chambers were passivated by flowing 0.57 mg/mL of 3.5 grafting ration PLL-PEG into the chamber and incubating for 2 min. Next, ultrapure water was flushed through the chambers, followed by GEF buffer (for non-lysate experiments) or extraction buffer (for lysate experiments) 20 mM HEPES pH 7.4, 100 mM KCl, 1 mM EGTA, 0.1 mM EDTA, 2 mM $MgCl_2$ 2.5 mM DTT, 0.5 mM ATP). Chambers were placed on the Olympus IX81 (CellR) widefield microscope (Olympus Waltham MA, USA), controlled by Excellence software (Olympus Waltham MA, USA) and images captured using a UPLSAPO 20X 0.75 NA objective at 100 ms exposure using the arc lamp with appropriate filters, in this case RFP filters to observe Cy3. Images were captured using an ORCA-Quest qCMOS camera (Hamamatsu Photonics, Japan).

Analysis

Single molecule spot tracking

Dual colour single molecule TIRF data was analysed using Fiji[259] from ImageJ. Data from NIS-Elements was first imported with BioFormats[260] to preserve metadata essential for analysis scripts. To track particles, images were processed using Trackmate[261] within Fiji and the output files ran through our in-house-developed colocalisation scripts[244]. In brief, track data from trackmate analysed from the two channels gathered simultaneously in the microscope was analysed in a two-step process. The first step was to filter and assign new track IDs to the tracks in both channels. The first filter step used was to limit the analysis region to spots which occur in the upper left 75% of the chip, as this is where the TIRF field was found to be uniform and appropriate for single molecule analysis. Next it is determined if the sample is a control (glass) or experimental (lipid), this is to determine all spots are analysed or new landing events. Next experimental data sets are filtered to exclude tracks < 5

frames, as these are not considered true membrane association events as they are incredibly short and sporadic (< 100 ms). Following this, the number of frames to be analysed is to be input (excluding control, this by default takes all frames). For this work the first 3 frames were excluded due to laser ramp, and the final frame was frame 1000. Once these parameters are set, the script will analyse both channel data and generate an X,Y,T coordinate for each spot within a track and give this data as an output file. The second scrip then was used to match this data and determine several parameters, but crucially for this work, how many of these events are colocalising, and at what rate are spots arriving at the membrane.

Bead intensity scans

Bead data was analysed using Fiji. Images were set to matching intensity values and a line (1 pt thick) was drawn across the diameter of beads. A fluorescence intensity plot was taken across this line. A further intensity plot was taken away from the beads as a background measure for subtraction.

Figure preparation and statistics

Data analysis was completed using Prism 9 from GraphPad Software and Origin 9 from Origin corporation. Statistics were calculated in Prism 9 (Graphpad Software).

References

1. Dehmelt, L. & Bastiaens, P. I. H. Spatial organization of intracellular communication: insights from imaging. *Nat. Rev. Mol. Cell Biol.* **11**, 440–452 (2010).
2. Kinkhabwala, A. & Bastiaens, P. I. Spatial aspects of intracellular information processing. *Curr. Opin. Genet. Dev.* **20**, 31–40 (2010).
3. Paterson, H. *et al.* Microinjection of recombinant p21Rho induces rapid changes in cell morphology. *J. Cell Biol.* **111**, 1001–7 (1990).
4. Ridley, A. J., Paterson, H. F., Johnston, C. L., Diekmann, D. & Hall, A. The small GTP-binding protein rac regulates growth factor-induced membrane ruffling. *Cell* **70**, 401–410 (1992).
5. Munemitsu, S. *et al.* Molecular cloning and expression of a G25K cDNA, the human homolog of the yeast cell cycle gene CDC42. *Mol. Cell. Biol.* **10**, 5977–5982 (1990).
6. Shinjo, K. *et al.* Molecular cloning of the gene for the human placental GTP-binding protein Gp (G25K): identification of this GTP-binding protein as the human homolog of the yeast cell-division-cycle protein CDC42. *Proc. Natl. Acad. Sci. U. S. A.* **87**, 9853–9857 (1990).
7. de Beco, S. *et al.* Optogenetic dissection of Rac1 and Cdc42 gradient shaping. *Nat. Commun.* **9**, (2018).
8. Yang, H. W., Collins, S. R. & Meyer, T. Locally excitable Cdc42 signals steer cells during chemotaxis. *Nat. Cell Biol.* **18**, 191 (2016).
9. Haspel, N., Jang, H. & Nussinov, R. Active and Inactive Cdc42 Differ in Their Insert Region Conformational Dynamics. *Biophys. J.* **0**, (2020).
10. Garcia-Mata, R., Boulter, E. & Burridge, K. The 'invisible hand': regulation of RHO GTPases by RHOGDIs. *Nat. Rev. Mol. Cell Biol.* **12**, 493–504 (2011).
11. Williams, C. L. The polybasic region of Ras and Rho family small GTPases: a regulator of protein interactions and membrane association and a site of nuclear localization signal sequences. *Cell. Signal.* **15**, 1071–1080 (2003).
12. Roberts, P. J. *et al.* Rho Family GTPase Modification and Dependence on CAAX Motif-signaled Posttranslational Modification*. *J. Biol. Chem.* **283**, 25150–25163 (2008).
13. Hoffman, G. R., Nassar, N. & Cerione, R. A. Structure of the Rho Family GTP-Binding Protein Cdc42 in Complex with the Multifunctional Regulator RhoGDI. *Cell* **100**, 345–356 (2000).
14. Mogilner, A. & Oster, G. Cell motility driven by actin polymerization. *Biophys. J.* **71**, 3030–3045 (1996).

15. Bretschneider, T. *et al.* Dynamic Actin Patterns and Arp2/3 Assembly at the Substrate-Attached Surface of Motile Cells. *Curr. Biol.* **14**, 1–10 (2004).
16. Worthylake, R. A., Lemoine, S., Watson, J. M. & Burridge, K. RhoA is required for monocyte tail retraction during transendothelial migration. *J. Cell Biol.* **154**, 147–160 (2001).
17. Pertz, O. Spatio-temporal Rho GTPase signaling – where are we now? *J Cell Sci* **123**, 1841–1850 (2010).
18. Benink, H. A. & Bement, W. M. Concentric zones of active RhoA and Cdc42 around single cell wounds., Concentric zones of active RhoA and Cdc42 around single cell wounds. *J. Cell Biol. J. Cell Biol.* **168, 168**, 429, 429–439 (2005).
19. Martin, K. *et al.* Spatio-temporal co-ordination of RhoA, Rac1 and Cdc42 activation during prototypical edge protrusion and retraction dynamics. *Sci. Rep.* **6**, 21901 (2016).
20. Fritz, R. D. & Pertz, O. The dynamics of spatio-temporal Rho GTPase signaling: formation of signaling patterns. *F1000Research* **5**, F1000 Faculty Rev-749 (2016).
21. Hanna, S., Miskolci, V., Cox, D. & Hodgson, L. A New Genetically Encoded Single-Chain Biosensor for Cdc42 Based on FRET, Useful for Live-Cell Imaging. *PLoS ONE* **9**, (2014).
22. Damiano-Guercio, J. *et al.* Loss of Ena/VASP interferes with lamellipodium architecture, motility and integrin-dependent adhesion. *eLife* **9**, e55351 (2020).
23. Mondal, S., Hsiao, K. & Goueli, S. A. A Homogenous Bioluminescent System for Measuring GTPase, GTPase Activating Protein, and Guanine Nucleotide Exchange Factor Activities. *ASSAY Drug Dev. Technol.* **13**, 444–455 (2015).
24. Dudzinska, W., Lubkowska, A., Dolegowska, B., Safranow, K. & Jakubowska, K. Adenine, guanine and pyridine nucleotides in blood during physical exercise and restitution in healthy subjects. *Eur. J. Appl. Physiol.* **110**, 1155–1162 (2010).
25. Bourne, H. R., Sanders, D. A. & McCormick, F. The GTPase superfamily: conserved structure and molecular mechanism. *Nature* **349**, 117–127 (1991).
26. Wennerberg, K., Rossman, K. L. & Der, C. J. The Ras superfamily at a glance. *J. Cell Sci.* **118**, 843–846 (2005).
27. Hodge, R. G., Schaefer, A., Howard, S. V. & Der, C. J. RAS and RHO family GTPase mutations in cancer: twin sons of different mothers? *Crit. Rev. Biochem. Mol. Biol.* **55**, 386–407 (2020).
28. Müller, M. P. & Goody, R. S. Molecular control of Rab activity by GEFs, GAPs and GDI. *Small GTPases* **9**, 5–21 (2018).

29. Jaiswal, M., Dvorsky, R. & Ahmadian, M. R. Deciphering the Molecular and Functional Basis of Dbl Family Proteins A NOVEL SYSTEMATIC APPROACH TOWARD CLASSIFICATION OF SELECTIVE ACTIVATION OF THE Rho FAMILY PROTEINS. *J. Biol. Chem.* **288**, 4486–4500 (2013).
30. Amin, E. *et al.* Deciphering the Molecular and Functional Basis of RHOGAP Family Proteins: A SYSTEMATIC APPROACH TOWARD SELECTIVE INACTIVATION OF RHO FAMILY PROTEINS. *J. Biol. Chem.* **291**, 20353–20371 (2016).
31. Vartak, N. & Bastiaens, P. Spatial cycles in G-protein crowd control. *EMBO J.* **29**, 2689–2699 (2010).
32. Boulter, E. *et al.* Regulation of Rho GTPase crosstalk, degradation and activity by RhoGDI1. *Nat. Cell Biol.* **12**, 477–483 (2010).
33. Cox, A. D. & Der, C. J. Protein prenylation: more than just glue? *Curr. Opin. Cell Biol.* **4**, 1008–1016 (1992).
34. Chandra, A. *et al.* The GDI-like solubilizing factor PDEδ sustains the spatial organization and signalling of Ras family proteins. *Nat. Cell Biol.* **14**, 148–158 (2011).
35. Nancy, V., Callebaut, I., El Marjou, A. & de Gunzburg, J. The delta subunit of retinal rod cGMP phosphodiesterase regulates the membrane association of Ras and Rap GTPases. *J. Biol. Chem.* **277**, 15076–15084 (2002).
36. Gosser, Y. Q. *et al.* C-terminal binding domain of Rho GDP-dissociation inhibitor directs N-terminal inhibitory peptide to GTPases. *Nature* **387**, 814–819 (1997).
37. Longenecker, K. *et al.* How RhoGDI binds Rho. *Acta Crystallogr. D Biol. Crystallogr.* **55**, 1503–1515 (1999).
38. Golding, A. E., Visco, I., Bieling, P. & Bement, W. M. Extraction of active RhoGTPases by RhoGDI regulates spatiotemporal patterning of RhoGTPases. *eLife* **8**, e50471 (2019).
39. Del Pozo, M. A. *et al.* Integrins regulate GTP-Rac localized effector interactions through dissociation of Rho-GDI. *Nat. Cell Biol.* **4**, 232–239 (2002).
40. Ren, X. D., Kiosses, W. B. & Schwartz, M. A. Regulation of the small GTP-binding protein Rho by cell adhesion and the cytoskeleton. *EMBO J.* **18**, 578–585 (1999).
41. Müller, P. M. *et al.* Systems analysis of RhoGEF and RhoGAP regulatory proteins reveals spatially organized RAC1 signalling from integrin adhesions. *Nat. Cell Biol.* **22**, 498–511 (2020).

42. Boureux, A., Vignal, E., Faure, S. & Fort, P. Evolution of the Rho family of ras-like GTPases in eukaryotes. *Mol. Biol. Evol.* **24**, 203–216 (2007).
43. Gupton, S. L. & Gertler, F. B. Filopodia: the fingers that do the walking. *Sci. STKE Signal Transduct. Knowl. Environ.* **2007**, re5 (2007).
44. Tao, W., Pennica, D., Xu, L., Kalejta, R. F. & Levine, A. J. Wrch-1, a novel member of the Rho gene family that is regulated by Wnt-1. *Genes Dev.* **15**, 1796–1807 (2001).
45. Aspenström, P., Fransson, A. & Saras, J. Rho GTPases have diverse effects on the organization of the actin filament system. *Biochem. J.* **377**, 327–337 (2004).
46. Govek, E.-E., Newey, S. E. & Van Aelst, L. The role of the Rho GTPases in neuronal development. *Genes Dev.* **19**, 1–49 (2005).
47. Chen, L. *et al.* Rac1 Controls the Formation of Midline Commissures and the Competency of Tangential Migration in Ventral Telencephalic Neurons. *J. Neurosci.* **27**, 3884–3893 (2007).
48. Wu, X. *et al.* Cdc42 is crucial for the establishment of epithelial polarity during early mammalian development. *Dev. Dyn. Off. Publ. Am. Assoc. Anat.* **236**, 2767–2778 (2007).
49. Hall, A. Rho GTPases and the actin cytoskeleton. *Science* **279**, 509–514 (1998).
50. Fritz, R. D. *et al.* A versatile toolkit to produce sensitive FRET biosensors to visualize signaling in time and space. *Sci. Signal.* **6**, rs12 (2013).
51. Heasman, S. J. & Ridley, A. J. Mammalian Rho GTPases: new insights into their functions from in vivo studies. *Nat. Rev. Mol. Cell Biol.* **9**, 690–701 (2008).
52. Katayama, M. *et al.* The posttranslationally modified C-terminal structure of bovine aortic smooth muscle rhoA p21. *J. Biol. Chem.* **266**, 12639–12645 (1991).
53. Adamson, P., Marshall, C. J., Hall, A. & Tilbrook, P. A. Post-translational modifications of p21rho proteins. *J. Biol. Chem.* **267**, 20033–20038 (1992).
54. Michaelson, D. *et al.* Differential localization of Rho GTPases in live cells: regulation by hypervariable regions and RhoGDI binding. *J. Cell Biol.* **152**, 111–126 (2001).
55. Hodge, R. G. & Ridley, A. J. Regulating Rho GTPases and their regulators. *Nat. Rev. Mol. Cell Biol.* **17**, 496–510 (2016).
56. Wang, D.-A. & Sebti, S. M. Palmitoylated cysteine 192 is required for RhoB tumor-suppressive and apoptotic activities. *J. Biol. Chem.* **280**, 19243–19249 (2005).

57. Pérez-Sala, D., Boya, P., Ramos, I., Herrera, M. & Stamatakis, K. The C-Terminal Sequence of RhoB Directs Protein Degradation through an Endo-Lysosomal Pathway. *PLOS ONE* **4**, e8117 (2009).
58. Berzat, A. C. *et al.* Transforming activity of the Rho family GTPase, Wrch-1, a Wnt-regulated Cdc42 homolog, is dependent on a novel carboxyl-terminal palmitoylation motif. *J. Biol. Chem.* **280**, 33055–33065 (2005).
59. Chenette, E. J., Mitin, N. Y. & Der, C. J. Multiple Sequence Elements Facilitate Chp Rho GTPase Subcellular Location, Membrane Association, and Transforming Activity. *Mol. Biol. Cell* **17**, 3108–3121 (2006).
60. Navarro-Lérida, I. *et al.* A palmitoylation switch mechanism regulates Rac1 function and membrane organization. *EMBO J.* **31**, 534–551 (2012).
61. Nishimura, A. & Linder, M. E. Identification of a Novel Prenyl and Palmitoyl Modification at the CaaX Motif of Cdc42 That Regulates RhoGDI Binding. *Mol. Cell. Biol.* **33**, 1417–1429 (2013).
62. Tu, S., Wu, W. J., Wang, J. & Cerione, R. A. Epidermal growth factor-dependent regulation of Cdc42 is mediated by the Src tyrosine kinase. *J. Biol. Chem.* **278**, 49293–49300 (2003).
63. Forget, M.-A., Desrosiers, R. R., Gingras, D. & Béliveau, R. Phosphorylation states of Cdc42 and RhoA regulate their interactions with Rho GDP dissociation inhibitor and their extraction from biological membranes. *Biochem. J.* **361**, 243–254 (2002).
64. Tong, J., Li, L., Ballermann, B. & Wang, Z. Phosphorylation of Rac1 T108 by extracellular signal-regulated kinase in response to epidermal growth factor: a novel mechanism to regulate Rac1 function. *Mol. Cell. Biol.* **33**, 4538–4551 (2013).
65. Kwon, T., Kwon, D. Y., Chun, J., Kim, J. H. & Kang, S. S. Akt protein kinase inhibits Rac1-GTP binding through phosphorylation at serine 71 of Rac1. *J. Biol. Chem.* **275**, 423–428 (2000).
66. Takemoto, K., Ishihara, S., Mizutani, T., Kawabata, K. & Haga, H. Compressive stress induces dephosphorylation of the myosin regulatory light chain via RhoA phosphorylation by the adenylyl cyclase/protein kinase A signaling pathway. *PloS One* **10**, e0117937 (2015).
67. Rolli-Derkinderen, M., Toumaniantz, G., Pacaud, P. & Loirand, G. RhoA Phosphorylation Induces Rac1 Release from Guanine Dissociation Inhibitor α and Stimulation of Vascular Smooth Muscle Cell Migration. *Mol. Cell. Biol.* **30**, 4786–4796 (2010).

68. Garcia-Mata, R., Boulter, E. & Burridge, K. The 'invisible hand': regulation of RHO GTPases by RHOGDIs. *Nat. Rev. Mol. Cell Biol.* **12**, 493 (2011).
69. Leonard, D. *et al.* The identification and characterization of a GDP-dissociation inhibitor (GDI) for the CDC42Hs protein. *J. Biol. Chem.* **267**, 22860–22868 (1992).
70. Newcombe, A. R., Stockley, R. W., Hunter, J. L. & Webb, M. R. The interaction between rac1 and its guanine nucleotide dissociation inhibitor (GDI), monitored by a single fluorescent coumarin attached to GDI. *Biochemistry* **38**, 6879–6886 (1999).
71. Bourmeyster, N., Boquet, P. & Vignais, P. V. Role of bound GDP in the stability of the rho A-rho GDI complex purified from neutrophil cytosol. *Biochem. Biophys. Res. Commun.* **205**, 174–179 (1994).
72. Lelias, J. M. *et al.* cDNA cloning of a human mRNA preferentially expressed in hematopoietic cells and with homology to a GDP-dissociation inhibitor for the rho GTP-binding proteins. *Proc. Natl. Acad. Sci. U. S. A.* **90**, 1479–1483 (1993).
73. Scherle, P., Behrens, T. & Staudt, L. M. Ly-GDI, a GDP-dissociation inhibitor of the RhoA GTP-binding protein, is expressed preferentially in lymphocytes. *Proc. Natl. Acad. Sci. U. S. A.* **90**, 7568–7572 (1993).
74. Platko, J. V. *et al.* A Single Residue can Modify Target-Binding Affinity and Activity of the Functional Domain of the Rho-Subfamily GDP Dissociation Inhibitors. *Proc. Natl. Acad. Sci. U. S. A.* **92**, 2974–2978 (1995).
75. Scheffzek, K., Stephan, I., Jensen, O. N., Illenberger, D. & Gierschik, P. The Rac-RhoGDI complex and the structural basis for the regulation of Rho proteins by RhoGDI. *Nat. Struct. Biol.* **7**, 122–126 (2000).
76. Zalcman, G. *et al.* RhoGDI-3 Is a New GDP Dissociation Inhibitor (GDI): IDENTIFICATION OF A NON-CYTOSOLIC GDI PROTEIN INTERACTING WITH THE SMALL GTP-BINDING PROTEINS RhoB AND RhoG *. *J. Biol. Chem.* **271**, 30366–30374 (1996).
77. Adra, C. N. *et al.* RhoGDIγ: A GDP-dissociation inhibitor for Rho proteins with preferential expression in brain and pancreas. *Proc. Natl. Acad. Sci. U. S. A.* **94**, 4279 (1997).
78. Brunet, N., Morin, A. & Olofsson, B. RhoGDI-3 Regulates RhoG and Targets This Protein to the Golgi Complex Through its Unique N-Terminal Domain. *Traffic* **3**, 342–358 (2002).
79. Hodgson, L. *et al.* FRET binding antenna reports spatiotemporal dynamics of GDI–Cdc42 GTPase interactions. *Nat. Chem. Biol.* **12**, 802–809 (2016).

80. Ueda, T., Kikuchi, A., Ohga, N., Yamamoto, J. & Takai, Y. Purification and characterization from bovine brain cytosol of a novel regulatory protein inhibiting the dissociation of GDP from and the subsequent binding of GTP to rhoB p20, a ras p21-like GTP-binding protein. *J. Biol. Chem.* **265**, 9373–9380 (1990).
81. Hart, M. J. *et al.* A GDP dissociation inhibitor that serves as a GTPase inhibitor for the Ras-like protein CDC42Hs. *Science* **258**, 812–815 (1992).
82. DerMardirossian, C. & Bokoch, G. M. GDIs: central regulatory molecules in Rho GTPase activation. *Trends Cell Biol.* **15**, 356–363 (2005).
83. Schrödinger, LLC. The PyMOL Molecular Graphics System, Version 1.8. (2015).
84. Tnimov, Z. *et al.* Quantitative Analysis of Prenylated RhoA Interaction with Its Chaperone, RhoGDI. *J. Biol. Chem.* **287**, 26549–26562 (2012).
85. Graziano, B. R. *et al.* A module for Rac temporal signal integration revealed with optogenetics. *J. Cell Biol.* **216**, 2515–2531 (2017).
86. Gandhi, P. N. *et al.* An activating mutant of Rac1 that fails to interact with Rho GDP-dissociation inhibitor stimulates membrane ruffling in mammalian cells. *Biochem. J.* **378**, 409–419 (2004).
87. Gibson, R. M. & Wilson-Delfosse, A. L. RhoGDI-binding-defective mutant of Cdc42Hs targets to membranes and activates filopodia formation but does not cycle with the cytosol of mammalian cells. *Biochem. J.* **359**, 285–294 (2001).
88. Tiedje, C., Sakwa, I., Just, U. & Höfken, T. The Rho GDI Rdi1 Regulates Rho GTPases by Distinct Mechanisms. *Mol. Biol. Cell* **19**, 2885–2896 (2008).
89. Lin, Q., Fuji, R. N., Yang, W. & Cerione, R. A. RhoGDI Is Required for Cdc42-Mediated Cellular Transformation. *Curr. Biol.* **13**, 1469–1479 (2003).
90. Chianale, F. *et al.* Diacylglycerol kinase α mediates HGF-induced Rac activation and membrane ruffling by regulating atypical PKC and RhoGDI. *Proc. Natl. Acad. Sci.* **107**, 4182–4187 (2010).
91. Nevins, A. K. & Thurmond, D. C. Caveolin-1 functions as a novel Cdc42 guanine nucleotide dissociation inhibitor in pancreatic beta-cells. *J. Biol. Chem.* **281**, 18961–18972 (2006).
92. Slaughter, B. D., Das, A., Schwartz, J. W., Rubinstein, B. & Li, R. Dual Modes of Cdc42 Recycling Fine-Tune Polarized Morphogenesis. *Dev. Cell* **17**, 823–835 (2009).
93. Rittinger, K. *et al.* Crystal structure of a small G protein in complex with the GTPase-activating protein rhoGAP. *Nature* **388**, 693–697 (1997).

94. Goody, R. S. How not to do kinetics: examples involving GTPases and guanine nucleotide exchange factors. *FEBS J.* **281**, 593–600 (2014).
95. Guo, Z., Ahmadian, M. R. & Goody, R. S. Guanine Nucleotide Exchange Factors Operate by a Simple Allosteric Competitive Mechanism. *Biochemistry* **44**, 15423–15429 (2005).
96. Zhang, B., Zhang, Y., Wang, Z. & Zheng, Y. The Role of Mg2+ Cofactor in the Guanine Nucleotide Exchange and GTP Hydrolysis Reactions of Rho Family GTP-binding Proteins. *J. Biol. Chem.* **275**, 25299–25307 (2000).
97. Rossman, K. L., Der, C. J. & Sondek, J. GEF means go: turning on RHO GTPases with guanine nucleotide-exchange factors. *Nat. Rev. Mol. Cell Biol.* **6**, 167–180 (2005).
98. Cook, D. R., Rossman, K. L. & Der, C. J. Rho guanine nucleotide exchange factors: regulators of Rho GTPase activity in development and disease. *Oncogene* **33**, 4021–4035 (2014).
99. Kukimoto-Niino, M., Ihara, K., Murayama, K. & Shirouzu, M. Structural insights into the small GTPase specificity of the DOCK guanine nucleotide exchange factors. *Curr. Opin. Struct. Biol.* **71**, 249–258 (2021).
100. Gadea, G. & Blangy, A. Dock-family exchange factors in cell migration and disease. *Eur. J. Cell Biol.* **93**, 466–477 (2014).
101. Nishikimi, A., Kukimoto-Niino, M., Yokoyama, S. & Fukui, Y. Immune regulatory functions of DOCK family proteins in health and disease. *Exp. Cell Res.* **319**, 2343–2349 (2013).
102. Jiang, H. *et al.* Deletion of DOCK2, a regulator of the actin cytoskeleton in lymphocytes, suppresses cardiac allograft rejection. *J. Exp. Med.* **202**, 1121–1130 (2005).
103. Zhang, Q. *et al.* Combined Immunodeficiency Associated with DOCK8 Mutations. *N. Engl. J. Med.* **361**, 2046–2055 (2009).
104. Hirsch, E. *et al.* Defective dendrite elongation but normal fertility in mice lacking the Rho-like GTPase activator Dbl. *Mol. Cell. Biol.* **22**, 3140–3148 (2002).
105. van der Crabben, S. *et al.* Constitutional RUNX1 deletion presenting as non-syndromic thrombocytopenia with myelodysplasia: 21q22 ITSN1 as a candidate gene in mental retardation. *Leuk. Res.* **34**, e8–e12 (2010).
106. Lindstrand, A. *et al.* Detailed molecular and clinical characterization of three patients with 21q deletions. *Clin. Genet.* **77**, 145–154 (2010).
107. Hunter, M. P., Russo, A. & O'Bryan, J. P. Emerging Roles for Intersectin (ITSN) in Regulating Signaling and Disease Pathways. *Int. J. Mol. Sci.* **14**, 7829–7852 (2013).

108. Malliri, A. *et al.* Mice deficient in the Rac activator Tiam1 are resistant to Ras-induced skin tumours. *Nature* **417**, 867–871 (2002).

109. Engelhardt, K. R. *et al.* Large deletions and point mutations involving the dedicator of cytokinesis 8 (DOCK8) in the autosomal-recessive form of hyper-IgE syndrome. *J. Allergy Clin. Immunol.* **124**, 1289-1302.e4 (2009).

110. Eva, A., Vecchio, G., Rao, C. D., Tronick, S. R. & Aaronson, S. A. The predicted DBL oncogene product defines a distinct class of transforming proteins. *Proc. Natl. Acad. Sci. U. S. A.* **85**, 2061–2065 (1988).

111. Hart, M. J., Eva, A., Evans, T., Aaronsont, S. A. & Cerione, R. A. Catalysis of guanine nucleotide exchange on the CDC42Hs protein by the db/ oncogene product. **354**, 4 (1991).

112. Di Fiore, P. P., Pelicci, P. G. & Sorkin, A. EH: a novel protein-protein interaction domain potentially involved in intracellular sorting. *Trends Biochem. Sci.* **22**, 411–413 (1997).

113. Zhang, D. & Aravind, L. Identification of novel families and classification of the C2 domain superfamily elucidate the origin and evolution of membrane targeting activities in eukaryotes. *Gene* **469**, 18–30 (2010).

114. Snyder, J. T. *et al.* Structural basis for the selective activation of Rho GTPases by Dbl exchange factors. *Nat. Struct. Biol.* **9**, 468–475 (2002).

115. Boriack-Sjodin, P. A., Margarit, S. M., Bar-Sagi, D. & Kuriyan, J. The structural basis of the activation of Ras by Sos. *Nature* **394**, 337–343 (1998).

116. Goldberg, J. Structural basis for activation of ARF GTPase: mechanisms of guanine nucleotide exchange and GTP-myristoyl switching. *Cell* **95**, 237–248 (1998).

117. Renault, L., Kuhlmann, J., Henkel, A. & Wittinghofer, A. Structural basis for guanine nucleotide exchange on Ran by the regulator of chromosome condensation (RCC1). *Cell* **105**, 245–255 (2001).

118. Traut, T. W. Physiological concentrations of purines and pyrimidines. *Mol. Cell. Biochem.* **140**, 1–22 (1994).

119. Snyder, J. T. *et al.* Quantitative Analysis of the Effect of Phosphoinositide Interactions on the Function of Dbl Family Proteins *. *J. Biol. Chem.* **276**, 45868–45875 (2001).

120. Goicoechea, S. M., Awadia, S. & Garcia-Mata, R. I'm coming to GEF you: Regulation of RhoGEFs during cell migration. *Cell Adhes. Migr.* **8**, 535–549 (2014).

121. Pegtel, D. M. *et al.* The Par-Tiam1 Complex Controls Persistent Migration by Stabilizing Microtubule-Dependent Front-Rear Polarity. *Curr. Biol.* **17**, 1623–1634 (2007).

122. Wang, S. *et al.* Tiam1 interaction with the PAR complex promotes talin-mediated Rac1 activation during polarized cell migration. *J. Cell Biol.* **199**, 331–345 (2012).

123. Jenna, S. *et al.* The activity of the GTPase-activating protein CdGAP is regulated by the endocytic protein intersectin. *J. Biol. Chem.* **277**, 6366–6373 (2002).

124. Dergai, O. *et al.* Intersectin 1 forms complexes with SGIP1 and Reps1 in clathrin-coated pits. *Biochem. Biophys. Res. Commun.* **402**, 408–413 (2010).

125. Zheng, Y., Zangrilli, D., Cerione, R. A. & Eva, A. The Pleckstrin Homology Domain Mediates Transformation by Oncogenic Dbl through Specific Intracellular Targeting *. *J. Biol. Chem.* **271**, 19017–19020 (1996).

126. Vanni, C. *et al.* Phosphorylation-independent membrane relocalization of ezrin following association with Dbl in vivo. *Oncogene* **23**, 4098–4106 (2004).

127. Brugnera, E. *et al.* Unconventional Rac-GEF activity is mediated through the Dock180-ELMO complex. *Nat. Cell Biol.* **4**, 574–582 (2002).

128. Côté, J.-F., Motoyama, A. B., Bush, J. A. & Vuori, K. A novel and evolutionarily conserved PtdIns(3,4,5)P3-binding domain is necessary for DOCK180 signalling. *Nat. Cell Biol.* **7**, 797–807 (2005).

129. Premkumar, L. *et al.* Structural basis of membrane targeting by the Dock180 family of Rho family guanine exchange factors (Rho-GEFs). *J. Biol. Chem.* **285**, 13211–13222 (2010).

130. Grimsley, C. M. *et al.* Dock180 and ELMO1 Proteins Cooperate to Promote Evolutionarily Conserved Rac-dependent Cell Migration *. *J. Biol. Chem.* **279**, 6087–6097 (2004).

131. Gumienny, T. L. *et al.* CED-12/ELMO, a novel member of the CrkII/Dock180/Rac pathway, is required for phagocytosis and cell migration. *Cell* **107**, 27–41 (2001).

132. deBakker, C. D. *et al.* Phagocytosis of Apoptotic Cells Is Regulated by a UNC-73/TRIO-MIG-2/RhoG Signaling Module and Armadillo Repeats of CED-12/ELMO. *Curr. Biol.* **14**, 2208–2216 (2004).

133. Côté, J.-F. & Vuori, K. GEF what? Dock180 and related proteins help Rac to polarize cells in new ways. *Trends Cell Biol.* **17**, 383–393 (2007).

134. Schmidt, A. & Hall, A. Guanine nucleotide exchange factors for Rho GTPases: turning on the switch. *Genes Dev.* **16**, 1587–1609 (2002).

135. Aghazadeh, B., Lowry, W. E., Huang, X. Y. & Rosen, M. K. Structural basis for relief of autoinhibition of the Dbl homology domain of proto-oncogene Vav by tyrosine phosphorylation. *Cell* **102**, 625–633 (2000).

136. Zamanian, J. L. & Kelly, R. B. Intersectin 1L Guanine Nucleotide Exchange Activity Is Regulated by Adjacent src Homology 3 Domains That Are Also Involved in Endocytosis. *Mol. Biol. Cell* **14**, 1624–1637 (2003).

137. Kintscher, C., Wuertenberger, S., Eylenstein, R., Uhlendorf, T. & Groemping, Y. Autoinhibition of GEF activity in intersectin 1 is mediated by the short SH3-DH domain linker. *Protein Sci.* **19**, 2164–2174 (2010).

138. Adam, G. & Delbrück, M. Reduction of Dimensionality in Biological Diffusion Processes. in *Structural Chemistry and Molecular Biology* (eds. Rich, A. & Davidson, N.) (W H Freeman and Co., 1968).

139. Vetter, I. R. Interface analysis of small GTP binding protein complexes suggests preferred membrane orientations. *Biol. Chem.* **398**, 637–651 (2017).

140. Gureasko, J. *et al.* Membrane-dependent signal integration by the Ras activator Son of sevenless. *Nat. Struct. Mol. Biol.* **15**, 452–461 (2008).

141. Levskaya, A., Weiner, O. D., Lim, W. A. & Voigt, C. A. Spatiotemporal control of cell signalling using a light-switchable protein interaction. *Nature* **461**, 997–1001 (2009).

142. Kamps, D. *et al.* Optogenetic Tuning Reveals Rho Amplification-Dependent Dynamics of a Cell Contraction Signal Network. *Cell Rep.* **33**, (2020).

143. van Unen, J. *et al.* Plasma membrane restricted RhoGEF activity is sufficient for RhoA-mediated actin polymerization. *Sci. Rep.* **5**, 14693 (2015).

144. Jaiswal, M., Dubey, B. N., Koessmeier, K. T., Gremer, L. & Ahmadian, M. R. Biochemical Assays to Characterize Rho GTPases. *Rho GTPases* 37–58 (2012) doi:10.1007/978-1-61779-442-1_3.

145. Garrett, M. D., Major, G. N., Totty, N. & Hall, A. Purification and N-terminal sequence of the p21rho GTPase-activating protein, rho GAP. *Biochem. J.* **276**, 833–836 (1991).

146. Moon, S. Y. & Zheng, Y. Rho GTPase-activating proteins in cell regulation. *Trends Cell Biol.* **13**, 13–22 (2003).

147. Peck, J., Douglas, G., Wu, C. H. & Burbelo, P. D. Human RhoGAP domain-containing proteins: structure, function and evolutionary relationships. *FEBS Lett.* **528**, 27–34 (2002).

148. Endris, V. *et al.* SrGAP3 interacts with lamellipodin at the cell membrane and regulates Rac-dependent cellular protrusions. *J. Cell Sci.* **124**, 3941–3955 (2011).

149. Lamarche, N. & Hall, A. GAPs for rho-related GTPase. *Trends Genet.* **10**, 436–440 (1994).

150. Tcherkezian, J. & Lamarche-Vane, N. Current knowledge of the large RhoGAP family of proteins. *Biol. Cell* **99**, 67–86 (2007).

151. Lamarche-Vane, N. & Hall, A. CdGAP, a novel proline-rich GTPase-activating protein for Cdc42 and Rac. *J. Biol. Chem.* **273**, 29172–29177 (1998).

152. Ko, F. C. F. *et al.* PKA-induced dimerization of the RhoGAP DLC1 promotes its inhibition of tumorigenesis and metastasis. *Nat. Commun.* **4**, 1618 (2013).

153. Pullikuth, A. K. & Catling, A. D. Extracellular signal-regulated kinase promotes Rho-dependent focal adhesion formation by suppressing p190A RhoGAP. *Mol. Cell. Biol.* **30**, 3233–3248 (2010).

154. Mullins, R. D., Bieling, P. & Fletcher, D. A. From solution to surface to filament: actin flux into branched networks. *Biophys. Rev.* **10**, 1537–1551 (2018).

155. Bisi, S. *et al.* Membrane and actin dynamics interplay at lamellipodia leading edge. *Curr. Opin. Cell Biol.* **25**, 565–573 (2013).

156. Field, C., Li, R. & Oegema, K. Cytokinesis in eukaryotes: a mechanistic comparison. *Curr. Opin. Cell Biol.* **11**, 68–80 (1999).

157. Drubin, D. G. & Nelson, W. J. Origins of cell polarity. *Cell* **84**, 335–344 (1996).

158. Dominguez, R. & Holmes, K. C. Actin Structure and Function. *Annu. Rev. Biophys.* **40**, 169–186 (2011).

159. Funk, J. *et al.* Profilin and formin constitute a pacemaker system for robust actin filament growth. *eLife* **8**, e50963 (2019).

160. Koestler, S. A. *et al.* Arp2/3 complex is essential for actin network treadmilling as well as for targeting of capping protein and cofilin. *Mol. Biol. Cell* **24**, 2861–2875 (2013).

161. Machesky, L. M. & Insall, R. H. Scar1 and the related Wiskott–Aldrich syndrome protein, WASP, regulate the actin cytoskeleton through the Arp2/3 complex. *Curr. Biol.* **8**, 1347–1356 (1998).

162. Rohatgi, R. *et al.* The Interaction between N-WASP and the Arp2/3 Complex Links Cdc42-Dependent Signals to Actin Assembly. *Cell* **97**, 221–231 (1999).

163. Kim, A. S., Kakalis, L. T., Abdul-Manan, N., Liu, G. A. & Rosen, M. K. Autoinhibition and activation mechanisms of the Wiskott-Aldrich syndrome protein. *Nature* **404**, 151–158 (2000).

164. Koronakis, V. *et al.* WAVE regulatory complex activation by cooperating GTPases Arf and Rac1. *Proc. Natl. Acad. Sci.* **108**, 14449–14454 (2011).

165. Lebensohn, A. M. & Kirschner, M. W. Activation of the WAVE complex by coincident signals controls actin assembly. *Mol. Cell* **36**, 512–524 (2009).

166. Miki, H., Suetsugu, S. & Takenawa, T. WAVE, a novel WASP-family protein involved in actin reorganization induced by Rac. *EMBO J.* **17**, 6932–6941 (1998).

167. Oikawa, T. *et al.* PtdIns(3,4,5)P3 binding is necessary for WAVE2-induced formation of lamellipodia. *Nat. Cell Biol.* **6**, 420–426 (2004).

168. Mullins, R. D., Heuser, J. A. & Pollard, T. D. The interaction of Arp2/3 complex with actin: nucleation, high affinity pointed end capping, and formation of branching networks of filaments. *Proc. Natl. Acad. Sci. U. S. A.* **95**, 6181–6186 (1998).

169. Mullins, R. D., Stafford, W. F. & Pollard, T. D. Structure, subunit topology, and actin-binding activity of the Arp2/3 complex from Acanthamoeba. *J. Cell Biol.* **136**, 331–343 (1997).

170. Robinson, R. C. *et al.* Crystal structure of Arp2/3 complex. *Science* **294**, 1679–1684 (2001).

171. Chhabra, E. S. & Higgs, H. N. The many faces of actin: matching assembly factors with cellular structures. *Nat. Cell Biol.* **9**, 1110–1121 (2007).

172. Brunetti, R. M. *et al.* WASP integrates substrate topology and cell polarity to guide neutrophil migration. *J. Cell Biol.* **221**, e202104046 (2022).

173. Weiner, O. D., Marganski, W. A., Wu, L. F., Altschuler, S. J. & Kirschner, M. W. An Actin-Based Wave Generator Organizes Cell Motility. *PLoS Biol.* **5**, e221 (2007).

174. Pipathsouk, A. *et al.* The WAVE complex associates with sites of saddle membrane curvature. *J. Cell Biol.* **220**, (2021).

175. Millius, A., Watanabe, N. & Weiner, O. D. Diffusion, capture and recycling of SCAR/WAVE and Arp2/3 complexes observed in cells by single-molecule imaging. *J. Cell Sci.* **125**, 1165–1176 (2012).

176. Leung, T., Manser, E., Tan, L. & Lim, L. A novel serine/threonine kinase binding the Ras-related RhoA GTPase which translocates the kinase to peripheral membranes. *J. Biol. Chem.* **270**, 29051–29054 (1995).

177. Ishizaki, T. *et al.* The small GTP-binding protein Rho binds to and activates a 160 kDa Ser/Thr protein kinase homologous to myotonic dystrophy kinase. *EMBO J.* **15**, 1885–1893 (1996).

178. Matsui, T. *et al.* Rho-associated kinase, a novel serine/threonine kinase, as a putative target for small GTP binding protein Rho. *EMBO J.* **15**, 2208–2216 (1996).

179. Amano, M., Nakayama, M. & Kaibuchi, K. Rho-Kinase/ROCK: A Key Regulator of the Cytoskeleton and Cell Polarity. *Cytoskelet. Hoboken Nj* **67**, 545–554 (2010).

180. Julian, L. & Olson, M. F. Rho-associated coiled-coil containing kinases (ROCK): structure, regulation, and functions. *Small GTPases* **5**, e29846 (2014).

181. Amano, M. *et al.* Phosphorylation and activation of myosin by Rho-associated kinase (Rho-kinase). *J. Biol. Chem.* **271**, 20246–20249 (1996).

182. Huttenlocher, A., Sandborg, R. R. & Horwitz, A. F. Adhesion in cell migration. *Curr. Opin. Cell Biol.* **7**, 697–706 (1995).

183. Reymann, A.-C. *et al.* Actin network architecture can determine myosin motor activity. *Science* **336**, 1310–1314 (2012).

184. Blanchoin, L., Boujemaa-Paterski, R., Sykes, C. & Plastino, J. Actin dynamics, architecture, and mechanics in cell motility. *Physiol. Rev.* **94**, 235–263 (2014).

185. Thoresen, T., Lenz, M. & Gardel, M. L. Thick filament length and isoform composition determine self-organized contractile units in actomyosin bundles. *Biophys. J.* **104**, 655–665 (2013).

186. Sugimoto, K., Fujii, S. & Yamashita, K. Expression of stress fibers in bullfrog mesothelial cells in response to tension. *Exp. Cell Res.* **196**, 353–361 (1991).

187. Murakami, T. & Ishikawa, H. Stress fibers in situ in proximal tubules of the rat kidney. *Cell Struct. Funct.* **16**, 231–240 (1991).

188. Schiller, H. B. & Fässler, R. Mechanosensitivity and compositional dynamics of cell-matrix adhesions. *EMBO Rep.* **14**, 509–519 (2013).

189. Grecco, H. E., Schmick, M. & Bastiaens, P. I. H. Signaling from the living plasma membrane. *Cell* **144**, 897–909 (2011).

190. van Meer, G., Voelker, D. R. & Feigenson, G. W. Membrane lipids: where they are and how they behave. *Nat. Rev. Mol. Cell Biol.* **9**, 112–124 (2008).

191. Ma, L., Cantley, L. C., Janmey, P. A. & Kirschner, M. W. Corequirement of specific phosphoinositides and small GTP-binding protein Cdc42 in inducing actin assembly in Xenopus egg extracts. *J. Cell Biol.* **140**, 1125–1136 (1998).

192. Lassing, I. & Lindberg, U. Specific interaction between phosphatidylinositol 4,5-bisphosphate and profilactin. *Nature* **314**, 472–474 (1985).

193. Di Paolo, G. & De Camilli, P. Phosphoinositides in cell regulation and membrane dynamics. *Nature* **443**, 651–657 (2006).

194. Berquez, M. *et al.* The phosphoinositide 3-kinase inhibitor alpelisib restores actin organization and improves proximal tubule dysfunction in vitro and in a mouse model of Lowe syndrome and Dent disease. *Kidney Int.* **98**, 883–896 (2020).

195. Daste, F. *et al.* Control of actin polymerization via the coincidence of phosphoinositides and high membrane curvature. *J. Cell Biol.* **216**, 3745–3765 (2017).

196. Knight, Z. A., Feldman, M. E., Balla, A., Balla, T. & Shokat, K. M. A membrane capture assay for lipid kinase activity. *Nat. Protoc.* **2**, 2459–2466 (2007).

197. Ferguson, G. J. *et al.* PI(3)Kγ has an important context-dependent role in neutrophil chemokinesis. *Nat. Cell Biol.* **9**, 86–91 (2007).

198. Krahn, M. P. & Wodarz, A. Phosphoinositide lipids and cell polarity: linking the plasma membrane to the cytocortex. *Essays Biochem.* **53**, 15–27 (2012).

199. Catimel, B. *et al.* The PI(3,5)P2 and PI(4,5)P2 interactomes. *J. Proteome Res.* **7**, 5295–5313 (2008).

200. Fritsch, R. *et al.* RAS and RHO families of GTPases directly regulate distinct phosphoinositide 3-kinase isoforms. *Cell* **153**, 1050–1063 (2013).

201. Campa, C. C., Ciraolo, E., Ghigo, A., Germena, G. & Hirsch, E. Crossroads of PI3K and Rac pathways. *Small GTPases* **6**, 71–80 (2015).

202. McCormick, B., Chu, J. Y. & Vermeren, S. Cross-talk between Rho GTPases and PI3K in the neutrophil. *Small GTPases* **10**, 187–195 (2019).

203. Weiner, O. D. Rac Activation: P-Rex1 — A Convergence Point for PIP3 and Gβγ? *Curr. Biol.* **12**, R429–R431 (2002).

204. Houk, A. R. *et al.* Membrane Tension Maintains Cell Polarity by Confining Signals to the Leading Edge during Neutrophil Migration. *Cell* **148**, 175–188 (2012).

205. Singer, S. J. & Nicolson, G. L. The fluid mosaic model of the structure of cell membranes. *Science* **175**, 720–731 (1972).

206. Nicolson, G. L. The Fluid—Mosaic Model of Membrane Structure: Still relevant to understanding the structure, function and dynamics of biological membranes after more than 40years. *Biochim. Biophys. Acta BBA - Biomembr.* **1838**, 1451–1466 (2014).

207. Shi, Z., Graber, Z. T., Baumgart, T., Stone, H. A. & Cohen, A. E. Cell Membranes Resist Flow. *Cell* **0**, (2018).

208. Mosaddeghzadeh, N. *et al.* Electrostatic Forces Mediate the Specificity of RHO GTPase-GDI Interactions. *Int. J. Mol. Sci.* **22**, 12493 (2021).

209. Silvius, J. R. & l'Heureux, F. Fluorometric Evaluation of the Affinities of Isoprenylated Peptides for Lipid Bilayers. *Biochemistry* **33**, 3014–3022 (1994).

210. Johnson, J. L., Erickson, J. W. & Cerione, R. A. C-terminal Di-arginine Motif of Cdc42 Protein Is Essential for Binding to Phosphatidylinositol 4,5-Bisphosphate-containing Membranes and Inducing Cellular Transformation. *J. Biol. Chem.* **287**, 5764–5774 (2012).

211. Cadart, C. *et al.* Size control in mammalian cells involves modulation of both growth rate and cell cycle duration. *Nat. Commun.* **9**, 3275 (2018).

212. Gauthier, N. C., Rossier, O. M., Mathur, A., Hone, J. C. & Sheetz, M. P. Plasma membrane area increases with spread area by exocytosis of a GPI-anchored protein compartment. *Mol. Biol. Cell* **20**, 3261–3272 (2009).

213. Ingólfsson, H. I. *et al.* Lipid Organization of the Plasma Membrane. *J. Am. Chem. Soc.* **136**, 14554–14559 (2014).

214. Schmick, M. *et al.* KRas localizes to the plasma membrane by spatial cycles of solubilization, trapping and vesicular transport. *Cell* **157**, 459–471 (2014).

215. Dharmaiah, S. *et al.* Structural basis of recognition of farnesylated and methylated KRAS4b by PDEδ. *Proc. Natl. Acad. Sci.* **113**, E6766–E6775 (2016).

216. Pfeffer, S. R., Dirac-Svejstrup, A. B. & Soldati, T. Rab GDP dissociation inhibitor: putting rab GTPases in the right place. *J. Biol. Chem.* **270**, 17057–17059 (1995).

217. Sivars, U., Aivazian, D. & Pfeffer, S. R. Yip3 catalyses the dissociation of endosomal Rab–GDI complexes. *Nature* **425**, 856–859 (2003).

218. Dirac-Svejstrup, A. B., Sumizawa, T. & Pfeffer, S. R. Identification of a GDI displacement factor that releases endosomal Rab GTPases from Rab-GDI. *EMBO J.* **16**, 465–472 (1997).

219. Machner, M. P. & Isberg, R. R. A Bifunctional Bacterial Protein Links GDI Displacement to Rab1 Activation. *Science* **318**, 974–977 (2007).

220. Schoebel, S., Oesterlin, L. K., Blankenfeldt, W., Goody, R. S. & Itzen, A. RabGDI Displacement by DrrA from Legionella Is a Consequence of Its Guanine Nucleotide Exchange Activity. *Mol. Cell* **36**, 1060–1072 (2009).

221. Maeda, M., Matsui, T., Imamura, M., Tsukita, S. & Tsukita, S. Expression level, subcellular distribution and rho-GDI binding affinity of merlin in comparison with Ezrin/Radixin/Moesin proteins. *Oncogene* **18**, 4788–4797 (1999).

222. Takahashi, K. *et al.* Direct Interaction of the Rho GDP Dissociation Inhibitor with Ezrin/Radixin/Moesin Initiates the Activation of the Rho Small G Protein. *J. Biol. Chem.* **272**, 23371–23375 (1997).

223. Yamashita, T. & Tohyama, M. The p75 receptor acts as a displacement factor that releases Rho from Rho-GDI. *Nat. Neurosci.* **6**, 461–467 (2003).

224. Takahashi, K. *et al.* Interaction of radixin with Rho small G protein GDP/GTP exchange protein Dbl. *Oncogene* **16**, 3279–3284 (1998).

225. DerMardirossian, C., Schnelzer, A. & Bokoch, G. M. Phosphorylation of RhoGDI by Pak1 Mediates Dissociation of Rac GTPase. *Mol. Cell* **15**, 117–127 (2004).

226. DerMardirossian, C., Rocklin, G., Seo, J.-Y. & Bokoch, G. M. Phosphorylation of RhoGDI by Src Regulates Rho GTPase Binding and Cytosol-Membrane Cycling. *Mol. Biol. Cell* **17**, 4760–4768 (2006).

227. Lang, P. *et al.* Protein kinase A phosphorylation of RhoA mediates the morphological and functional effects of cyclic AMP in cytotoxic lymphocytes. *EMBO J.* **15**, 510–519 (1996).

228. Chuang, T. H., Bohl, B. P. & Bokoch, G. M. Biologically active lipids are regulators of Rac.GDI complexation. *J. Biol. Chem.* **268**, 26206–26211 (1993).

229. Robbe, K., Otto-Bruc, A., Chardin, P. & Antonny, B. Dissociation of GDP Dissociation Inhibitor and Membrane Translocation Are Required for Efficient Activation of Rac by the Dbl Homology-Pleckstrin Homology Region of Tiam*. *J. Biol. Chem.* **278**, 4756–4762 (2003).

230. Bos, J. L., Rehmann, H. & Wittinghofer, A. GEFs and GAPs: critical elements in the control of small G proteins. *Cell* **129**, 865–877 (2007).

231. Graessl, M. *et al.* An excitable Rho GTPase signaling network generates dynamic subcellular contraction patterns. *J Cell Biol* jcb.201706052 (2017) doi:10.1083/jcb.201706052.

232. Rossman, K. L. *et al.* A crystallographic view of interactions between Dbs and Cdc42: PH domain-assisted guanine nucleotide exchange. *EMBO J.* **21**, 1315–1326 (2002).

233. Worthylake, D. K., Rossman, K. L. & Sondek, J. Crystal structure of the DH/PH fragment of Dbs without bound GTPase. *Struct. Lond. Engl. 1993* **12**, 1078–1086 (2004).

234. Boulter, E. & Garcia-Mata, R. RhoGDI. *Small GTPases* **1**, 65–68 (2010).

235. Farhan, H. & Hsu, V. W. Cdc42 and Cellular Polarity: Emerging Roles at the Golgi. *Trends Cell Biol.* **26**, 241–248 (2016).

236. Zhang, S.-C. *et al.* Liposome Reconstitution and Modulation of Recombinant Prenylated Human Rac1 by GEFs, GDI1 and Pak1. *PLOS ONE* **9**, e102425 (2014).

237. Roskoski, R. Protein prenylation: a pivotal posttranslational process. *Biochem. Biophys. Res. Commun.* **303**, 1–7 (2003).

238. Popp, M. W., Antos, J. M., Grotenbreg, G. M., Spooner, E. & Ploegh, H. L. Sortagging: a versatile method for protein labeling. *Nat. Chem. Biol.* **3**, 707–708 (2007).

239. Hancock, J. f. & Hall, A. A novel role for RhoGDI as an inhibitor of GAP proteins. *EMBO J.* **12**, 1915–1921 (1993).

240. Nomanbhoy, T. K. & Cerione, R. A. Characterization of the Interaction between RhoGDI and Cdc42Hs Using Fluorescence Spectroscopy. *J. Biol. Chem.* **271**, 10004–10009 (1996).

241. Lee, K., Gallop, J. L., Rambani, K. & Kirschner, M. W. Self-Assembly of Filopodia-Like Structures on Supported Lipid Bilayers. *Science* **329**, 1341–1345 (2010).

242. Hume, P. J., Humphreys, D. & Koronakis, V. Chapter Twenty - WAVE Regulatory Complex Activation. in *Methods in Enzymology* (ed. Vale, R. D.) vol. 540 363–379 (Academic Press, 2014).

243. Nye, J. A. & Groves, J. T. Kinetic Control of Histidine-Tagged Protein Surface Density on Supported Lipid Bilayers. *Langmuir* **24**, 4145–4149 (2008).

244. iamankitroy/Single-Molecule-Colocalization: Scripts for analysing colocalizations in dual channel single molecule TIRF microscopy data of GTPase and GDI recruitment/extraction events on lipid bilayers. *GitHub* https://github.com/iamankitroy/Single-Molecule-Colocalization.

245. Meca, J. *et al.* Avidity-driven polarity establishment via multivalent lipid–GTPase module interactions. *EMBO J.* **38**, (2019).

246. Golovanov, A. P. *et al.* Structure-activity relationships in flexible protein domains: regulation of rho GTPases by RhoGDI and D4 GDI. *J. Mol. Biol.* **305**, 121–135 (2001).

247. Lam, B. D. & Hordijk, P. L. The Rac1 hypervariable region in targeting and signaling. *Small GTPases* **4**, 78–89 (2013).

248. Mouritsen, O. G. & Zuckermann, M. J. What's so special about cholesterol? *Lipids* **39**, 1101–1113 (2004).

249. Schmick, M., Kraemer, A. & Bastiaens, P. I. H. Ras moves to stay in place. *Trends Cell Biol.* **25**, 190–197 (2015).

250. Roder, F., Birkholz, O., Beutel, O., Paterok, D. & Piehler, J. Spatial Organization of Lipid Phases in Micropatterned Polymer-Supported Membranes. *J. Am. Chem. Soc.* **135**, 1189–1192 (2013).

251. Ramella, M., Ribolla, L. M. & de Curtis, I. Liquid-Liquid Phase Separation at the Plasma Membrane-Cytosol Interface: Common Players in Adhesion, Motility, and Synaptic Function. *J. Mol. Biol.* **434**, 167228 (2022).

252. Sala, K. *et al.* The ERC1 scaffold protein implicated in cell motility drives the assembly of a liquid phase. *Sci. Rep.* **9**, 13530 (2019).

253. Rossman, K. L. *et al.* Multifunctional Roles for the PH Domain of Dbs in Regulating Rho GTPase Activation *. *J. Biol. Chem.* **278**, 18393–18400 (2003).

254. Frisch, T. & Thoumine, O. Predicting the kinetics of cell spreading. *J. Biomech.* **35**, 1137–1141 (2002).

255. Hansen, S. D. *et al.* Stochastic geometry sensing and polarization in a lipid kinase–phosphatase competitive reaction. *Proc. Natl. Acad. Sci.* **116**, 15013–15022 (2019).

256. Gibson, D. G. Enzymatic assembly of overlapping DNA fragments. *Methods Enzymol.* **498**, 349–361 (2011).

257. Gibson, D. G. *et al.* Enzymatic assembly of DNA molecules up to several hundred kilobases. *Nat. Methods* **6**, 343–345 (2009).

258. Huang, N. P. *et al.* Poly(L-lysine)-g-poly(ethylene glycol) layers on metal oxide surfaces: surface-analytical characterization and resistance to serum and fibrinogen adsorption. *Langmuir* **17**, 489–498 (2001).

259. Schindelin, J. *et al.* Fiji: an open-source platform for biological-image analysis. *Nat. Methods* **9**, 676–682 (2012).

260. Linkert, M. *et al.* Metadata matters: access to image data in the real world. *J. Cell Biol.* **189**, 777–782 (2010).

261. Tinevez, J.-Y. *et al.* TrackMate: An open and extensible platform for single-particle tracking. *Methods* **115**, 80–90 (2017).